Journal of the
OPTICAL SOCIETY *of* AMERICA

VOLUME 35, NUMBER 10 OCTOBER, 1945

Effects of Temperature and Pressure on the Focus of Aerial Cameras

EDWARD B. WOODFORD AND RICHARD N. NIERENBERG
Army Air Forces Photographic Laboratory, Engineering Division, Wright Field, Dayton, Ohio
(Received June 25, 1945)

LENSES of long focal length are coming into more common use in aerial cameras because of the higher and higher altitudes to which photographic reconnaissance airplanes are being forced. The effects of varying temperature and pressure on the focus of aerial cameras are of considerable importance for long focus lenses, and therefore a study was initiated to determine the magnitude of the effects of changes in barometric pressure, and temperature, on several standard Army Air Forces cameras.

In this study, it is assumed that the change in flange focus caused by a temperature change is proportional to the temperature change. This shift in focus is caused by: (1) changes in the length of the camera; (2) changes in the lens separations, or air spaces, in the lens barrel; (3) changes in the shape of the lens elements; and (4) changes in the refractive indices of the lens elements and of the air. The net result of these effects (K_1) might be called the "temperature coefficient" of the camera, and Table I shows values for this constant for six Army Air Forces cameras.

It can be shown that the change in the flange focus of a lens, caused by a change in the index of the air, is proportional to that index change. It has been found, experimentally, that the relationship between index of air (μ) and barometric pressure (P), at a given temperature, is linear. Therefore, a linear relationship holds between change in flange focus ($F.F.$) and barometric pressure.

$$\Delta F.F. = C\Delta\mu$$

and

$$\mu - 1 = C_1 P,$$
$$\Delta\mu = C_1 \Delta P,$$
$$\Delta F.F. = K_2 \Delta P.$$

Flange focus is herein defined as the distance from the focal plane to the mounting shoulder of the rear cell of the lens. K_2 might be called "pressure coefficient" of the camera, and in Table I values of this coefficient are given for four cameras. Measurements on the temperature and pressure effects for two aerial cameras are

TABLE I.

Lens	K_1 Focus shift in mm per degree centrigade change in temperature.	K_2 Focus shift in mm per mm change in barometric pressure.
48-inch $f/6.3$	-195×10^{-4}	
*40-inch $f/8.0$	-348×10^{-4}	13.5×10^{-4}
*40-inch $f/8.0$	-320×10^{-4}	13.3×10^{-4}
**40-inch $f/8$	-117×10^{-4}	
36-inch $f/8$	-294×10^{-4}	
24-inch $f/6.0$ Manufacturer A	-214×10^{-4}	4.9×10^{-4}
24-inch $f/6.0$ Manufacturer B	-90×10^{-4}	4.3×10^{-4}
12-inch $f/5$	-105×10^{-4}	1.3×10^{-4}

* These two sets of measurements on the 40-inch $f/8$ lens were made by different observers using different apparatus and on dates approximately two years apart.
** This lens was mounted in an Invar barrel.

BOSTON UNIVERSITY
COLLEGE OF LIBERAL ARTS
LIBRARY

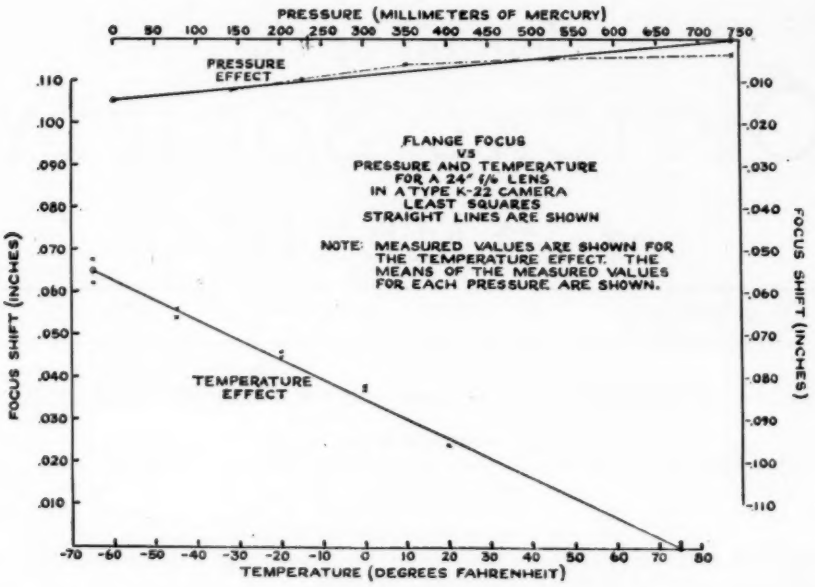
PRESSURE (MILLIMETERS OF MERCURY)
0 50 100 150 200 250 300 350 400 450 500 550 600 650 700 750
PRESSURE EFFECT
FLANGE FOCUS VS PRESSURE AND TEMPERATURE FOR A 24" f/6 LENS IN A TYPE K-22 CAMERA LEAST SQUARES STRAIGHT LINES ARE SHOWN
NOTE: MEASURED VALUES ARE SHOWN FOR THE TEMPERATURE EFFECT. THE MEANS OF THE MEASURED VALUES FOR EACH PRESSURE ARE SHOWN.
TEMPERATURE EFFECT
FOCUS SHIFT (INCHES)
.110 .100 .090 .080 .070 .060 .050 .040 .030 .020 .010
-.010 -.020 -.030 -.040 -.050 -.060 -.070 -.080 -.090 -.100 -.110
-70 -60 -50 -40 -30 -20 -10 0 10 20 30 40 50 60 70 80
TEMPERATURE (DEGREES FAHRENHEIT)

FIG. 1.

recorded on the two curve sheets Figs. 1 and 2. The values shown in Table I were taken from the slopes of the least squares straight lines.

Figure 2 shows the average of ten measurements of the flange focus shift in the 40-inch $f/8$ telephoto lens, at each indicated pressure. These values indicate a departure from a straight line, which was verified by eight repetitions of the test and by a statistical analysis of the data. The statistical study included an analysis of 110 observations (10 observations at each of 11 pressures) by use of the analysis of variance technique applied to the least squares straight line fitted to the data. This least squares line, plotted in Fig. 2, is $Y=-0.03547+0.00005229P$, where Y is the focus shift in inches corresponding to a pressure of P millimeters. No explanation is offered for this departure from a straight line, but further investigation is planned.

METHOD OF MEASUREMENT

An autocollimation system, described herein, was designed to permit measurements of the change in flange focus of complete cameras in a low pressure chamber and in a "cold room." The microscope, with target in position, was placed in the cold room at -65°F for six hours, and the zero adjustment was checked to determine how much shift in focus caused by temperature variation may be attributed to the microscope. No shift was discernible. The axial focus position for each of the six standard Army Air Forces cameras was measured with the autocollimation apparatus at room temperature, 75° F. These were taken as the normal or zero positions for these cameras. One of the cameras, a K-17 with the 12-inch $f/5$ lens, was placed in the cold chamber at -65°F, and the autocollimated image was observed. The appearance of the image was very poor for the first 35 minutes, because of the turbulence of the air surrounding the camera and the lens elements. The image became progressively better during the last 5 of the 35 minutes, until the image was good and could be brought into focus easily. At least 2 hours are required, however, for this lens to reach a truly stable condition. Six cameras, a 12-inch $f/5$ Type K-17, a 24-inch $f/6$ Type K-17, a 24-inch $f/6$ Type K-22, a 36-inch $f/8$, Type K-18, a 40-inch $f/8$ Type K-22, and a 48-inch $f/6.3$ Type K-22, were placed in the cold room at $+20$° F and were maintained within 2° F of that temperature for 20 hours before measurements of the axial focus position were made. A

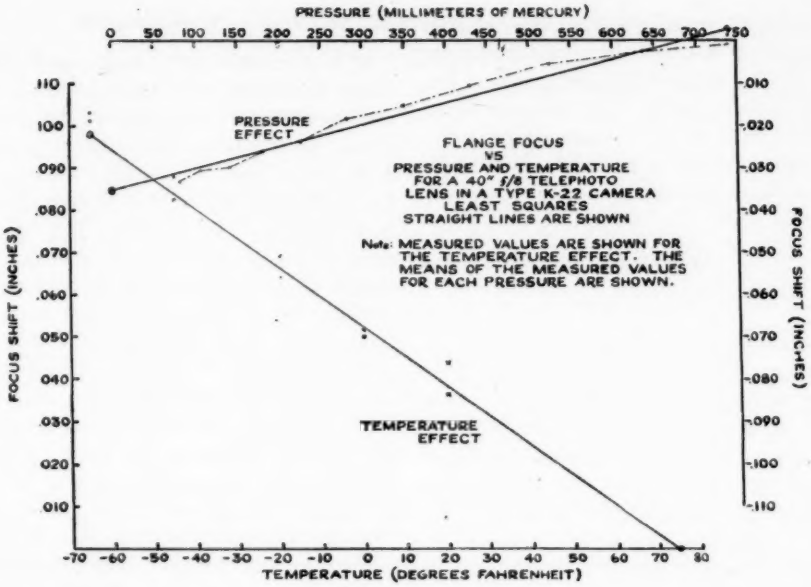
PRESSURE (MILLIMETERS OF MERCURY)
0 50 100 150 200 250 300 350 400 450 500 550 600 650 700 750
FOCUS SHIFT (INCHES)
110 100 .090 .080 .070 .060 050 040 .030 020 .010
FOCUS SHIFT (INCHES)
.010 .020 .030 .040 .050 .060 .070 .080 .090 .100 .110
PRESSURE EFFECT
FLANGE FOCUS VS PRESSURE AND TEMPERATURE FOR A 40" f/8 TELEPHOTO LENS IN A TYPE K-22 CAMERA LEAST SQUARES STRAIGHT LINES ARE SHOWN
Note: MEASURED VALUES ARE SHOWN FOR THE TEMPERATURE EFFECT. THE MEANS OF THE MEASURED VALUES FOR EACH PRESSURE ARE SHOWN.
TEMPERATURE EFFECT
-70 -60 -50 -40 -30 -20 -10 0 10 20 30 40 50 60 70 80
TEMPERATURE (DEGREES FAHRENHEIT)

FIG. 2.

Duraluminum fixture with the autocollimating microscope was attached to the cone to be measured. Similarly, measurements were made at 0°, −20°, −45°, and −65° F. The measurements were made by two observers. Figure 3 is a view of the installation of the autocollimation apparatus in the low temperature chamber for making measurements of the shift in focus caused by a change in temperature. The low pressure chamber is capable of producing and maintaining a pressure much lower than 83 mm of mercury, which was the lowest pressure at which readings were made.

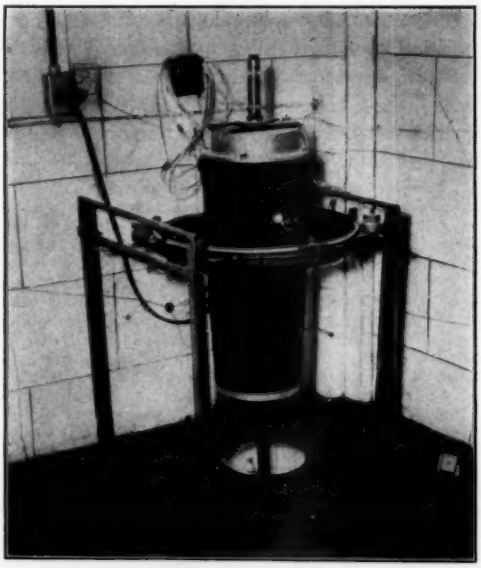

FIG. 3. Auto collimation apparatus for focus shift, measurements at low temperatures.

Measurements of focus position were made with the focusing microscope at air pressures corresponding to 0 to 50,000 feet of altitude in 10,000 foot steps, both on "ascent" and "descent." The focusing microscope was installed through a porthole in the chamber. A rubber gasket was used to seal against air leaks. The altimeter of the chamber was calibrated against an open tube mercury manometer. The changes in the temperature of the air in the chamber, with changes in pressure, were measured. Although calculations indicate that these small temperature changes were negligible, the measurements of focus change were not made until the temperature of the air in the chamber had been restored to 75° F. An investigation was made of the possibility that errors might be

caused by residual pressure differences between the air outside of the lens and that in the air spaces within. The 40-inch $f/8$ telephoto lens was used in this investigation, and measurements were made at 740-mm to 83-mm air pressure. Holes were then drilled in the walls of the lens cells to insure equal pressure, and the measurements were repeated. No measurable effect was found.

AUTOCOLLIMATOR

The autocollimation system, consists of a 100× focusing microscope, an illuminated target, a Duraluminum fixture to replace the camera body, and an optically flat, front-surfaced mirror. The target is placed in the object position of the microscope, and is held in place by a slotted cylindrical jig fastened to the objective. This element permits the microscope to be moved in and out, carrying the target with it without rotation. The illumination is supplied by 3 very small, 3-volt, 0.19-ampere lamps located between the objective of the microscope and the target. The autocollimating microscope assembly is mounted in the focal plane of the camera to be tested. The mirror is placed in front of the lens and is adjusted so that the reflected image appears in the center of the field of the microscope. The microscope, with the illuminated target, is then moved in and out by a micrometer screw, to locate the position in which the target is considered to be in the focal plane of the lens.

CONCLUSIONS

It is concluded that temperature and pressure effects should be taken into account in the design and use of aerial cameras having long focal length lenses. It is further concluded from this study, and from studies of a similar nature conducted by C. W. Kendall, at the Photographic Laboratory, Wright Field, in 1941, that there are two aspects to the problem of correcting for the effects of temperature on a photographic objective. One of these is a change in flange focus caused by a temperature change, and the other is the loss in definition which results where there are temperature gradients within the optical system. Compensation for the former can be achieved by adjusting the focus of the lens of the camera for the temperature at which it is to be used. No compensation for the effect of temperature gradients is possible, and the only solution to this problem is to maintain the lens at a uniform temperature for considerable time prior to use (for example, 3 hours for the 40-inch $f/8$ telephoto lenses), and at the same temperature during use. This may be accomplished by suitable insulation and adequate, thermostatically-controlled heating.

The authors wish to express their indebtedness to Colonel Barron C. Powers, Chief, Photographic Laboratory, Wright Field, to Mr. C. W. Kendall, under whose direction this work was carried out, and to Mr. A. H. Katz for his assistance with the statistical analysis of the observed data.

JOURNAL OF THE OPTICAL SOCIETY OF AMERICA VOLUME 35, NUMBER 10 OCTOBER, 1945

Focal Plane Anomalies in Roof Prisms*

A. I. MAHAN
Optical Design Section, Design and Drafting Division, Naval Gun Factory, Washington, D. C.
(Received August 14, 1945)

A description is given of a focal plane anomaly occurring in a roof prism when parallel light passing through the prism is brought to a focus by a lens. The anomaly consists of a doubling of the image in a direction perpendicular to the roof edge while parallel to the roof edge, the image remains single and sharp. If plane polarized light is allowed to enter the prism, the form of the doubling can be changed by rotating the incident azimuth angle of the entering plane polarized light. Usually in roof prisms, such a doubling is to be associated with a roof angle error. It is the purpose of this paper to show that such is not the case for this particular prism. The following development also suggests that all roof prisms can be expected to possess to some degree these same characteristics. The magnitude of the doubling in unpolarized light and the changes in the doubling in plane polarized light when the incident azimuth angle is rotated will be shown to be a function of the geometry of the prism and its refractive index.

INTRODUCTION

IN the course of the making of some roof prisms for military purposes, a prism shown in Fig. 1 came to our attention which had some rather unusual properties. It was found that if light from a distant target consisting of narrow horizontal and vertical lines is allowed to enter the prism in the direction indicated in the top view shown in Fig. 2 and upon emergence is collected by a telescope of rather high power (about sixteen), lines in the direction of the horizontal (parallel to the roof edge) were always found to be doubled while the vertical lines remained single and sharp. Simultaneously these prisms always showed a higher resolving power in the vertical direction If the prism roofs however were silvered, the definition and resolving power in the two directions became nearly equivalent. Normally when a doubling of the image of this type is found in an Amici roof prism, it is usually to be associated with a roof angle error. Since silvering of the roof surfaces eliminated the apparent roof angle error, there was considerable evidence that a different phenomenon was effective in this particular case. In fact, it will be the purpose of this paper to show that even with a perfect 90° roof angle on the prism

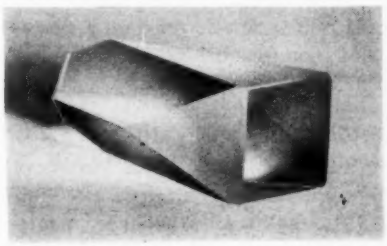

FIG. 1.

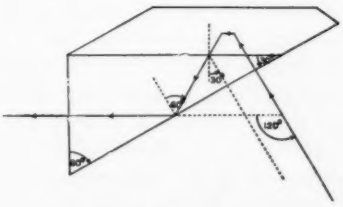

FIG. 2.

* This paper was completed a little over a year ago but because of the war, publication was not permitted. Since that time an article on the same general subject has been called to the author's attention. For a copy of this article the author is indebted to Dr. I. C. Gardner of the Bureau of Standards who on his trip to Europe sent a copy of this paper back to the Bureau of Standards. The title of the paper was "Image Deterioration by Roof Prisms" by Dr. G. Joos (Zeiss Nachrichten **4**, 9 (July 1943)). This paper was made available to the author by Dr. R. E. Stephens and Dr. L. W. Tilton of the optics division of the Bureau of Standards. The occasion for the writing of this paper by Dr. Joos was identical (with the exception that a different type roof prism was used) with that of the present paper. The roof prism in Fig. 1 always gave poor definition, but after silvering of the roof surfaces (first suggested by Max Zwillinger of the Optics Laboratory in January 1943) the definition was greatly increased. Dr. Joos' paper is more general in nature and is concerned primarily with the polarization properties for a two internal reflection roof prism when illuminated with parallel light. No attempt is made to evaluate the forms of the diffraction patterns for different incident azimuth angles for polarized light or for unpolarized light.

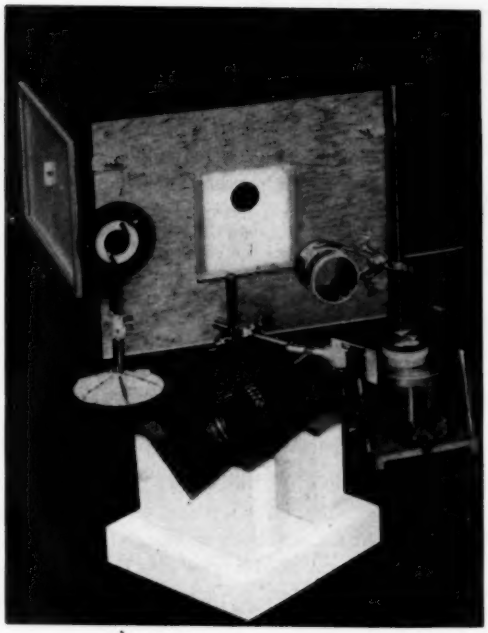

FIG. 3.

shown in Fig. 1, this doubling of the image parallel to the roof edge will persist.

To magnify this effect sufficiently to record it photographically, the following experimental apparatus was used. A cross consisting of lines about .01 mm wide was ruled on a silvered glass plate and mounted behind the hole in the box shown in Fig. 3. An AH4 high pressure mercury arc, green filter, and auxiliary lens were also placed inside the box to illuminate the previously mentioned cross. This box served as a unit to provide a monochromatically illuminated target (5461A) for all the experiments (room completely darkened) in connection with this paper. A 500-mm E.F. telescope objective was mounted in front of the illuminated cross at a distance equal to the back focus of the lens. The collimated light from this lens was allowed to fall on the prism (see Fig. 3) in the manner suggested by Fig. 2 and the emergent light brought to a focus by the 2839-mm E.F. lens. To magnify further the diffraction effects involved, a 5-mm square aperture (made with razor blades) was centrally placed over the emergent aperture of the prism. The resulting picture obtained in the focal plane of the 2839-mm lens after being enlarged about four times is shown in Fig. 4. This picture although somewhat overexposed shows clearly the characteristic behavior of such prisms. In addition to the doubling of the horizontal lines, it will be noted that the minima of the weaker adjacent diffraction bands have twice the separation of the corresponding minima in the vertical direction.

The problem therefore is to show why the diffraction pattern for this prism takes this particular form. Once this is done for the 5461 light used above, the same procedure can be applied to other wave-lengths which might be present in any given source. When reasons for the diffraction patterns in the two directions of Fig. 4 have been determined, the different resolving powers in the two directions can also be understood.

For ease of presentation, the following theoretical treatment of the problem will be divided into four parts. The first will concern itself with the polarization properties of the prism and is designated as "Polarization Properties." The second will be called the "Focal Plane Properties" since this part will develop the mathematics necessary to describe the diffraction pattern for any arbitrary incident azimuth of the entering plane polarized light. The third part is concerned with the actual evaluation of the different forms of the diffraction patterns for polarized light of different incident azimuth angles and is called the "Form of Diffraction Pattern in Polarized Light." The fourth and last part derives the form to be expected in unpolarized light and is accordingly called "Form of the Diffraction Pattern in Unpolarized Light." The equations themselves will be developed in general terms so that they may be applied to any roof prism having three internal reflections,

FIG. 4.

but they will be evaluated only for the prism under consideration.

1. POLARIZATION PROPERTIES

It might be rather surprising that it is necessary to bring polarized light into the problem for, in use, the prism normally is illuminated with unpolarized light. Unpolarized light itself however may be looked upon as consisting of plane polarized light having all possible incident azimuth angles. If the problem can be solved for several incident azimuth angles and inferences drawn from these solutions as to the form of the diffraction pattern when all incident azimuth angles are present, the solution to the problem will be more clearly understood and will also serve as a check on any other method.

If now a plane wave of monochromatic light having amplitude A_0 and phase φ_i is allowed to enter the prism in the direction indicated in Fig. 2, at a time "t" it can be designated by[1]

$$A_0 \sin (\omega t + \varphi_i). \tag{1}$$

This light after entering the prism may travel by one of two paths. Either it may enter the upper half of the prism aperture and emerge from the lower, or it may enter the lower and emerge from the upper. In either case it should be clear from the geometry of the prism that the path in glass for a perfectly made prism must have the same value for both directions. If therefore one views the plane wave at the same time "t" emerging from the upper or lower halves of the aperture (assuming no phase changes upon reflection at the internal prism surfaces or amplitude losses due to reflection and absorption), it would be expected to be of the form

$$A_0 \sin (\omega t + \varphi_i + \varphi_g), \tag{2}$$

where φ_g is the difference in phase created by the geometrical path in the prism.

Actually the problem is much more complex. It will be found for instance that if a polarizer and analyzer are inserted in front and in back of the prism, respectively, for any given initial position of the polarizer, light of different ellipticities will be found to emerge from the upper and lower halves of the prism aperture. Thus although geometrically the two paths in the prism are identical, from the standpoint of physical optics they are different. This difference in ellipticity will later be shown to be brought about by the phase changes after reflection at each of the internal prism reflecting surfaces.

To define the initial incident azimuth angle for light entering the upper or lower halves of the prism aperture, a sign convention for the "s" and "p" vibrations[2] at each surface must be chosen since the various azimuth angles in proceeding along the path through the prism are located with respect to these vibrations and it is necessary to have the correct signs if the azimuth angles are to have the correct values. For each ray therefore reflected inside the prism, the positive direction of the "p" vibration will be chosen in the direction of the inward surface normal, and the positive direction of the "s" vibration 90° clockwise from that of the positive direction of "p" when looking along the path of travel of the light.

In the following treatment, the case in which light enters the upper half of the prism (see Fig. 2) and emerges from the lower will be treated in complete detail. After this is done, it will be possible by analogy to write down immediately the corresponding expressions for the case in which light enters the lower half and emerges from the upper.

The initial incident azimuth angle of the plane polarized light entering the upper half of the prism will be designated by α. Its value will be assumed positive when measured counterclockwise from the positive direction of the "s" vibration at the first roof surface when looking along the path of travel of the light. If the incident plane polarized wave at the first roof surface is given by expression (2), the corresponding "s" and "p" vibrations before reflection are

$$A_{s1} = A_0 \cos \alpha \sin (\omega t + \varphi_i + \varphi_g),$$

$$A_{p1} = A_0 \sin \alpha \sin (\omega t + \varphi_i + \varphi_g).$$

After reflection at the first roof surface, the

[1] Actually in practice incoherent light is used so that A_0 and φ_i will have a wide range of values. The form of the solution to the problem as will be seen later is however independent of the values of A_0 and φ_i.

[2] The "s" vibration will be assumed to be that with the electric vector vibrating perpendicular to the plane of incidence, while the "p" vibration will be that vibratng in the plane of incidence.

amplitudes[3] remain unchanged[4] since reflection occurs beyond the critical angle. The changes which do occur however are an abrupt change in phase[5] at the surface for both "s" and "p" vibrations and a change in direction for the "p" vibration. The two waves after reflection can then be written in the form

$$A_{s1}' = A_0 \cos\alpha \sin(\omega t + \varphi_i + \varphi_g + \varphi_{s1}), \quad (3)$$

$$A_{p1}' = A_0 \sin\alpha \sin(\omega t + \varphi_i + \varphi_g + \varphi_{p1}), \quad (4)$$

φ_{s1}, and φ_{p1}, being the changes in phase upon reflection for each of the two waves.

At the second roof surface both A_{s1}' and A_{p1}' must again be resolved into "s" and "p" components for the plane of incidence (determined by the incident ray and surface normal) for this surface will be found to be different from that of the first surface. The determination of the "s" and "p" components at the second roof surface reduces therefore to resolving A_{s1}' and A_{p1}' into components about a set of coplanar axes which are rotated with respect to A_{s1}' and A_{p1}'. If β is the angle between the positive directions of A_{s2} and A_{s1}' (also assumed positive when measured in a counterclockwise direction from the positive direction of A_{s2} when looking along the path of the ray) the "s" and "p" components before reflection at the second roof surface can be written

$$A_{s2} = A_0 \cos\alpha \cos\beta \sin(\omega t + \varphi_i + \varphi_g + \varphi_{s1}) - A_0 \sin\alpha \sin\beta \sin(\omega t + \varphi_i + \varphi_g + \varphi_{p1}),$$

$$A_{p2} = A_0 \cos\alpha \sin\beta \sin(\omega t + \varphi_i + \varphi_g + \varphi_{s1}) + A_0 \sin\alpha \cos\beta \sin(\omega t + \varphi_i + \varphi_g + \varphi_{p1}).$$

If each of these expressions is expanded (retaining $\omega t + \varphi_i + \varphi_g$ as a constant term) and then in each case multiplied and divided by the square root of the sums of the squares of the coefficients of the time dependent sine and cosine terms, they can be written in the form of a single wave with amplitude and phase. After reflection the values of A_{s2}' and A_{p2}' become[6]

$$A_{s2}' = A_0\{\cos^2\alpha\cos^2\beta + \sin^2\alpha\sin^2\beta - \tfrac{1}{2}\sin 2\alpha \sin 2\beta \cos(\varphi_{s1} - \varphi_{p1})\} \times \sin(\omega t + \varphi_i + \varphi_g + R_{s2} + \varphi_{s2}), \quad (5)$$

$$A_{p2}' = A_0\{\cos^2\alpha\sin^2\beta + \sin^2\alpha\cos^2\beta + \tfrac{1}{2}\sin 2\alpha \sin 2\beta \cos(\varphi_{s1} - \varphi_{p1})\} \times \sin(\omega t + \varphi_i + \varphi_g + R_{p2} + \varphi_{p2}). \quad (6)$$

In these expressions, R_{s2} and R_{p2} are given by

$$\tan R_{s2} = \frac{\cos\alpha\cos\beta\sin\varphi_{s1} - \sin\alpha\sin\beta\sin\varphi_{p1}}{\cos\alpha\cos\beta\cos\varphi_{s1} - \sin\alpha\sin\beta\cos\varphi_{p1}}, \quad (7)$$

$$\tan R_{p2} = \frac{\cos\alpha\sin\beta\sin\varphi_{s1} + \sin\alpha\cos\beta\sin\varphi_{p1}}{\cos\alpha\sin\beta\cos\varphi_{s1} + \sin\alpha\cos\beta\cos\varphi_{p1}}. \quad (8)$$

The two waves given by A_{s2}' and A_{p2}' are then incident upon the third and last internal reflecting surface of the prism. These waves must be resolved about the directions of the "s" and "p" vibrations for this surface for again the plane of incidence for this surface will be different from the preceding one. If we let γ (also positive when measured in a counterclockwise direction from the positive direction of A_{s3} when looking along the path of the light) be the angle between the positive directions of A_{s3} and A_{s2}', the "s" and "p" components before reflection at the third surface can in a similar manner to A_{s2} and A_{p2} be written in the form

$$A_{s3} = A_{s2}'\cos\gamma - A_{p2}'\sin\gamma,$$

$$A_{p3} = A_{s2}'\sin\gamma + A_{p2}'\cos\gamma.$$

Each of these equations can again be expressed in the form of a single vibration of fixed amplitude and phase. To do this, the two terms of each equation must be combined. This procedure is the same as that used in obtaining

[3] Decreases in amplitude due to reflection at the entering and emerging surfaces and absorption along the geometrical path will for simplicity be neglected throughout the paper. These losses can for exactness be included in the final terms if desired by multiplying by appropriate transmission factors. See F. A. Jenkins and H. E. White, *Fundamentals of Physical Optics* (McGraw-Hill Book Company, Inc., New York, 1937), p. 389, 21.

[4] M. Born, *Optik* (Verlagsbuchhandlung, Julius Springer, Berlin, 1933), p. 42.

[5] M. Born, *Optik* (Verlagsbuchhandlung, Julius Springer, Berlin, 1933), p. 43.

[6] It is possible to check the correctness of these expressions by setting $\varphi_{s1} = \varphi_{p1} = \varphi_{s2} = \varphi_{p2} = 0$ and then combining them vectorially. When this is done, the starting wave given by expression (2) will result.

Eqs. (5) and (6) and although it is not difficult, the mathematics necessary is quite long so only the result will be given. The "s" and "p" components after reflection can be written in the form[6]

$$A_{s3}' = A_0\{\cos^2\alpha(\cos^2\beta\cos^2\gamma+\sin^2\beta\sin^2\gamma)+\sin^2\alpha(\sin^2\beta\cos^2\gamma+\cos^2\beta\sin^2\gamma)$$
$$-\tfrac{1}{2}\sin 2\alpha\sin 2\beta\cos 2\gamma\cos(\varphi_{s1}-\varphi_{p1})-2\sin\gamma\cos\gamma[\cos^2\alpha\cos^2\beta+\sin^2\alpha\sin^2\beta$$
$$-\tfrac{1}{2}\sin 2\alpha\sin 2\beta\cos(\varphi_{s1}-\varphi_{p1})]^{\frac{1}{2}}\cdot[\cos^2\alpha\sin^2\beta+\sin^2\alpha\cos^2\beta$$
$$+\tfrac{1}{2}\sin 2\alpha\sin 2\beta\cos(\varphi_{s1}-\varphi_{p1})]^{\frac{1}{2}}\cdot\cos[(R_{s2}-R_{p2})+(\varphi_{s2}-\varphi_{p2})]\}^{\frac{1}{2}}$$
$$\times\sin(\omega t+\varphi_i+\varphi_g+R_{s3}+\varphi_{s3}), \quad (9)$$

$$A_{p3}' = A_0\{\cos^2\alpha(\cos^2\beta\sin^2\gamma+\sin^2\beta\cos^2\gamma)+\sin^2\alpha(\sin^2\beta\sin^2\gamma+\cos^2\beta\cos^2\gamma)$$
$$+\tfrac{1}{2}\sin 2\alpha\sin 2\beta\cos 2\gamma\cos(\varphi_{s1}-\varphi_{p1})+2\sin\gamma\cos\gamma[\cos^2\alpha\cos^2\beta+\sin^2\alpha\sin^2\beta$$
$$-\tfrac{1}{2}\sin 2\alpha\sin 2\beta\cos(\varphi_{s1}-\varphi_{p1})]^{\frac{1}{2}}\cdot[\cos^2\alpha\sin^2\beta+\sin^2\alpha\cos^2\beta$$
$$+\tfrac{1}{2}\sin 2\alpha\sin 2\beta\cos(\varphi_{s1}-\varphi_{p1})]^{\frac{1}{2}}\cdot\cos[(R_{s2}-R_{p2})+(\varphi_{s2}-\varphi_{p2})]\}^{\frac{1}{2}}$$
$$\times\sin(\omega t+\varphi_i+\varphi_g+R_{p3}+\varphi_{p3}), \quad (10)$$

where R_{s3} and R_{p3} are given by

$$\tan R_{s3} = \frac{C\sin(R_{s2}+\varphi_{s2})-D\sin(R_{p2}+\varphi_{p2})}{C\cos(R_{s2}+\varphi_{s2})-D\cos(R_{p2}+\varphi_{p2})}, \quad (11)$$

$$\tan R_{p3} = \frac{E\sin(R_{s2}+\varphi_{s2})+F\sin(R_{p2}+\varphi_{p2})}{E\cos(R_{s2}+\varphi_{s2})+F\cos(R_{p2}+\varphi_{p2})}, \quad (12)$$

and C, D, E, and F are given by

$$C=\cos\gamma\{\cos^2\alpha\cos^2\beta+\sin^2\alpha\sin^2\beta-\tfrac{1}{2}\sin 2\alpha\sin 2\beta\cos(\varphi_{s1}-\varphi_{p1})\}^{\frac{1}{2}}, \quad (13)$$

$$D=\sin\gamma\{\cos^2\alpha\sin^2\beta+\sin^2\alpha\cos^2\beta+\tfrac{1}{2}\sin 2\alpha\sin 2\beta\cos(\varphi_{s1}-\varphi_{p1})\}^{\frac{1}{2}}, \quad (14)$$

$$E=\sin\gamma\{\cos^2\alpha\cos^2\beta+\sin^2\alpha\sin^2\beta-\tfrac{1}{2}\sin 2\alpha\sin 2\beta\cos(\varphi_{s1}-\varphi_{p1})\}^{\frac{1}{2}}, \quad (15)$$

$$F=\cos\gamma\{\cos^2\alpha\sin^2\beta+\sin^2\alpha\cos^2\beta+\tfrac{1}{2}\sin 2\alpha\sin 2\beta\cos(\varphi_{s1}-\varphi_{p1})\}^{\frac{1}{2}}. \quad (16)$$

If instead of entering the upper half of the prism aperture the light is permitted to enter the lower and hence to emerge from the upper (see Fig. 2), the procedure for arriving at the final "s" and "p" components emerging from the prism is exactly the same as the previous one. Asssuming for this case that δ, ϵ, and η are the incident azimuth angles corresponding to α, β, and γ at each of the three reflecting surfaces, the resultant "s" and "p" components emerging from the upper half of the prism aperture are then directly[7]

$$\mathfrak{A}_{s3}' = A_0\{\cos^2\delta(\cos^2\epsilon\cos^2\eta+\sin^2\epsilon\sin^2\eta)+\sin^2\delta(\sin^2\epsilon\cos^2\eta+\cos^2\epsilon\sin^2\eta)$$
$$-\tfrac{1}{2}\sin 2\delta\sin 2\epsilon\cos 2\eta\cos(\varphi_{s1}-\varphi_{p1})-2\sin\eta\cos\eta[\cos^2\delta\cos^2\epsilon+\sin^2\delta\sin^2\epsilon$$
$$-\tfrac{1}{2}\sin 2\delta\sin 2\epsilon\cos(\varphi_{s1}-\varphi_{p1})]^{\frac{1}{2}}\cdot[\cos^2\delta\sin^2\epsilon+\sin^2\delta\cos^2\epsilon$$
$$+\tfrac{1}{2}\sin 2\delta\sin 2\epsilon\cos(\varphi_{s1}-\varphi_{p1})]^{\frac{1}{2}}\cdot\cos[(\mathfrak{R}_{s2}-\mathfrak{R}_{p2})+(\varphi_{s2}-\varphi_{p2})]\}^{\frac{1}{2}}$$
$$\times\sin(\omega t+\varphi_i+\varphi_g+\mathfrak{R}_{s3}+\varphi_{s3}), \quad (17)$$

[7] The only assumption involved in writing these equations is that the angles of incidence on each of the successive reflecting surfaces have the same values in sequence when the light travels either of the two suggested paths. This assumption appears in the assumed equality of the various φ's and these as will be seen later depend only upon the angles of incidence and the refractive index.

$$\mathfrak{A}_{p3}' = A_0\{\cos^2\delta(\cos^2\epsilon\sin^2\eta+\sin^2\epsilon\cos^2\eta)+\sin^2\delta(\sin^2\epsilon\sin^2\eta+\cos^2\epsilon\cos^2\eta)$$
$$+\tfrac{1}{2}\sin 2\delta\sin 2\epsilon\cos 2\eta\cos(\varphi_{s1}-\varphi_{p1})+2\sin\eta\cos\eta[\cos^2\delta\cos^2\epsilon+\sin^2\delta\sin^2\epsilon$$
$$-\tfrac{1}{2}\sin 2\delta\sin 2\epsilon\cos(\varphi_{s1}-\varphi_{p1})]^{\frac{1}{2}}\cdot[\cos^2\delta\sin^2\epsilon+\sin^2\delta\cos^2\epsilon$$
$$+\tfrac{1}{2}\sin 2\delta\sin 2\epsilon\cos(\varphi_{s1}-\varphi_{p1})]^{\frac{1}{2}}\cdot\cos[(\mathfrak{R}_{s2}-\mathfrak{R}_{p2})+(\varphi_{s2}-\varphi_{p2})]\}^{\frac{1}{2}}$$
$$\times\sin(\omega t+\varphi_i+\varphi_g+\mathfrak{R}_{p3}+\varphi_{p3}), \quad (18)$$

where $\mathfrak{R}_{s2}$, $\mathfrak{R}_{p2}$, $\mathfrak{R}_{s3}$, and $\mathfrak{R}_{p3}$ are given by

$$\tan\mathfrak{R}_{s2}=\frac{\cos\delta\cos\epsilon\sin\varphi_{s1}-\sin\delta\sin\epsilon\sin\varphi_{p1}}{\cos\delta\cos\epsilon\cos\varphi_{s1}-\sin\delta\sin\epsilon\cos\varphi_{p1}}, \quad (19)$$

$$\tan\mathfrak{R}_{p2}=\frac{\cos\delta\sin\epsilon\sin\varphi_{s1}+\sin\delta\cos\epsilon\sin\varphi_{p1}}{\cos\delta\sin\epsilon\cos\varphi_{s1}+\sin\delta\cos\epsilon\cos\varphi_{p1}}, \quad (20)$$

$$\tan\mathfrak{R}_{s3}=\frac{\mathfrak{C}\sin(\mathfrak{R}_{s2}+\varphi_{s2})-\mathfrak{D}\sin(\mathfrak{R}_{p2}+\varphi_{p2})}{\mathfrak{C}\cos(\mathfrak{R}_{s2}+\varphi_{s2})-\mathfrak{D}\cos(\mathfrak{R}_{p2}+\varphi_{p2})}, \quad (21)$$

$$\tan\mathfrak{R}_{p3}=\frac{\mathcal{E}\sin(\mathfrak{R}_{s2}+\varphi_{s2})+\mathfrak{F}\sin(\mathfrak{R}_{p2}+\varphi_{p2})}{\mathcal{E}\cos(\mathfrak{R}_{s2}+\varphi_{s2})+\mathfrak{F}\cos(\mathfrak{R}_{p2}+\varphi_{p2})}; \quad (22)$$

and the values of $\mathfrak{C}$, $\mathfrak{D}$, $\mathcal{E}$, and $\mathfrak{F}$ are given by

$$\mathfrak{C}=\cos\eta\{\cos^2\delta\cos^2\epsilon+\sin^2\delta\sin^2\epsilon-\tfrac{1}{2}\sin 2\delta\sin 2\epsilon\cos(\varphi_{s1}-\varphi_{p1})\}^{\frac{1}{2}}, \quad (23)$$

$$\mathfrak{D}=\sin\eta\{\cos^2\delta\sin^2\epsilon+\sin^2\delta\cos^2\epsilon+\tfrac{1}{2}\sin 2\delta\sin 2\epsilon\cos(\varphi_{s1}-\varphi_{p1})\}^{\frac{1}{2}}, \quad (24)$$

$$\mathcal{E}=\sin\eta\{\cos^2\delta\cos^2\epsilon+\sin^2\delta\sin^2\epsilon-\tfrac{1}{2}\sin 2\delta\sin 2\epsilon\cos(\varphi_{s1}-\varphi_{p1})\}^{\frac{1}{2}}, \quad (25)$$

$$\mathfrak{F}=\cos\eta\{\cos^2\delta\sin^2\epsilon+\sin^2\delta\cos^2\epsilon+\tfrac{1}{2}\sin 2\delta\sin 2\epsilon\cos(\varphi_{s1}-\varphi_{p1})\}^{\frac{1}{2}}. \quad (26)$$

If now one views the emergent aperture of the prism in a direction opposite to the oncoming light, it can be represented as shown in Fig. 5. As can be seen, the upper half of the aperture contains two superimposed plane waves (see Eqs. (17) and (18)) vibrating at right angles to each other and having different amplitudes and phases. Similarly the lower half also contains two superimposed plane waves (see Eqs. (9) and (10)) vibrating at right angles and having different amplitudes and phases. It is also of importance to note that each of the four waves has an amplitude and phase different from the others. To determine the ellipticity of the light in either half of the aperture, it is necessary to combine two vibrations at right angles to each other having different amplitudes and phases. The procedure for doing this is well known.[8] The orientation of the major axis of the resultant elliptical motion in either half of the aperture will be found to depend only upon the ratio of the amplitudes of the waves described by Eqs. (9) and (10) (or (17) and (18)) and their difference in phase. From these equations it can be said therefore that the ellipticity of the light in the two halves can be expected to be different.

Under experimental conditions, incoherent light rather than the single wave here pictured will be used for illumination purposes. This will not in any way change the form of the solution for as stated before, the resultant ellipticity for each initial wave is in each case determined by the ratios of the amplitudes and the differences in phase between the final emerging "s" and "p" vibrations. The resultant motion will then be the superposition of a large number of elliptical vibrations of arbitrary phase whose directions of major axes are all superimposed and whose ratio

[8] M. Born, *Optik* (Verlagsbuchhandlung, Julius Springer, Berlin, 1933), p. 21–23.

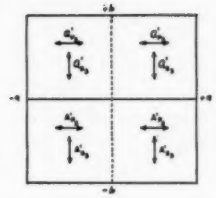

FIG. 5.

of major to minor axis in all cases are identical (see Eqs. (9) and (10)). Such an addition[9] will again show a resultant elliptical motion whose major axis is parallel to the major axes of the component vibrations and whose ratio of major to minor axis is also identical with the component elliptical vibrations. If therefore the ellipticity of the emergent light is determined for a plane polarized wave of the form of Eq. 1, the ellipticity of a plane polarized wave of incoherent light will simultaneously be known.

2. FOCAL PLANE PROPERTIES

The detailed evaluations of the ellipticities of the emergent light for given values of the initial azimuth angle α were not of so much interest as was the use of these polarization properties in explaining the anomalous behavior of the prism when used in conjunction with a telescope. To understand this behavior, it is necessary to combine in the focal plane of the telescope the four plane waves emerging from the prism (see Fig. 5). This addition must consist first of the combining of A_{s3}' and $\mathfrak{A}_{s3}'$, then A_{p3}' and $\mathfrak{A}_{p3}'$ and finally the adding together of these two resultant motions. The determination of the form of the image observed in the focal plane of the telescope is clearly an application of the type of diffraction designated as Fraunhofer Diffraction and the methods used in finding these diffraction patterns are available in many physical optics books.

For purposes of integration, it is now possible to express Eqs. (9), (10), (17), and (18) in a much more simplified form. Designating the amplitude of each by a single term and grouping all the phase factors, these equations can be written

$$\begin{aligned} A_{s3}' &= \bar{A}_{s3} \sin 2\pi(\nu t + N_{s3}), \\ A_{p3}' &= \bar{A}_{p3} \sin 2\pi(\nu t + N_{p3}), \\ \mathfrak{A}_{s3}' &= \bar{\mathfrak{A}}_{s3} \sin 2\pi(\nu t + \mathfrak{N}_{s3}), \\ \mathfrak{A}_{p3}' &= \bar{\mathfrak{A}}_{p3} \sin 2\pi(\nu t + \mathfrak{N}_{p3}). \end{aligned} \tag{27}$$

Following Professor Wood's treatment[10] on the usual rectangular diffracting aperture, the vibration in the focal plane of the telescope at a point (ξ, μ) off the optic axis due to the A_{s3}' and $\mathfrak{A}_{s3}'$ waves will be given by (see Fig. 5)[11]

$$V_{s3} = \bar{A}_{s3} \int_{-b}^{0} \int_{-a}^{+a} \sin 2\pi\left(\nu t + N_{s3} - \frac{F}{\lambda} + \frac{x\xi + y\mu}{\lambda F}\right) dx dy + \bar{\mathfrak{A}}_{s3} \int_{0}^{b} \int_{-a}^{+a} \sin 2\pi\left(\nu t + \mathfrak{N}_{s3} - \frac{F}{\lambda} + \frac{x\xi + y\mu}{\lambda F}\right) dx dy, \tag{28}$$

F being the effective focal length of the telescopic objective and λ the wave-length of the incident plane polarized light. If each of the integrands is expanded (grouping all terms not containing x and y into one term) the resulting expression will be found readily integrable. The integrals to be evaluated contain only sine and cosine terms and if these are evaluated for the limits of the aperture suggested by Fig. 5, the result will be found to be

$$V_{s3} = \frac{\lambda^2 F^2}{2\pi^2 \xi\mu} \sin U\{\bar{A}_{s3}[\sin V \sin 2\pi(\nu t - F/\lambda + N_{s3}) - (1 - \cos V) \cos 2\pi(\nu t - F/\lambda + N_{s3})] + \bar{\mathfrak{A}}_{s3}[\sin V \sin 2\pi(\nu t - F/\lambda + \mathfrak{N}_{s3}) + (1 - \cos V) \cos 2\pi(\nu t - F/\lambda + \mathfrak{N}_{s3})]\},$$

[9] This can be demonstrated by the addition of two sets of equations of the form of Eqs. (9) and (10) having different A_0's and φ_i's. In the proof it is necessary to designate one amplitude as A_0 and the other as cA_0, c being a constant.

[10] R. W. Wood, *Physical Optics* (The Macmillan Company, New York, 1914), p. 195.

[11] The problem of evaluating these integrals is not new for it was first done for the more simplified case of identical amplitudes by G. B. Airy, Phil. Trans. Roy. Soc. London **130**, part 2, 225 (1840); **131**, part 1, 1 (1841), in his much celebrated explanation of Talbot's bands.

where

$$U=\frac{2\pi a\xi}{\lambda F}, \quad V=\frac{2\pi b\mu}{\lambda F}. \tag{29}$$

If one multiplies and divides by the square root of the sum of the squares of the coefficients of the sine and cosine time dependent terms, this can be written in the form

$$V_{s3}=\frac{\lambda^2F^2}{2\pi^2\xi\mu}\sin U(2-2\cos V)^{\frac{1}{2}}\{\bar{A}_{s3}\sin[2\pi(\nu t-F/\lambda+N_{s3})-\Delta]+\bar{\alpha}_{s3}\sin[2\pi(\nu t-F/\lambda+\Re_{s3})+\Delta]\},$$

Δ having the value

$$\tan\Delta=(1-\cos V)/\sin V. \tag{30}$$

To reduce this equation to a more usable form, an expansion of the sine terms retaining $2\pi(\nu t-F/\lambda)$ as a constant factor is necessary. If in addition a substitution in terms of half angles is made for the radical and Eqs. (29) are used, the resulting equation will be

$$\begin{aligned}V_{s3}=2ab\cdot\frac{\sin U}{U}\cdot\frac{\sin V/2}{V/2}\{&\sin 2\pi(\nu t-F/\lambda)[\bar{A}_{s3}\cos 2\pi N_{s3}\cos\Delta+\bar{A}_{s3}\sin 2\pi N_{s3}\sin\Delta\\&+\bar{\alpha}_{s3}\cos 2\pi\Re_{s3}\cos\Delta-\bar{\alpha}_{s3}\sin 2\pi\Re_{s3}\sin\Delta]+\cos 2\pi(\nu t-F/\lambda)[\bar{A}_{s3}\sin 2\pi N_{s3}\cos\Delta\\&-\bar{A}_{s3}\cos 2\pi N_{s3}\sin\Delta+\bar{\alpha}_{s3}\sin 2\pi\Re_{s3}\cos\Delta+\bar{\alpha}_{s3}\cos 2\pi\Re_{s3}\sin\Delta]\}.\end{aligned}$$

Again multiplying and dividing by the square root of the sum of the squares of the sine and cosine time dependent terms, this can be expressed in the form of a single wave having an amplitude and phase. Thus,

$$\begin{aligned}V_{s3}=2ab\cdot\frac{\sin U}{U}\cdot\frac{\sin V/2}{V/2}\{&\bar{A}_{s3}^2+\bar{\alpha}_{s3}^2+2\bar{A}_{s3}\bar{\alpha}_{s3}\cos^2\Delta\cos 2\pi(N_{s3}-\Re_{s3})\\&+4\bar{A}_{s3}\bar{\alpha}_{s3}\sin\Delta\cos\Delta\sin 2\pi(N_{s3}-\Re_{s3})\\&-2\bar{A}_{s3}\bar{\alpha}_{s3}\sin^2\Delta\cos 2\pi(N_{s3}-\Re_{s3})\}^{\frac{1}{2}}\sin[2\pi(\nu t-F/\lambda)+\Phi_S].\end{aligned}$$

If we set $\theta_s=2\pi(N_{s3}-\Re_{s3})$ and substitute for Δ from Eq. 30, the equation in its simplest form is

$$V_{s3}=2ab\cdot\frac{\sin U}{U}\cdot\frac{\sin V/2}{V/2}\{\bar{A}_{s3}^2+\bar{\alpha}_{s3}^2+2\bar{A}_{s3}\bar{\alpha}_{s3}\cos(V-\theta_s)\}^{\frac{1}{2}}\sin[2\pi(\nu t-F/\lambda)+\Phi_s]. \tag{31}$$

A similar addition of the two "p" vibrations in the focal plane of the telescope will give an equation of exactly the same form. The resultant "p" vibration can then be written down immediately in the form

$$V_{p3}=2ab\cdot\frac{\sin U}{U}\cdot\frac{\sin V/2}{V/2}\{\bar{A}_{p3}^2+\bar{\alpha}_{p3}^2+2\bar{A}_{p3}\bar{\alpha}_{p3}\cos(V-\theta_p)\}^{\frac{1}{2}}\sin[2\pi(\nu t-F/\lambda)+\Phi_p], \tag{32}$$

θ_p here has a similar form as in the above equation with the value $2\pi(N_{p3}-\Re_{p3})$.

The resultant motion in the focal plane of the telescope can now be determined by combining these last two equations. If this is done, it will be seen[8] that for a given initial azimuth angle, the resultant motion will in general be an elliptical one whose ellipticity is constant in the direction of ξ but changes in the direction of μ.

The intensity distribution in the diffraction pattern observed in the focal plane of the telescope will, since these two vibrations are perpendicular to each other, be proportional to the sum of the squares of the amplitudes of each of the last two expressions. If the intensity is designated by J,

it will be proportional to

$$J=(2ab)^2\cdot\frac{\sin^2 U}{U^2}\cdot\frac{\sin^2 V/2}{(V/2)^2}\{\bar{A}_{s_2}^2+\bar{A}_{p_3}^2+\bar{\alpha}_{s_3}^2+\bar{\alpha}_{p_3}^2+2\bar{A}_{s_3}\bar{\alpha}_{s_3}\cos(V-\theta_S)+2\bar{A}_{p_3}\bar{\alpha}_{p_3}\cos(V-\theta_p)\}. \tag{33}$$

When the forms of Eqs. (9), (10), (17), and (18) are considered, this equation can be reduced to the final form used in calculating the diffraction patterns. Thus

$$J=2(2ab)^2\cdot\frac{\sin^2 U}{U^2}\cdot\frac{\sin^2 V/2}{(V/2)^2}\{A_0^2+\bar{A}_{s_3}\bar{\alpha}_{s_3}\cos[V-(\Re_{s_3}-R_{s_3})]+\bar{A}_{p_3}\bar{\alpha}_{p_3}\cos[V-(\Re_{p_3}-R_{p_3})]\}. \tag{34}$$

In the direction parallel to the roof edge (direction of ξ coordinate), the resulting diffraction pattern will according to this equation be of the usual symmetric form.[10] The intensity becomes zero for values of ξ given by

$$\xi=\frac{\lambda F}{2a}m \quad (m=1, 2, 3, 4\cdots). \tag{35}$$

If Eq. (34) is differentiated to obtain the zero positions in the μ direction, the intensity will be found to be zero for values of μ given by

$$\mu=\frac{\lambda F}{b}n \quad (n=1, 2, 3, 4, \cdots). \tag{36}$$

In the direction of the μ coordinate therefore, the spacing between the adjacent minima should be twice that in the ξ direction if a and b are set equal to each other. This is exactly what was observed in Fig. 4. From Eq. (34), however, it will be noticed that the form of the diffraction pattern in the μ direction is influenced by other factors such as the geometry of the prism and the incident azimuth angle of the entering plane polarized light.

3. FORM OF DIFFRACTION PATTERN IN POLARIZED LIGHT

Before the form of the diffraction pattern in the μ direction can be determined from Eq. (34), the amplitudes and the differences in phase between the corresponding vibrations in the upper and lower halves of the aperture (see Fig. 5) must be determined. In evaluating each of these, it will be found necessary (see Eqs. (9)–(26)) to know the incident azimuth of the plane polarized light, the angles between the positive directions of the "s" vibrations at each of the surfaces, the phase changes upon reflection, and the geometry of the rays throughout the prism. It is with the evaluation of these various factors and their final substitution in Eq. (34) that this part of the paper will concern itself.

Inside the prism, the light in going along either of the two paths previously described undergoes three internal reflections. The evaluation therefore of the various angles between the positive directions of the "s" vibrations and the angles of incidence at each surface consists of a sixfold repetition of the methods of solid geometry to determine the direction cosines of the incident ray, reflected ray, surface normal, and the positive directions of the "s" and "p" vibrations at each of the internal reflecting surfaces. For the sake of brevity therefore, the methods used will be shown in detail at one reflecting surface only and the values for the other surfaces simply written down directly in table form.

Before the direction cosines of any of the previously mentioned vibrations or rays can be determined, it is necessary to choose fixed directions for the axes of reference from which the direction cosines are to be measured. For convenience then at each point of incidence of a ray on a prism reflecting surface, there will be considered to be present a set of Cartesian axes whose origin coincides with the point of incidence of the ray on the surface. The positive direction of the "z" axis will be assumed to be parallel to the roof edge and directed toward the emerging

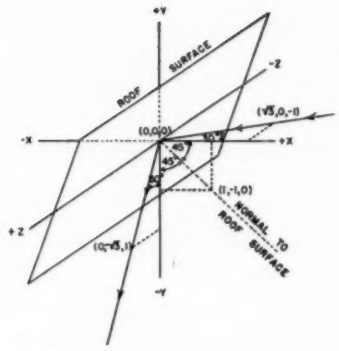

FIG. 6.

surface of the prism (see Fig. 2). The positive direction of the "y" axis will be always chosen perpendicular to the view of Fig. 2 and in an upward direction from the point of incidence. The positive direction of "x" must then be perpendicular to the plane of these two directions and in the general direction of the entering surface.

The sample reflection to be considered will be that for which the light enters the upper half of the prism aperture (see Fig. 2) and is incident upon the first roof surface. If the geometry of the prism is as assumed in Fig. 2 and the roof angle is an exact 90°, the geometry of the rays at this roof surface will be as shown in Fig. 6. It will be evident from Fig. 2 that the incident ray lies in the "$x-z$" plane and makes an angle of 30° with the positive "x" direction. Its direction cosines are then $+\sqrt{3}/2,\ 0,\ -\frac{1}{2}$. Reflection at the first roof surface changes the path of the ray to the "$y-z$" plane so that now it makes an angle of 30° with the minus "y" axis. After reflection therefore the direction cosines of the ray become $0,\ -\sqrt{3}/2,\ +\frac{1}{2}$. Also the normal to the roof surface as indicated lies in the "$x-y$" plane and makes a 45° angle with the positive "x" direction. Its direction cosines are then $+1/\sqrt{2},\ -1/\sqrt{2},\ 0$.

The direction cosines of the "s" vibration are found most directly by determining first the equation of the plane of incidence as defined by the incident ray and surface normal and then expressing this equation in the normal form.[12]

[12] C. E. Love, *Analytic Geometry* (The Macmillan Company, New York, 1927), p. 201.

The direction of the normal to the plane of incidence is by definition[2] also the direction of the "s" vibration. To determine the equation of the plane of incidence, it is necessary to write the equation of the plane through the points $(\sqrt{3},\ 0,\ -1)$, $(0,\ 0,\ 0)$, and $(1,\ -1,\ 0)$ shown in Fig. 6. There are different ways[13] of proceeding in the matter, but the simplest manner of designating the equation is to use the determinant form. The equation of the plane therefore passing through the three previously mentioned points will be

$$\begin{vmatrix} 1 & x & y & z \\ 1 & \sqrt{3} & 0 & -1 \\ 1 & 0 & 0 & 0 \\ 1 & 1 & -1 & 0 \end{vmatrix} = 0, \tag{37}$$

which after expansion becomes

$$x+y+\sqrt{3}z=0. \tag{38}$$

After reduction of this equation to the normal form, the direction cosines of the "s" vibration become $\pm 1/(5)^{\frac{1}{2}},\ \pm 1/(5)^{\frac{1}{2}},\ \pm(\frac{3}{5})^{\frac{1}{2}}$.

To determine the direction cosines of the "p" vibration, it is necessary again to resort to some well-known equations[14] from space geometry. It can be shown that if for each plane of incidence the "s" vibration has the direction cosines $l_1,\ m_1,\ n_1$ the desired ray the direction cosines $l_2,\ m_2,\ n_2$, the direction cosines of the "p" vibration (perpendicular to the other two) will be given by

$$\begin{aligned} l_3 &= m_2n_1-m_1n_2, \\ m_3 &= l_1n_2-l_2n_1, \\ n_3 &= l_2m_1-l_1m_2. \end{aligned} \tag{39}$$

Making numerical substitutions in these equations both before and after reflection at the roof surface indicated in Fig. 6, the direction cosines of the "p" vibrations are $\pm 1/2(5)^{\frac{1}{2}},\ \mp 2/(5)^{\frac{1}{2}},\ \pm\frac{1}{2}(\frac{3}{5})^{\frac{1}{2}}$ and $\pm 2/(5)^{\frac{1}{2}},\ \mp 1/2(5)^{\frac{1}{2}},\ \mp\frac{1}{2}(\frac{3}{5})^{\frac{1}{2}}$.

Knowing the direction cosines of all the rays and "s" and "p" vibrations at the roof surface indicated in Fig. 6, it is possible to find the angle between any two of them (designated by ρ) by using a further well-known equation of the

[13] C. E. Love, *Analytic Geometry* (The Macmillan Company, New York, 1927), p. 206.

[14] F. S. Woods, *Advanced Calculus* (Ginn & Company, New York, 1934), p. 123.

form[15]

$$\cos \rho = l_1 l_2 + m_1 m_2 + n_1 n_2, \qquad (40)$$

$l_1 m_1 n_1$ and $l_2 m_2 n_2$ being the direction cosines of the two rays or vibrations in question.

The only remaining difficulty at the first roof surface reflection is that of choosing the correct signs to correspond with the earlier adopted sign convention (see part 1) for the positive directions of the "s" and "p" vibrations. To aid in this matter and also to check the magnitudes and signs of the angles obtained by substituting values in Eq. (40), a model of the prism showing the various rays and "s" and "p" vibrations reflected at each surface of the prism was constructed from a series of strings and matches and mounted on the wooden base shown in Fig. 7. At each surface the unlighted part of the match was for both the "s" and "p" vibrations directed in the positive direction. At the first reflection on the lower roof surface, the unlighted part of the match corresponding to the positive direction of the "p" vibration was therefore directed toward the inward surface normal and the unlighted part of the match corresponding to the positive direction of the "s" vibration was located 90° clockwise from this when looking along the path of travel of the light. This same convention was followed at each of the surface reflections within the prism by a corresponding arrangement of the matches. The incident plane

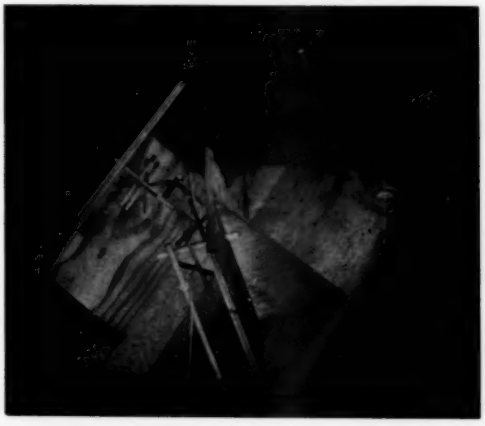

FIG. 7.

[15] C. E. Love, *Analytic Geometry* (The Macmillan Company, New York, 1927), p. 220.

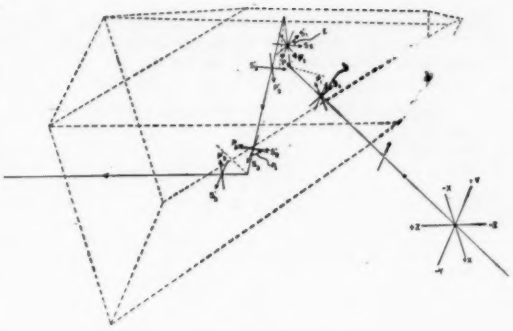

FIG. 7A.

of polarization of the initially polarized beam entering the prism is represented by a single match which is mounted first on the string. In the picture of the model shown, the light is incident in the lower half of the aperture and emerges from the upper. By removing the pegs corresponding to the surface normals and placing them in different holes, the opposite case in which the light enters the upper half of the aperture and emerges from the lower can also be represented.

In Fig. 7A an attempt has been made to show a perspective drawing for the case set up in the model picture. Here the coordinate directions and the angles δ, ϵ, and η are indicated. All the "s" and "p" vibrations both before and after reflection at each of the internally reflecting surfaces are also marked. At each surface, the arrow point is directed in the positive direction.

If the direction cosines of the various rays and "s" and "p" vibrations at each of the reflecting surfaces are determined in the same manner as shown in Fig. 6 and their magnitudes and signs in each case checked from the prism model shown in Fig. 7, direction cosine tables like Tables I and II can be constructed from which all the geometrical properties of the various rays and "s" and "p" vibrations can be determined. In each case in these tables, the signs corresponding to the various "s" and "p" vibrations are those for the positive directions.

Some of the immediate consequences of having Tables I and II available are that β, γ, δ, ϵ, and η can now be evaluated if Eq. (40) is utilized. In each case the signs and magnitudes of the angles have to be checked from the model keeping in

TABLE I. Direction cosines of incident and reflected rays and "s" and "p" vibrations when light enters upper half of prism aperture and emerges from lower.

Equation of first plane of incidence $x+y+(3)^{\frac{1}{2}}z=0$			
Incident ray	$+(3)^{\frac{1}{2}}/2$	0	$-1/2$
Surface normal	$+1/\sqrt{2}$	$-1/\sqrt{2}$	0
Reflected ray	0	$-(3)^{\frac{1}{2}}/2$	$+1/2$
S_1	$+1/(5)^{\frac{1}{2}}$	$+1/(5)^{\frac{1}{2}}$	$+(3)^{\frac{1}{2}}/(5)^{\frac{1}{2}}$
P_1 before reflection	$+1/2(5)^{\frac{1}{2}}$	$-2/(5)^{\frac{1}{2}}$	$+(3)^{\frac{1}{2}}/2(5)^{\frac{1}{2}}$
P_1 after reflection	$+2/(5)^{\frac{1}{2}}$	$-1/2(5)^{\frac{1}{2}}$	$-(3)^{\frac{1}{2}}/2(5)^{\frac{1}{2}}$
Equation of second plane of incidence $x-y-(3)^{\frac{1}{2}}z=0$			
Incident ray	0	$+(3)^{\frac{1}{2}}/2$	$-1/2$
Surface normal	$+1/\sqrt{2}$	$+1/\sqrt{2}$	0
Reflected ray	$+(3)^{\frac{1}{2}}/2$	0	$+1/2$
S_2	$-1/(5)^{\frac{1}{2}}$	$+1/(5)^{\frac{1}{2}}$	$+(3)^{\frac{1}{2}}/(5)^{\frac{1}{2}}$
P_2 before reflection	$+2/(5)^{\frac{1}{2}}$	$+1/2(5)^{\frac{1}{2}}$	$+(3)^{\frac{1}{2}}/2(5)^{\frac{1}{2}}$
P_2 after reflection	$+1/2(5)^{\frac{1}{2}}$	$+2/(5)^{\frac{1}{2}}$	$-(3)^{\frac{1}{2}}/2(5)^{\frac{1}{2}}$
Equation of third plane of incidence $y=0$			
Incident ray	$-(3)^{\frac{1}{2}}/2$	0	$-1/2$
Surface normal	$-(3)^{\frac{1}{2}}/2$	0	$+1/2$
Reflected ray	0	0	$+1$
S_3	0	-1	0
P_3 before reflection	$-1/2$	0	$+(3)^{\frac{1}{2}}/2$
P_3 after reflection	-1	0	0

mind the earlier adopted sign conventions. β for instance was defined as the angle between A_{s_2} and A_{s_1}' and was positive when measured in a counterclockwise direction from the positive direction of A_{s_2} when looking along the path of light. Consulting Table I,

$$\cos\beta=-\tfrac{1}{5}+\tfrac{1}{5}+\tfrac{3}{5}=\tfrac{3}{5},$$
$$\beta=53°7'42''.$$

The equation although giving the magnitude of β does not determine its sign and this will be found quite important upon substituting in Eqs. (9) and (10). For the determination of the sign, the model must again be consulted and when this is done, it will be seen that the positive direction of S_1 lies counterclockwise from the positive direction of S_2 when looking along the path of the light. By convention then β itself must be positive. Similar evaluations from Tables I and II show that the remainder of the above angles have the following values

$$\beta=+53°7'42'', \qquad \delta=\alpha+126°52'18'',$$
$$\gamma=+116°33'54'', \qquad \epsilon=-53°7'42'',$$
$$\eta=-116°33'54''.$$

The phase changes upon reflection at each of the prism surfaces must also be evaluated. These are determined from Fresnel's equations which for the case of incidence beyond the critical angle become complex. This complex form can be shown to be equivalent to a change in phase which when evaluated for each of the "s" and "p" components can be expressed in the forms[16]

$$\tan\frac{\varphi_s}{2}=\frac{(n^2\sin^2 i-1)^{\frac{1}{2}}}{n\cos i},$$
$$\tan\frac{\varphi_p}{2}=\frac{n(n^2\sin^2 i-1)^{\frac{1}{2}}}{\cos i}, \qquad (41)$$

n being the refractive index of the medium and "i" the angle of incidence for the surface in question. Again if the direction cosines of the incident ray and surface normal for each reflection are obtained from the tables and substituted in Eq. (40), all these angles of incidence at each surface may be found. As might be expected from the geometry of the prism, evaluations of these angles show that the angle of incidence on each roof surface is 52°14'20" and that on the last reflecting surface before emergence 60° (see Fig. 2). If these values of i are substituted in Eqs. (41) for a prism having a refractive index 1.517, the phase changes upon reflection will be found to be[7]

$$\varphi_{s_1}=\varphi_{s_2}=70°57'10'', \quad \varphi_{p_1}=\varphi_{p_2}=117°15'22'',$$
$$\varphi_{s_3}=96°38'32'', \quad \varphi_{p_3}=137°42'12''.$$

TABLE II. Direction cosines of incident and reflected rays and "s" and "p" vibrations when light enters lower half of prism aperture and emerges from upper.

Equation of first plane of incidence $x-y+(3)^{\frac{1}{2}}z=0$			
Incident ray	$+(3)^{\frac{1}{2}}/2$	0	$-1/2$
Surface normal	$+1/\sqrt{2}$	$+1/\sqrt{2}$	0
Reflected ray	0	$+(3)^{\frac{1}{2}}/2$	$+1/2$
S_1'	$-1/(5)^{\frac{1}{2}}$	$+1/(5)^{\frac{1}{2}}$	$-(3)^{\frac{1}{2}}/(5)^{\frac{1}{2}}$
P_1' before reflection	$+1/2(5)^{\frac{1}{2}}$	$+2/(5)^{\frac{1}{2}}$	$+(3)^{\frac{1}{2}}/2(5)^{\frac{1}{2}}$
P_1' after reflection	$+2/(5)^{\frac{1}{2}}$	$+1/2(5)^{\frac{1}{2}}$	$-(3)^{\frac{1}{2}}/2(5)^{\frac{1}{2}}$
Equation of second plane of incidence $x+y-(3)^{\frac{1}{2}}z=0$			
Incident ray	0	$-(3)^{\frac{1}{2}}/2$	$-1/2$
Surface normal	$+1/\sqrt{2}$	$-1/\sqrt{2}$	0
Reflected ray	$+(3)^{\frac{1}{2}}/2$	0	$+1/2$
S_2'	$+1/(5)^{\frac{1}{2}}$	$+1/(5)^{\frac{1}{2}}$	$-(3)^{\frac{1}{2}}/(5)^{\frac{1}{2}}$
P_2' before reflection	$+2/(5)^{\frac{1}{2}}$	$-1/2(5)^{\frac{1}{2}}$	$+(3)^{\frac{1}{2}}/2(5)^{\frac{1}{2}}$
P_2' after reflection	$+1/2(5)^{\frac{1}{2}}$	$-2/(5)^{\frac{1}{2}}$	$-(3)^{\frac{1}{2}}/2(5)^{\frac{1}{2}}$
Equation of third plane of incidence $y=0$			
Incident ray	$-(3)^{\frac{1}{2}}/2$	0	$-1/2$
Surface normal	$-(3)^{\frac{1}{2}}/2$	0	$+1/2$
Reflected ray	0	0	$+1$
S_3'	0	-1	0
P_3' before reflection	$-1/2$	0	$+(3)^{\frac{1}{2}}/2$
P_3' after reflection	-1	0	0

[16] M. Born, *Optik* (Verlagsbuchhandlung, Julius Springer, Berlin, 1933), p. 43.

It is now possible to simplify considerably the form of Eqs. (9)–(26) by substitution of the various azimuth and phase angles which have just been determined. The substitutions are simple numerical ones so only the results obtained will be given.[17]

$$A_{s3}' = A_0\{.584000\cos^2\alpha + .416000\sin^2\alpha + .198964\sin 2\alpha + .8[.360000\cos^2\alpha + .640000\sin^2\alpha - .331607\sin 2\alpha]^{\frac{1}{2}}\cdot[.640000\cos^2\alpha + .360000\sin^2\alpha + .331607\sin 2\alpha]^{\frac{1}{2}} \times\cos[(R_{s2}-R_{p2}) - 46°18'12'']\}^{\frac{1}{2}}\sin(\omega t+\varphi_i+\varphi_g+R_{s3}+96°38'32''), \quad (42)$$

$$A_{p3}' = A_0\{.416000\cos^2\alpha + .584000\sin^2\alpha - .198964\sin 2\alpha - .8[.360000\cos^2\alpha + .640000\sin^2\alpha - .331607\sin 2\alpha]^{\frac{1}{2}}\cdot[.640000\cos^2\alpha + .360000\sin^2\alpha + .331607\sin 2\alpha]^{\frac{1}{2}} \times\cos[(R_{s2}-R_{p2}) - 46°18'12'']\}^{\frac{1}{2}}\sin(\omega t+\varphi_i+\varphi_g+R_{p3}+137°42'12''), \quad (43)$$

$$\mathfrak{A}_{s3}' = A_0\{.332515\sin^2\alpha + .667485\cos^2\alpha + .136350\sin 2\alpha - .8[.779143\sin^2\alpha + .220857\cos^2\alpha - .227250\sin 2\alpha]^{\frac{1}{2}}\cdot[.220857\sin^2\alpha + .779143\cos^2\alpha + .227250\sin 2\alpha]^{\frac{1}{2}} \times\cos[(\mathfrak{R}_{s2}-\mathfrak{R}_{p2}) - 46°18'12'']\}^{\frac{1}{2}}\sin(\omega t+\varphi_i+\varphi_g+\mathfrak{R}_{s3}+96°38'32''), \quad (44)$$

$$\mathfrak{A}_{p3}' = A_0\{.667485\sin^2\alpha + .332515\cos^2\alpha - .136350\sin 2\alpha + .8[.779143\sin^2\alpha + .220857\cos^2\alpha - .227250\sin 2\alpha]^{\frac{1}{2}}\cdot[.220857\sin^2\alpha + .779143\cos^2\alpha + .227250\sin 2\alpha]^{\frac{1}{2}} \times\cos[(\mathfrak{R}_{s2}-\mathfrak{R}_{p2}) - 46°18'12'']\}^{\frac{1}{2}}\sin(\omega t+\varphi_i+\varphi_g+\mathfrak{R}_{p3}+137°42'12''); \quad (45)$$

$$\tan R_{s2} = \frac{.567150\cos\alpha - .711175\sin\alpha}{.195808\cos\alpha + .366375\sin\alpha}, \quad (46)$$

$$\tan R_{p2} = \frac{.756200\cos\alpha + .533381\sin\alpha}{.261078\cos\alpha - .274781\sin\alpha}, \quad (47)$$

$$\tan R_{s3} = \frac{C\sin(R_{s2}+70°57'10'') - D\sin(R_{p2}+117°15'22'')}{C\cos(R_{s2}+70°57'10'') - D\cos(R_{p2}+117°15'22'')}, \quad (48)$$

$$\tan R_{p3} = \frac{E\sin(R_{s2}+70°57'10'') + F\sin(R_{p2}+117°15'22'')}{E\cos(R_{s2}+70°57'10'') + F\cos(R_{p2}+117°15'22'')}; \quad (49)$$

$$C = -\{.072000\cos^2\alpha + .128000\sin^2\alpha - .066321\sin 2\alpha\}^{\frac{1}{2}}, \quad (50)$$

$$D = \{.512000\cos^2\alpha + .288000\sin^2\alpha + .265285\sin 2\alpha\}^{\frac{1}{2}}, \quad (51)$$

$$E = \{.288000\cos^2\alpha + .512000\sin^2\alpha - .265285\sin 2\alpha\}^{\frac{1}{2}}, \quad (52)$$

$$F = -\{.128000\cos^2\alpha + .072000\sin^2\alpha + .066321\sin 2\alpha\}^{\frac{1}{2}}; \quad (53)$$

$$\tan \mathfrak{R}_{s2} = \frac{.228650\cos\alpha - .880425\sin\alpha}{-.410585\cos\alpha + .063179\sin\alpha}, \quad (54)$$

$$\tan \mathfrak{R}_{p2} = \frac{.880425\cos\alpha + .284931\sin\alpha}{-.063179\cos\alpha + .373731\sin\alpha}, \quad (55)$$

$$\tan \mathfrak{R}_{s3} = \frac{\mathfrak{C}\sin(\mathfrak{R}_{s2}+70°57'10'') - \mathfrak{D}\sin(\mathfrak{R}_{p2}+117°15'22'')}{\mathfrak{C}\cos(\mathfrak{R}_{s2}+70°57'10'') - \mathfrak{D}\cos(\mathfrak{R}_{p2}+117°15'22'')}, \quad (56)$$

[17] In making the substitutions, an attempt was made to retain six significant figures. All calculations were made with the aid of a calculating machine.

$$\tan \mathfrak{R}_{p3}=\frac{\mathcal{E}\sin(\mathfrak{R}_{s2}+70°57'10'')+\mathfrak{F}\sin(\mathfrak{R}_{p2}+117°15'22'')}{\mathcal{E}\cos(\mathfrak{R}_{s2}+70°57'10'')+\mathfrak{F}\cos(\mathfrak{R}_{p2}+117°15'22'')}; \tag{57}$$

$$\mathfrak{C}=-\{.155828\sin^2\alpha+.044172\cos^2\alpha-.045450\sin 2\alpha\}^{\frac{1}{2}}, \tag{58}$$

$$\mathfrak{D}=-\{.176686\sin^2\alpha+.623314\cos^2\alpha+.181800\sin 2\alpha\}^{\frac{1}{2}}, \tag{59}$$

$$\mathcal{E}=-\{.623314\sin^2\alpha+.176686\cos^2\alpha-.181800\sin 2\alpha\}^{\frac{1}{2}}, \tag{60}$$

$$\mathfrak{F}=-\{.044172\sin^2\alpha+.155828\cos^2\alpha+.045450\sin 2\alpha\}^{\frac{1}{2}}. \tag{61}$$

The only remaining factor which is left undetermined in the above equations is α, the incident azimuth of the plane polarized light. When this is once chosen, the amplitudes of Eqs. (42)–(45) have fixed numerical values and all the other terms from Eqs. (46)–(61) likewise have fixed numerical values. If the amplitudes of Eqs. (42)–(45) are then substituted in the equation of the diffraction pattern (Eq. (34)), it becomes evident that its form is also fixed when once α is chosen.

The numerical evaluations of the above equations for different initial azimuth angles α are simply detailed arithmetical substitutions. They will be evaluated for a series of angles from 0° to 180° only for it was found that for values beyond 180°, the calculated form of the resulting diffraction pattern repeats itself. In Table III, the calculated values of the R's are given for the values of α indicated. The amplitudes of the Eqs. (42)–(45) for the same values of α are given in Table IV.

If Tables III and IV are used to make the final substitutions in Eq. (34), the equations describing the resultant form of the diffraction pattern for each incident azimuth angle can readily be found. Making the necessary substitutions, the following equations were found. For convenience in writing, the terms which do not depend upon V have been grouped into a constant term K.

$$J_{0°}=K\frac{\sin^2 V/2}{(V/2)^2}\{1+.538277\cos(V+148°26'57'')+.315117\cos(V+63°21'25'')\},$$

$$J_{20°}=K\frac{\sin^2 V/2}{(V/2)^2}\{1+.650566\cos(V-187°3'43'')+.337830\cos(V+13°41'39'')\},$$

$$J_{45°}=K\frac{\sin^2 V/2}{(V/2)^2}\{1+.597306\cos(V-159°17'17'')+.320703\cos(V-41°11'56'')\},$$

$$J_{70°}=K\frac{\sin^2 V/2}{(V/2)^2}\{1+.397726\cos(V-117°52'59'')+.375307\cos(V-110°29'40'')\},$$

$$J_{90°}=K\frac{\sin^2 V/2}{(V/2)^2}\{1+.315116\cos(V-63°21'31'')+.538277\cos(V-148°26'54'')\},$$

$$J_{110°}=K\frac{\sin^2 V/2}{(V/2)^2}\{1+.337830\cos(V-13°41'40'')+.650566\cos(V-172°56'17'')\},$$

$$J_{135°}=K\frac{\sin^2 V/2}{(V/2)^2}\{1+.320701\cos(V+41°12'1'')+.597307\cos(V+159°17'17'')\},$$

$$J_{160°}=K\frac{\sin^2 V/2}{(V/2)^2}\{1+.375308\cos(V+110°29'41'')+.397727\cos(V+117°52'58'')\}.$$

If each of these equations is evaluated (neglecting the constant K) for different values of V, diffrac-

TABLE III.

α	R_{s_2}	R_{p_2}	R_{s_3}	R_{p_3}
0°	70°57′10″	70°57′10″	356° 3′23″	100° 7′26″
20°	43° 7′35″	80°22′51″	4°52′25″	63°43′54″
45°	345°37′50″	90°36′31″	20°11′38″	41°27′ 7″
70°	310°55′37″	102°31′59″	51° 9′56″	28°43′ 3″
90°	297°15′22″	117°15′22″	96°17′38″	20°21′41″
110°	287°49′41″	145° 4′57″	132°41′12″	11°32′39″
135°	277°36′ 0″	202°34′42″	154°57′56″	356°13′25″
160°	265°40′33″	237°16′55″	167°42′ 1″	325°15′ 7″
180°	250°57′10″	250°57′10″	176° 3′23″	280° 7′26″
α	$\Re_{s_2}$	$\Re_{p_2}$	$\Re_{s_3}$	$\Re_{p_3}$
0°	150°53′14″	94° 6′16″	207°36′26″	36°46′ 2″
20°	193°19′29″	85°46′ 0″	191°56′ 8″	50° 2′13″
45°	241°56′30″	75° 4′42″	179°28′55″	82°39′ 3″
70°	263°49′28″	59°54′49″	169° 2′55″	139°12′43″
90°	274° 6′16″	37°19′18″	159°39′ 9″	168°48′35″
110°	282°26′33″	354°53′ 3″	146°22′51″	184°28′57″
135°	293° 7′51″	306°16′ 2″	113°45′55″	196°56′ 8″
160°	308°17′43″	284°23′ 5″	57°12′20″	207°22′ 9″
180°	330°53′14″	274° 6′16″	27°36′26″	216°46′ 1″

TABLE IV.

α	$\bar{A}_{s_2}$	$\bar{A}_{p_2}$	$\bar{\alpha}_{s_3}$	α_{p_3}
0°	.921565 A_0	.388224 A_0	.584090 A_0	.811689 A_0
20°	.852464 A_0	.522786 A_0	.763159 A_0	.646211 A_0
45°	.660619 A_0	.750721 A_0	.904161 A_0	.427193 A_0
70°	.437678 A_0	.899132 A_0	.908719 A_0	.417410 A_0
90°	.388223 A_0	.921565 A_0	.811689 A_0	.584090 A_0
110°	.522786 A_0	.852464 A_0	.646210 A_0	.763160 A_0
135°	.750721 A_0	.660619 A_0	.427191 A_0	.904162 A_0
160°	.899132 A_0	.437679 A_0	.417411 A_0	.908718 A_0
180°	.921565 A_0	.388224 A_0	.584090 A_0	.811689 A_0

tion patterns of the form shown in Figs. 8 to 15 result. For purposes of plotting, calculations were made for every 20° on the V scale.

Under experimental conditions, it is not possible to obtain a wave of fixed amplitude and phase as thus far used in the above treatment. The incoherent source such as the mercury arc in which the various atoms are all radiating at differen ttimes is the usual laboratory source. Classically such a source can in its simplest form be looked upon as giving off a large number of waves of the same frequency but having different amplitudes and phases. This will not however change the form of the solution[1] for the presence of a series of such waves means that they must first be combined and this addition will again give a wave of the same form but of different amplitude and phase. The only effect on Eq. (34) describing the diffraction pattern is that A_0 changes hence changing the magnitude of the patterns shown in the previous figures but not their form.

The above theoretical treatment of the problem was then checked experimentally. A good polaroid was mounted between the collimating lens and prism (see Fig. 3) and the image behavior observed in the focal plane of the 2839-mm lens with an eye piece. The changes in the horizontal image were exactly of the form predicted by the previous curves while the vertical image remained sharp and unaffected by the polaroid rotation. At a given position of the polaroid, the horizontal image appeared as a single broad line of about twice the width of the vertical line. Upon rotating the polaroid in a given direction a satellite would appear on a given side, reach a maximum of sharpness, and then recede back into the original line. Further rotation of the polaroid in the same direction would produce the satellite on the opposite side

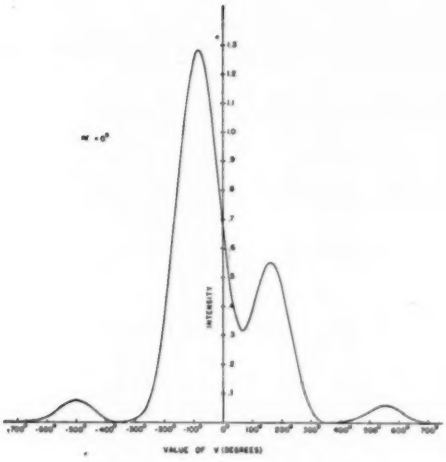

FIG. 8.

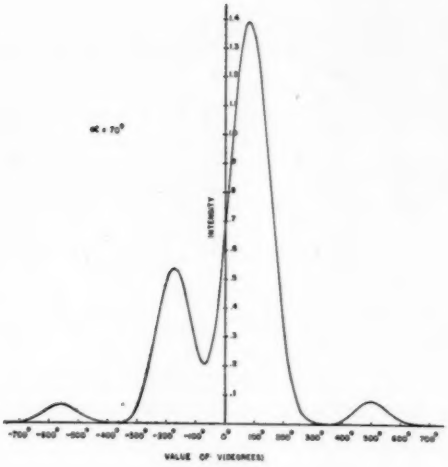

FIG. 11.

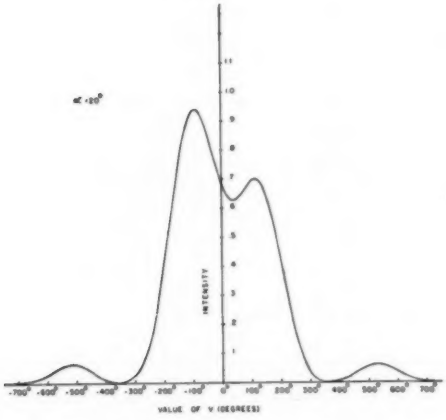

FIG. 9.

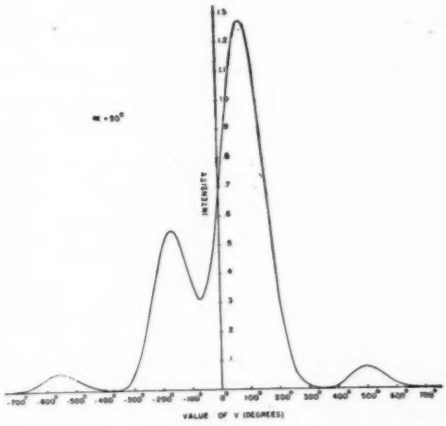

FIG. 12.

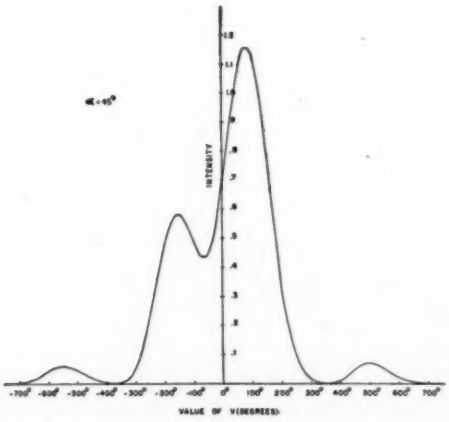

FIG.10.

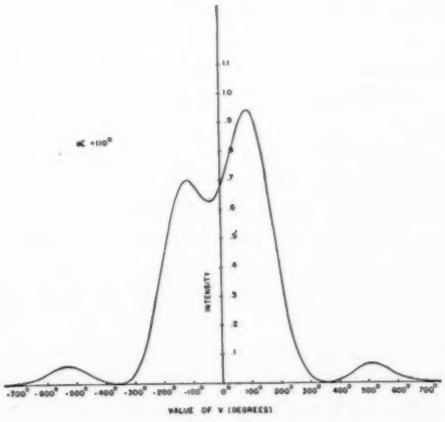

FIG. 13.

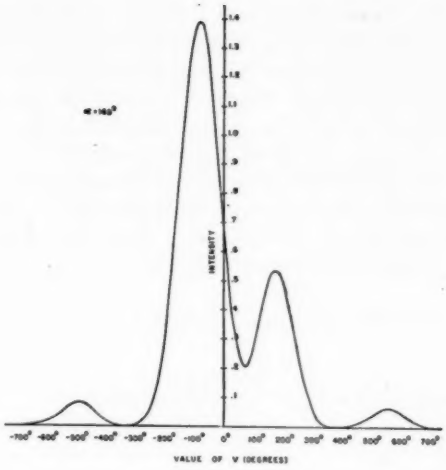

FIG. 14.

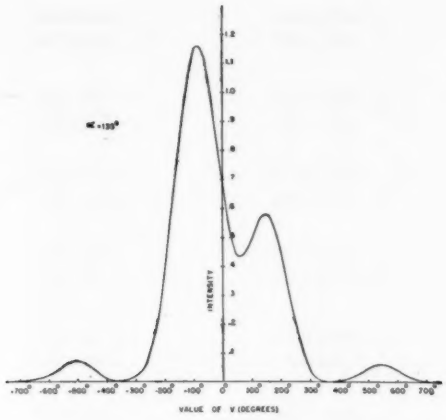

FIG. 15.

of the line. A complete cycle of these changes could always be observed for a rotation of the polaroid through 180°. To reproduce these changes for this paper, an attempt was made to photograph the image for every 20° rotation of the polaroid from an arbitrary initial incident azimuth angle. After contact prints were made from these negatives and mounted one above the other, Fig. 16 was obtained. Although the photographs are not too satisfactory, they do show that the behavior is that to be expected from the theoretical curves, the diffraction patterns repeating themselves every 180° rotation of the polaroid.

To show from Fig. 16 that the secondary minima are of the spacing predicted by the theoretical curves, the negative at 20° from the above series was used to make an enlarged longer exposure print. The result is shown in Fig. 17. Again it can be seen that the secondary minima in the horizontal direction have twice the separation of those in the vertical direction.

In the direction parallel to the roof edge (corresponding to the ξ direction), the diffraction pattern will according to Eq. (34) be of the usual symmetric form[10] shown in Fig. 18. It is important to notice that the form of the pattern in this direction is independent of the choice of α, hence its form should remain undisturbed by a rotation of the polaroid. This was seen to be the case and can be checked from any of the series of negatives used in Fig. 16. This pattern therefore can be expected to represent the diffraction patterns in the vertical direction in Figs. 4, 16, and 17. If the aperture of the prism is square ($a=b$), the spacing of the minima in the vertical direction should upon comparison with the previous curves be just half that in the horizontal direction. Experimentally such was found to be the case.

4. FORM OF DIFFRACTION PATTERN IN UNPOLARIZED LIGHT

The only remaining fact necessary to complete the problem is that of showing theoretically that the behavior of the prism with unpolarized light in a direction perpendicular to the roof edge is that shown in Fig. 4. To arrive at such a solution, the intensity J must be averaged for values of α from 0° to 180°. If all values of α are equally probable, this means that for each value of V an integral of the form $(1/\pi)\int_0^\pi J d\alpha$ (where J is given by Eq. (34)) must be evaluated. If an attempt is made to integrate Eq. (34), it will soon be found to be a rather discouraging task. Before proceeding with another means of evaluation, the easier method of graphical integration using the previous values of J for different incident azimuth angles was used to give an independent check on the later exact integration. In performing these graphical integrations, it is necessary to plot curves of the form shown in Fig. 19 in which now V is constant and α the variable. These curves were plotted for values of

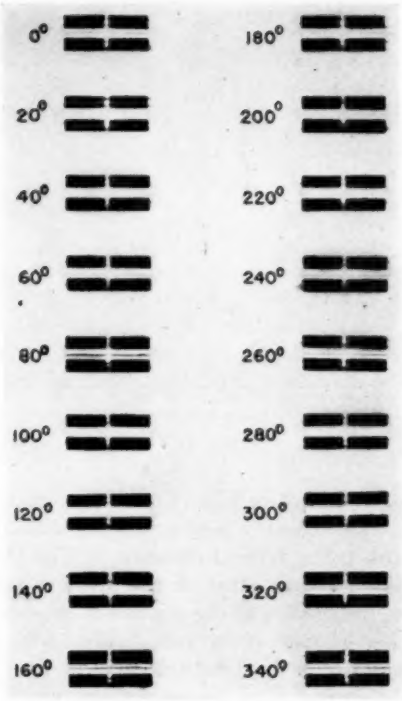

FIG. 16.

FIG. 17.

V at every 20° in the range from 0° to 720° hence only a few illustrative curves appear in Fig. 19. Once having these curves, an average value of J for each value of V can be found by evaluating the areas under the curves with a planimeter and then dividing these areas by the total length of the abscissa. It will be noted that for a given value of V, the curves corresponding to the plus and minus values are shifted horizontally 90°. The areas under both of the curves will in each case be found to be equal so that the diffraction pattern will be expected to be symmetrical about the zero position of V. In Table V are given the values of J obtained as a result of these graphical integrations.

If the values of J from Table V are plotted for the values of V indicated, Fig. 20 will result. This pattern, except for the small minimum in the center which would be difficult to obtain photographically, is of the experimentally observed form shown in Fig. 4. As might be expected from Figs. 8 to 15, the positions of the secondary minima have been unchanged so that the separation of the minima in the horizontal direction is still twice that in the vertical direction.

Although the result arrived at by graphical

TABLE V.

V	J	V	J	V	J
0°	.683	260°	.123	520°	.061
20°	.694	280°	.065	540°	.059
40°	.727	300°	.031	560°	.052
60°	.770	320°	.011	580°	.042
80°	.800	340°	.002	600°	.031
100°	.815	360°	.000	620°	.021
120°	.791	380°	.002	640°	.013
140°	.734	400°	.007	660°	.007
160°	.644	420°	.015	680°	.002
180°	.534	440°	.026	700°	.001
200°	.412	460°	.038	720°	.000
220°	.300	480°	.049		
240°	.198	500°	.057		

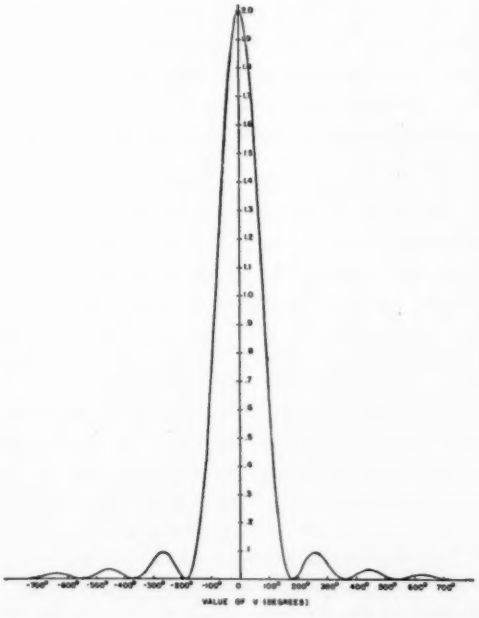

FIG. 18.

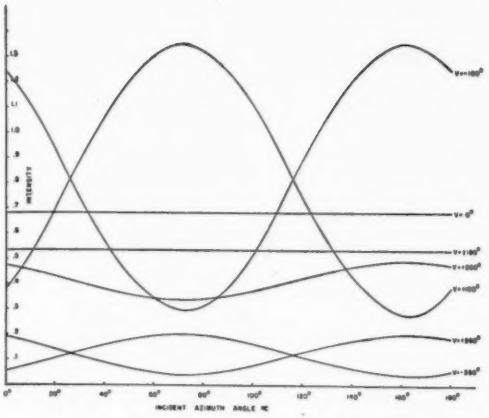

FIG. 19.

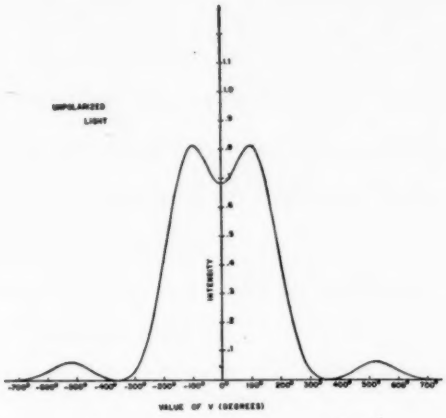

FIG. 20.

integration in Fig. 20 is sufficiently exact for most purposes, it should not be necessary for each particular prism to calculate all these values for each incident azimuth angle to arrive at the form of the diffraction pattern for unpolarized light. Obviously if this is to be avoided, it is necessary to obtain an equation equivalent to (34) which is readily integrable over values of α. To arrive at such an equation, it is necessary first to replace Eqs. (9), (10), (17), and (18) by equivalent expressions in which all the terms involving α appear in the amplitude of the time dependent sine and cosine terms and never in a phase factor. The manner of arriving at these expressions is the same as that used in deriving the earlier expressions for A_{s_3}', A_{p_3}', $\mathfrak{A}_{s_3}'$, and $\mathfrak{A}_{p_3}'$ with the exception that no attempt is made to combine sine and cosine time dependent terms into a single wave with amplitude and phase factor. The complete problem both in polarized and unpolarized light can be solved in this manner also, but the equations involved are much more complex. An added disadvantage to the second method is that one ceases to think of the longer expressions as single waves and therefor soon loses the physical significance of what is happening at each reflection. The final expressions derived by this method also are not readily susceptible to ellipticity calculations should such calculations be desired.

If the resulting waves are to be in a form which is readily integrable over the effective aperture of the prism, the various terms contributing to A_{s_3}', A_{p_3}', $\mathfrak{A}_{s_3}'$, and $\mathfrak{A}_{p_3}'$ (see equations preceding (9) and (10)) must be collected so that they can be written in the form

$$
\begin{aligned}
A_{s_3}' &= A_0(S_1 \cos\alpha - S_2 \sin\alpha)\sin(\omega t+\varphi_i+\varphi_g)+A_0(S_3\cos\alpha - S_4\sin\alpha)\cos(\omega t+\varphi_i+\varphi_g),\\
A_{p_3}' &= A_0(P_1 \cos\alpha - P_2 \sin\alpha)\sin(\omega t+\varphi_i+\varphi_g)+A_0(P_3\cos\alpha - P_4\sin\alpha)\cos(\omega t+\varphi_i+\varphi_g),\\
\mathfrak{A}_{s_3}' &= A_0(\mathfrak{S}_1 \cos\alpha - \mathfrak{S}_2 \sin\alpha)\sin(\omega t+\varphi_i+\varphi_g)+A_0(\mathfrak{S}_3\cos\alpha - \mathfrak{S}_4\sin\alpha)\cos(\omega t+\varphi_i+\varphi_g),\\
A_{p_3}' &= A_0(\mathfrak{P}_1 \cos\alpha - \mathfrak{P}_2 \sin\alpha)\sin(\omega t+\varphi_i+\varphi_g)+A_0(\mathfrak{P}_3\cos\alpha - \mathfrak{P}_4\sin\alpha)\cos(\omega t+\varphi_i+\varphi_g).
\end{aligned}
\tag{62}
$$

The various S's, P's, $\mathfrak{S}$'s, and $\mathfrak{P}$'s when written out in detail have the following values

$$
\begin{aligned}
S_1 &= \cos\beta\cos\gamma\cos(\varphi_{s_1}+\varphi_{s_2}+\varphi_{s_3})-\sin\beta\sin\gamma\cos(\varphi_{s_1}+\varphi_{p_2}+\varphi_{s_3}),\\
S_2 &= \sin\beta\cos\gamma\cos(\varphi_{p_1}+\varphi_{s_2}+\varphi_{s_3})+\cos\beta\sin\gamma\cos(\varphi_{p_1}+\varphi_{p_2}+\varphi_{s_3}),\\
S_3 &= \cos\beta\cos\gamma\sin(\varphi_{s_1}+\varphi_{s_2}+\varphi_{s_3})-\sin\beta\sin\gamma\sin(\varphi_{s_1}+\varphi_{p_2}+\varphi_{s_3}),\\
S_4 &= \sin\beta\cos\gamma\sin(\varphi_{p_1}+\varphi_{s_2}+\varphi_{s_3})+\cos\beta\sin\gamma\sin(\varphi_{p_1}+\varphi_{p_2}+\varphi_{s_3}),
\end{aligned}
$$

$$P_1=\cos\beta\sin\gamma\cos(\varphi_{s1}+\varphi_{s2}+\varphi_{p3})+\sin\beta\cos\gamma\cos(\varphi_{s1}+\varphi_{p2}+\varphi_{p3}),$$

$$P_2=\sin\beta\sin\gamma\cos(\varphi_{p1}+\varphi_{s2}+\varphi_{p3})-\cos\beta\cos\gamma\cos(\varphi_{p1}+\varphi_{p2}+\varphi_{p3}),$$

$$P_3=\cos\beta\sin\gamma\sin(\varphi_{s1}+\varphi_{s2}+\varphi_{p3})+\sin\beta\cos\gamma\sin(\varphi_{s1}+\varphi_{p2}+\varphi_{p3}),$$

$$P_4=\sin\beta\sin\gamma\sin(\varphi_{p1}+\varphi_{s2}+\varphi_{p3})-\cos\beta\cos\gamma\sin(\varphi_{p1}+\varphi_{p2}+\varphi_{p3}),$$

$$\begin{aligned}
S_1&=\cos H[\cos\epsilon\cos\eta\cos(\varphi_{s1}+\varphi_{s2}+\varphi_{s3})-\sin\epsilon\sin\eta\cos(\varphi_{s1}+\varphi_{p2}+\varphi_{s3})]\\
&\quad-\sin H[\sin\epsilon\cos\eta\cos(\varphi_{p1}+\varphi_{s2}+\varphi_{s3})+\cos\epsilon\sin\eta\cos(\varphi_{p1}+\varphi_{p2}+\varphi_{s3})],\\
S_2&=\sin H[\cos\epsilon\cos\eta\cos(\varphi_{s1}+\varphi_{s2}+\varphi_{s3})-\sin\epsilon\sin\eta\cos(\varphi_{s1}+\varphi_{p2}+\varphi_{s3})]\\
&\quad+\cos H[\sin\epsilon\cos\eta\cos(\varphi_{p1}+\varphi_{s2}+\varphi_{s3})+\cos\epsilon\sin\eta\cos(\varphi_{p1}+\varphi_{p2}+\varphi_{s3})],\\
S_3&=\cos H[\cos\epsilon\cos\eta\sin(\varphi_{s1}+\varphi_{s2}+\varphi_{s3})-\sin\epsilon\sin\eta\sin(\varphi_{s1}+\varphi_{p2}+\varphi_{s3})]\\
&\quad-\sin H[\sin\epsilon\cos\eta\sin(\varphi_{p1}+\varphi_{s2}+\varphi_{s3})+\cos\epsilon\sin\eta\sin(\varphi_{p1}+\varphi_{p2}+\varphi_{s3})],\\
S_4&=\sin H[\cos\epsilon\cos\eta\sin(\varphi_{s1}+\varphi_{s2}+\varphi_{s3})-\sin\epsilon\sin\eta\sin(\varphi_{s1}+\varphi_{p2}+\varphi_{s3})]\\
&\quad+\cos H[\sin\epsilon\cos\eta\sin(\varphi_{p1}+\varphi_{s2}+\varphi_{s3})+\cos\epsilon\sin\eta\sin(\varphi_{p1}+\varphi_{p2}+\varphi_{s3})],\\
P_1&=\cos H[\cos\epsilon\sin\eta\cos(\varphi_{s1}+\varphi_{s2}+\varphi_{p3})+\sin\epsilon\cos\eta\cos(\varphi_{s1}+\varphi_{p2}+\varphi_{p3})]\\
&\quad-\sin H[\sin\epsilon\sin\eta\cos(\varphi_{p1}+\varphi_{s2}+\varphi_{p3})-\cos\epsilon\cos\eta\cos(\varphi_{p1}+\varphi_{p2}+\varphi_{p3})],\\
P_2&=\sin H[\cos\epsilon\sin\eta\cos(\varphi_{s1}+\varphi_{s2}+\varphi_{p3})+\sin\epsilon\cos\eta\cos(\varphi_{s1}+\varphi_{p2}+\varphi_{p3})]\\
&\quad+\cos H[\sin\epsilon\sin\eta\cos(\varphi_{p1}+\varphi_{s2}+\varphi_{p3})-\cos\epsilon\cos\eta\cos(\varphi_{p1}+\varphi_{p2}+\varphi_{p3})],\\
P_3&=\cos H[\cos\epsilon\sin\eta\sin(\varphi_{s1}+\varphi_{s2}+\varphi_{p3})+\sin\epsilon\cos\eta\sin(\varphi_{s1}+\varphi_{p2}+\varphi_{p3})]\\
&\quad-\sin H[\sin\epsilon\sin\eta\sin(\varphi_{p1}+\varphi_{s2}+\varphi_{p3})-\cos\epsilon\cos\eta\sin(\varphi_{p1}+\varphi_{p2}+\varphi_{p3})],\\
P_4&=\sin H[\cos\epsilon\sin\eta\sin(\varphi_{s1}+\varphi_{s2}+\varphi_{p3})+\sin\epsilon\cos\eta\sin(\varphi_{s1}+\varphi_{p2}+\varphi_{p3})]\\
&\quad+\cos H[\sin\epsilon\sin\eta\sin(\varphi_{p1}+\varphi_{s2}+\varphi_{p3})-\cos\epsilon\cos\eta\sin(\varphi_{p1}+\varphi_{p2}+\varphi_{p3})].
\end{aligned}\tag{63}$$

In each of the above equations, the angle H is the difference between the angles δ and α.

To obtain the intensity function J for any given incident azimuth angle α, it is necessary to integrate each of the waves from Eqs. (62) over the region of the prism aperture as described before (see Eq. (28)). In the case of the previous waves however, the integrations for both the "s" and "p" waves will consist of a sum of four integrals for each. For purposes of integration it is again simpler to write these equations with a single term for each amplitude and phase (see Eqs. (27)). If this is done, Eqs. (62) can be written

$$\begin{aligned}
A_{s3}'&=\bar{A}_{s1}\sin 2\pi(\nu t+\Phi)+\bar{A}_{s2}\cos 2\pi(\nu t+\Phi),\\
A_{p3}'&=\bar{A}_{p1}\sin 2\pi(\nu t+\Phi)+\bar{A}_{p2}\cos 2\pi(\nu t+\Phi),\\
\mathfrak{A}_{s3}'&=\bar{\mathfrak{A}}_{s1}\sin 2\pi(\nu t+\Phi)+\bar{\mathfrak{A}}_{s2}\cos 2\pi(\nu t+\Phi),\\
\mathfrak{A}_{p3}'&=\bar{\mathfrak{A}}_{p1}\sin 2\pi(\nu t+\Phi)+\bar{\mathfrak{A}}_{p2}\cos 2\pi(\nu t+\Phi).
\end{aligned}\tag{64}$$

If now the integrations for each of these components is carried out over the region of the aperture suggested by Fig. 5 and the squares of the amplitudes of the resulting "s" and "p" vibrations added

TABLE VI.

$S_1=-.043384$	$P_1=-.206719$	$\mathcal{S}_1=+.328724$	$\mathcal{P}_1=-.807901$
$S_2=+.378370$	$P_2=+.854850$	$\mathcal{S}_2=+.192321$	$\mathcal{P}_2=-.347560$
$S_3=+.920543$	$P_3=-.328610$	$\mathcal{S}_3=-.482823$	$\mathcal{P}_3=+.078226$
$S_4=+.086910$	$P_4=-.344258$	$\mathcal{S}_4=+.788566$	$\mathcal{P}_4=+.469446$

(see Eqs. (23) to (34)), the resultant intensity will be found to be

$$J=2(2ab)^2\cdot\frac{\sin^2 U}{U^2}\cdot\frac{\sin^2 V/2}{(V/2)^2}\{\tfrac{1}{2}[\bar{A}_{s1}{}^2+\bar{\alpha}_{s1}{}^2+\bar{A}_{s2}{}^2+\bar{\alpha}_{s2}{}^2+\bar{A}_{p1}{}^2+\bar{\alpha}_{p1}{}^2+\bar{A}_{p2}{}^2+\bar{\alpha}_{p2}{}^2]$$
$$+[\bar{A}_{s2}\bar{\alpha}_{s1}-\bar{A}_{s1}\bar{\alpha}_{s2}+\bar{A}_{p2}\bar{\alpha}_{p1}-\bar{A}_{p1}\bar{\alpha}_{p2}]\sin V+[\bar{A}_{s1}\bar{\alpha}_{s1}+\bar{A}_{s2}\bar{\alpha}_{s2}+\bar{A}_{p1}\bar{\alpha}_{p1}+\bar{A}_{p2}\bar{\alpha}_{p2}]\cos V\}. \quad (65)$$

If the various amplitude factors are replaced by their equivalents from Eqs. (62) and the terms are squared out and collected, the following rather long expression for J is found.

$$J=2A_0{}^2(2ab)^2\cdot\frac{\sin^2 U}{U^2}\cdot\frac{\sin^2 V/2}{(V/2)^2}\Big\{\frac{\cos^2\alpha}{2}[S_1{}^2+S_3{}^2+\mathcal{S}_1{}^2+\mathcal{S}_3{}^2+P_1{}^2+P_3{}^2+\mathcal{P}_1{}^2+\mathcal{P}_3{}^2]$$
$$-\sin\alpha\cos\alpha[S_1S_2+S_3S_4+\mathcal{S}_1\mathcal{S}_2+\mathcal{S}_3\mathcal{S}_4+P_1P_2+P_3P_4+\mathcal{P}_1\mathcal{P}_2+\mathcal{P}_3\mathcal{P}_4]$$
$$+\frac{\sin^2\alpha}{2}[S_2{}^2+S_4{}^2+\mathcal{S}_2{}^2+\mathcal{S}_4{}^2+P_2{}^2+P_4{}^2+\mathcal{P}_2{}^2+\mathcal{P}_4{}^2]+\cos^2\alpha[S_3\mathcal{S}_1-S_1\mathcal{S}_3+P_3\mathcal{P}_1-P_1\mathcal{P}_3]\sin V$$
$$-\sin\alpha\cos\alpha[S_3\mathcal{S}_2+S_4\mathcal{S}_1-S_1\mathcal{S}_4-S_2\mathcal{S}_3+P_3\mathcal{P}_2+P_4\mathcal{P}_1-P_1\mathcal{P}_4-P_2\mathcal{P}_3]\sin V$$
$$+\sin^2\alpha[S_4\mathcal{S}_2-S_2\mathcal{S}_4+P_4\mathcal{P}_2-P_2\mathcal{P}_4]\sin V+\cos^2\alpha[S_1\mathcal{S}_1+S_3\mathcal{S}_3+P_1\mathcal{P}_1+P_3\mathcal{P}_3]\cos V$$
$$-\sin\alpha\cos\alpha[S_1\mathcal{S}_2+S_2\mathcal{S}_1+S_3\mathcal{S}_4+S_4\mathcal{S}_3+P_1\mathcal{P}_2+P_2\mathcal{P}_1+P_3\mathcal{P}_4+P_4\mathcal{P}_3]\cos V$$
$$+\sin^2\alpha[S_2\mathcal{S}_2+S_4\mathcal{S}_4+P_2\mathcal{P}_2+P_4\mathcal{P}_4]\cos V\Big\}. \quad (66)$$

This equation is completely equivalent to Eq. (34) but it will now be seen that the above equation can readily be integrated over values of α. Averaging this equation for values of α between 0 and π, all terms involving $(1/\pi)\int_0^\pi \sin\alpha\cos\alpha d\alpha$ will vanish and all terms containing $(1/\pi)\int_0^\pi \sin^2\alpha d\alpha$ or $(1/\pi)\int_0^\pi \cos^2\alpha d\alpha$ will appear with these integrals replaced by $\frac{1}{2}$. Collecting all the terms after these substitutions, the above equation reduces to

$$J=2A_0{}^2(2ab)^2\frac{\sin^2 U}{U^2}\cdot\frac{\sin^2 V/2}{(V/2)^2}\{\tfrac{1}{4}[S_1{}^2+S_2{}^2+S_3{}^2+S_4{}^2+\mathcal{S}_1{}^2+\mathcal{S}_2{}^2+\mathcal{S}_3{}^2+\mathcal{S}_4{}^2+P_1{}^2+P_2{}^2+P_3{}^2+P_4{}^2$$
$$+\mathcal{P}_1{}^2+\mathcal{P}_2{}^2+\mathcal{P}_3{}^2+\mathcal{P}_4{}^2]+\tfrac{1}{2}[-S_1\mathcal{S}_3-S_2\mathcal{S}_4+S_3\mathcal{S}_1+S_4\mathcal{S}_2-P_1\mathcal{P}_3-P_2\mathcal{P}_4+P_3\mathcal{P}_1+P_4\mathcal{P}_2]\sin V$$
$$+\tfrac{1}{2}[S_1\mathcal{S}_1+S_2\mathcal{S}_2+S_3\mathcal{S}_3+S_4\mathcal{S}_4+P_1\mathcal{P}_1+P_2\mathcal{P}_2+P_3P_3+P_4\mathcal{P}_4]\cos V\}. \quad (67)$$

For any roof prism involving three internal reflections, the intensity function J due to the forms of the coefficients given in Eqs. (63) will be found to reduce to the following simpler form.

$$J=2A_0{}^2(2ab)^2\cdot\frac{\sin^2 U}{U^2}\cdot\frac{\sin^2 V/2}{(V/2)^2}\{1+\tfrac{1}{2}[S_1\mathcal{S}_1+S_2\mathcal{S}_2+S_3\mathcal{S}_3+S_4\mathcal{S}_4+P_1\mathcal{P}_1+P_2\mathcal{P}_2+P_3\mathcal{P}_3+P_4\mathcal{P}_4]\cos V\}. \quad (68)$$

For the roof prism of Fig. 1, the various coefficients given by Eqs. (63) have the values given in Table VI when the known azimuth angles and phase changes upon reflection are substituted. If sub-

TABLE VII.

V	J	V	J	V	J
0°	.682154	260°	.120281	520°	.061165
20°	.694286	280°	.065383	540°	.059345
40°	.726267	300°	.030679	560°	.052739
60°	.766958	320°	.011348	580°	.042860
80°	.800942	340°	.002402	600°	.031705
100°	.813096	360°	.000000	620°	.021152
120°	.792604	380°	.001923	640°	.012515
140°	.735634	400°	.007263	660°	.006338
160°	.646048	420°	.015652	680°	.002513
180°	.534101	440°	.026477	700°	.000567
200°	.413474	460°	.038426	720°	.000000
220°	.297901	480°	.049538		
240°	.198154	500°	.057673		

stitutions from Table VI are made in Eq. (68) and all the terms which do not depend upon V are grouped into a constant term K, the resulting equation for the diffraction pattern in unpolarized light becomes

$$J=K\frac{\sin^2 V/2}{(V/2)^2}\{1-.317846\cos V\}. \tag{69}$$

If this equation is evaluated for different values of V, the resulting values will be found to agree quite closely with the graphically integrated values in Table V. In Table VII are given the calculated values for J as obtained from Eq. (69).

It should be emphasized that the form of the diffraction pattern shown in Fig. 20 is only to be expected when the prism is illuminated with completely unpolarized light (mathematically speaking, all values of α are equally probable). If for any reason there is present in the incident light an excess of plane polarized light in any given direction, the form of the diffraction pattern may be expected to change.

The mathematics as developed for this particular prism suggests strongly that all roof prisms involving two or three internal reflections are susceptible to some degree to this doubling of the image in a direction perpendicular to the roof edge. The magnitude of this doubling will be dependent upon the geometry and refractive index of the particular prism. In roof prisms therefore where an apparent persistent roof angle error is present, it is suggested that an analysis of the above type be made to see if a single sharp image is possible.

This paper should be looked upon more as an introduction to the problem. The experimental evidence for its existence is fairly complete but more accurate checks should be made. Diffraction patterns should be obtained for known incident azimuth angles and microphotometer tracings made to see if they compare in form to the calculated patterns of Fig. 8 to Fig. 15. The more embarassing problem of the changes taking place in the diffraction pattern as the roof angle is changed has not been touched. It is conceivable from Eqs. (9), (10), (17), and (18) that a fixed difference in phase between the two "s" and "p" components in the upper and lower halves of the aperture (see Fig. 5) might be introduced by changing the roof angle a small amount so as to make the resultant phase difference effectively zero for either the "s" or "p" (but not for both) vibrations for any given incident azimuth angle. It seems plausible therefore that the doubling for a given incident azimuth angle may be changed but not theoretically reduced to zero. The magnitude of these changes in the diffraction pattern for both polarized and unpolarized light for known changes in the roof angle remains to be determined. For the prism of Fig. 1, small roof angle changes apparently do not produce noticeable changes in the diffraction pattern for the doubling (hence difference in resolving powers in the vertical and horizontal directions) has always been observed in all prisms of this type investigated.

The problem of evaluating the form of the diffraction pattern when the prism roofs are silvered has been avoided in the writing of this paper. The solution of this problem is however essentially the same as the present solution with the exception that the phase changes of the "*s*" and "*p*" components after reflection at each of the glass-silver surfaces of the prism roofs will be different from the present values for the unsilvered roof surfaces.

The author is much indebted to Mr. Max Zwillinger of the Optical Laboratory whose suggestion of the problem and original interest in it was largely responsible for this paper. Many of the preliminary investigations on the problem were made in conjunction with Mr. Zwillinger. Other departmental contacts were also stimulating since the problem has also been worked on by other staff members. Mr. S. G. Hall of our laboratory also has another completely independent solution to the problem. Additional suggestions were also obtained as a result of discussions with Dr. W. F. Brown of the Naval Ordnance Laboratory. For help in doing many of the routine calculations as well as in the preparation of the paper itself, the author is indebted to his wife, Dr. Frances F. Mahan.

JOURNAL OF THE OPTICAL SOCIETY OF AMERICA VOLUME 35, NUMBER 10 OCTOBER, 1945

An Application of Multiplier Photo-Tubes to the Spectrochemical Analysis of Magnesium Alloy

GEORGE A. NAHSTOLL AND FORD R. BRYAN
Chemical Engineering Department, Ford Motor Company, Dearborn, Michigan
(Received August 6, 1945)

THE possibilities of increased speed and accuracy together with reduced material and labor costs have aroused an intensive interest in photo-tube methods of industrial spectroscopic analysis. The following pages describe a method used successfully in one of the Ford Motor Company spectrographic control laboratories.

A spectrographic installation engaged in the analysis of magnesium castings was selected as a suitable trial laboratory. This selection was made because of the comparatively moderate number of samples analyzed, the single type of alloy being cast, and the normally limited range of alloying elements contained in the metal both before and after the melting operation.

EQUIPMENT AND OPERATION

The equipment heretofore used for the work in this laboratory consisted of a Feussner interrupted high voltage spark source, a Bausch & Lomb medium quartz spectrograph, photographic plate processing apparatus, and a non-recording microphotometer. Of this equipment the spark source was retained for use without alteration. The spectrograph required an attachment for photo-tube reception of radiation. The processing equipment and microphotometer were not used.

The spectrograph camera head was removed, and in its place was substituted an attachment for isolating and measuring the lines of the elements to be determined. Figure 1 shows many of the details. The attachment consists mainly of three parts. One part is a rack located on the focal plane of the spectrograph and built to hold several adjustable width slits in a rigid position. The rack used for magnesium analysis provides for two rows of slit assemblies. One row is located above the other, and either row is positionable in the spectrum exit plane by means of a vertical movement of the entire rack. The slits, themselves, consist of mounted, sharpened, and lapped blades which form an exit for the specific wave-length chosen for measurement. The second principle part of the attachment consists of a mechanism for the horizontal displacement of a photo-tube to a position adjacent to any slit assembly so as to intercept the light emerging from that slit. Thus, it is possible to isolate the desired element line by means of the rigidly positioned slit and to measure the intensity of the line by the horizontal crank and screw movement of the photo-tube to the desired position in the spectrum. The third division of the attachment functions as an internal standard measuring device. An exit slit which would normally transmit a reference line is constructed to reflect that same line to a second photo-tube located in the scale lamp housing inside the spectrograph proper. The reflector is glass with an aluminized front surface, and is mounted directly behind the slit opening. The construction is such as to permit a wide angular adjustment of this assembly, and thus provide usefulness at any chosen wave-length. The remote location of the photo-tube which measures the reference line allows a full sweep of the spectrum by the movable photo-tube.

A great deal of the current enthusiasm regarding direct reading possibilities is centered about

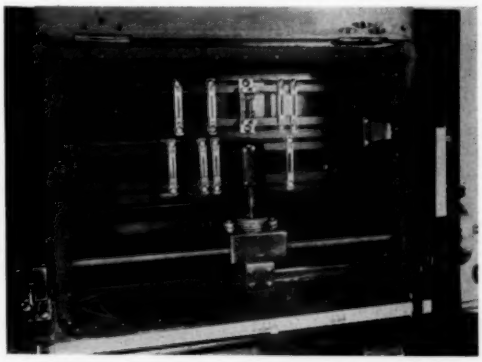

FIG. 1. Spectrograph photo-tube attachment.

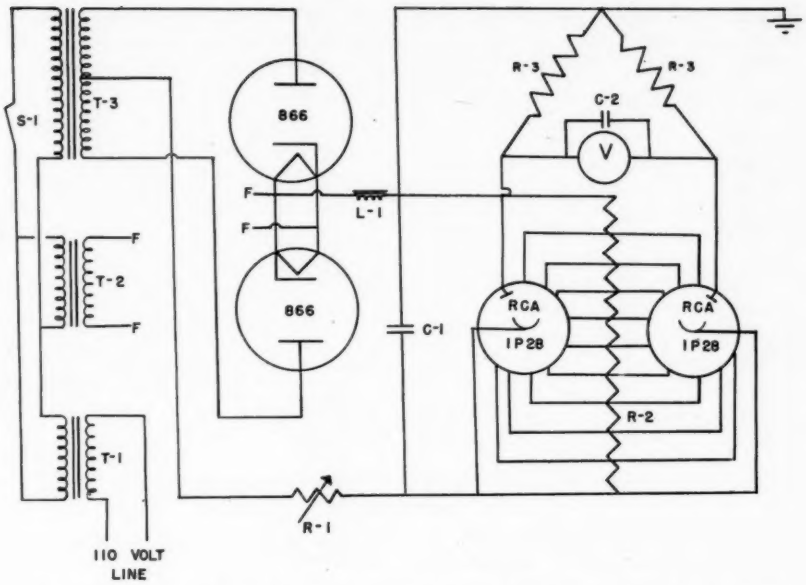

FIG. 2. Diagram of power and measuring circuits used for the comparison of two spectral line intensities.

S-1	Power switch	R-1	100,000 ohm, 200-watt variable resistor
T-1	Voltage regulator transformer	R-2	100,000 ohm, 200-watt voltage divider
T-2	2.5-volt filament transformer	L-1	30–40 henry choke coil
F-	Filament leads	C-1	2-microfarad filter condenser
T-3	3120-volt C.T. power transformer	C-2	0.1-microfarad condenser

the use of the RCA 1P28 multiplier photo-tube.[1,2] This photo-tube has a relatively high luminous sensitivity and a satisfactory spectral response to the wave-length region commonly used for industrial emission spectrography. Its rated current amplification of 200,000 times and the special glass envelope allowing sensitivity in the ultraviolet to nearly 2000 Angstroms give it practical advantages over the ordinary commercially available vacuum and gas photo-tubes as well as over barrier layer cells.

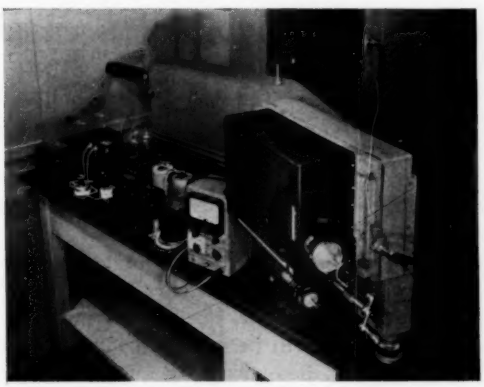

FIG. 3. General view of the apparatus.

To supply the necessary voltages to the 1P28 multiplier photo-tube, a power source was constructed. The electrical circuit employed is shown in Fig. 2. A full wave filtered direct current at about 1500 volts is supplied to a tapped voltage dividing resistor. Voltages up to 150 volts per stage can thus be supplied to the nine electron multiplying stages. In actual use it is found that increases in steps of 90 volts are satisfactory from the photo-cathode to the ninth stage. Twice this voltage, or 180 volts, is supplied between the ninth stage and the anode to permit current saturation at relatively high light values.

[1] V. K. Zworykin and J. A. Rajchman, "The Electrostatic Electron Multiplier," Proc. I.R.E., **27**, 558–566 (Sept. 1939).

[2] Bulletin 1P28, Radio Corporation of America, Harrison, New Jersey, 1944.

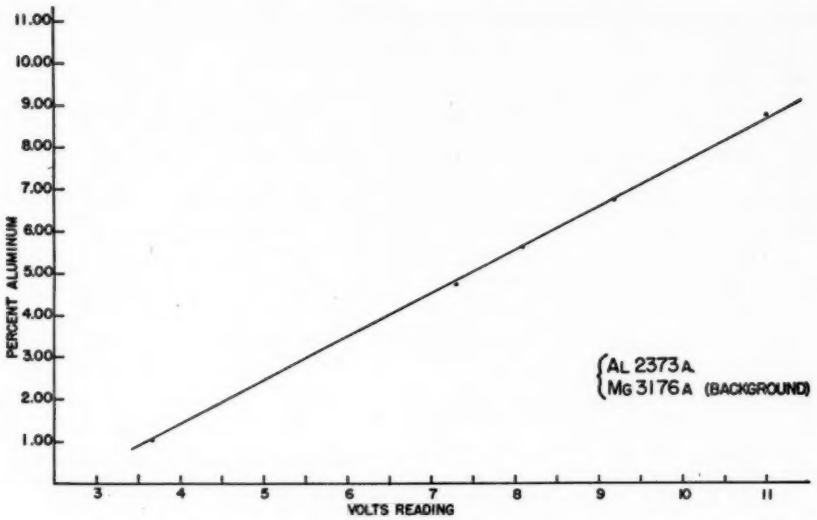

FIG. 4. A typical working curve showing relationships between voltmeter readings and percentage composition.

Some of the required voltage stabilization is provided by a comparatively large bleeder current. Additional regulation is obtained by the addition of a voltage regulating transformer located in the primary of the circuit. Further regulation by gaseous voltage regulator tubes or by separate stabilization circuits has not been attempted. Voltages for both the movable and the fixed multiplier photo-tubes are supplied by the common tapped voltage divider of the one power source. An unenclosed power source of this type is shown at the left of center in Fig. 3.

As a compromise choice among sensitivity, simplicity, and availability factors, a vacuum tube voltmeter is used to measure the output of either of the two multiplier photo-tubes. A load resistance of 20 megohms provides a voltage drop of sufficient magnitude to give a spectral background reading considerably above the tube dark current value. A less resistive load lessens the sensitivity of the method for very small light values, and a greater resistive load excessively taxes the insulation of the measuring circuit. A ratio between outputs of the two photo-tubes is obtained by using the vacuum tube voltmeter to indicate the difference of potential between the anodes of the two photo-tubes when each is connected to its 20-megohm load. Light fluctuations of the spectrographic spark source cause instantaneous irregularities in the multiplier photo-tube output. A condenser of 0.1 microfarad capacitance placed across the vacuum tube voltmeter leads tends to average these output values over a period of a few seconds. With proper consideration given to the time of wait necessary for light source equilibrium, no further integration was deemed necessary. A general view of the equipment as used is shown in Fig. 3.

To operate the apparatus described above, exit slits were placed so as to intercept lines of eight constituents of A.M.S. 4422 alloy. These slits were adjusted to a width sufficient to fully include a line formed by a 100 micron entrance slit. Line height was fixed at 10 mm at the spectrograph entrance aperature. Spectrographic standards obtained from the Dow Chemical Company were used to construct working curves. A typical example of these working curves is shown in Fig. 4. These same curves were then transposed as scales to the voltmeter itself, so that the meter indicates directly in percentage composition as Fig. 5 depicts. The use of a projection type meter, however, greatly aids in reading and in adjusting such scales.

RESULTS

A test of reproducibility was immediately made on the determination of aluminum in the

magnesium alloy inasmuch as the aluminum determination was of major importance in the acceptance or rejection of the melts. With the movable multiplier photo-tube positioned to pick up the aluminum line at 2373 Angstroms and with the fixed reference multiplier photo-tube receiving a background area at 3176 Angstroms, two alloy standards were sparked 10 times each at intervals during an eight-hour period. No readjustments were made in either the spark source or the multiplier photo-tube power source during that time. Results in precision were as follows:

Standard "H" (5.9 percent Aluminum)

	Maximum	Average
Deviation from mean output voltage	0.09 volt	0.05 volt
Deviation from mean percent aluminum	0.15 percent	0.08 percent
Percent deviation	2.5 percent	1.3 percent

Standard "C" (8.7 percent Aluminum)

	Maximum	Average
Deviation from mean output voltage	0.08 volt	0.03 volt
Deviation from mean percent aluminum	0.13 percent	0.06 percent
Percent deviation	1.5 percent	0.7 percent

Later, to test reproducibility over a longer period of time, no readjustments were made for two weeks. During this interval the same two standards were analyzed for aluminum content about 15 times each with the following degree of precision:

Standard "H" (5.9 percent Aluminum)

	Maximum	Average
Deviation from mean output voltage	0.11 volt	0.07 volt
Deviation from mean percent aluminum	0.18 percent	0.12 percent
Percent deviation	3.1 percent	2.0 percent

Standard "C" (8.7 percent Aluminum)

	Maximum	Average
Deviation from mean output voltage	0.17 volt	0.08 volt
Deviation from mean percent aluminum	0.28 percent	0.13 percent
Percent deviation	3.3 percent	1.5 percent

In order to determine whether the direct-reading method was sufficiently accurate for control analysis, a series of 133 production samples of A.M.S. 4422 alloy was analyzed by both photographic plate and multiplier photo-tube. The average deviations in percentage composition between the routine photographic method and the multiplier photo-tube method are as follows:

Aluminum	0.17 percent	Copper	0.002 percent
Zinc	0.24 percent	Nickel	0.003 percent
Manganese	0.02 percent	Iron	0.003 percent
Silicon	0.02 percent	Lead	0.02 percent

A customary number of these same production samples was analyzed by routine wet chemical methods as a check on spectrochemical procedure. Results from these seven samples, involving determinations of the three elements of greatest percentage, show average deviations as follows: aluminum, 0.15 percent; zinc, 0.17 percent; and manganese 0.02 percent. These average deviations are of magnitudes similar to the deviations obtained by comparing photo-tube and photographic plate methods.

The eight determinations per sample are obtained by manual operation of the photo-tube apparatus during a sparking time of about 4 minutes. Allowing more time for the photo-tube at each line position would tend to increase accuracy. This extra time should become available with motor manipulation of the photo-tube without increasing the total time for each determination. At present one operator is able to make 80 determinations per hour from samples as received from the foundry. Two operators can

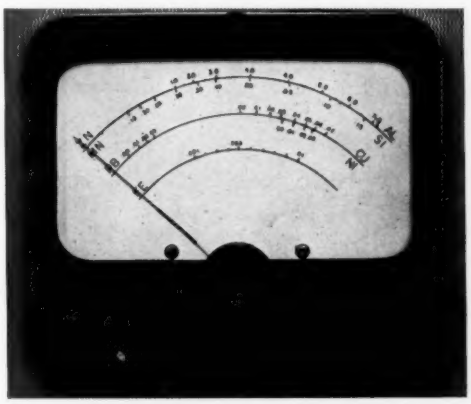

FIG. 5. A vacuum tube voltmeter dial calibrated from working curves to read directly the percentage composition.

increase this number of determinations to 100. The use of more operators will not speed the process. It would be possible to install several such units to permit greater capacity. However, for installations requiring the analysis of over 100 samples in an eight-hour day, simultaneously illuminated photo-tubes and their respective meters attached to an adequate single spectrograph would seem more feasible.

DIFFICULTIES ENCOUNTERED

There are several serious difficulties which we encountered during our attempt to apply the multiplier photo-tubes to standard equipment and to procedures designed for photographic reception of radiation. The size of the 1P28 multiplier photo-tube does not allow the focal plane placement of an individual photo-tube for each line to be measured. The desirable multiple and concurrent measurements, advocated by Boettner and Brewington,[3] have been reported only on the basis of rather elaborate reflecting systems.[4] Grating instruments of moderate to high dispersion would seem to fill more nearly the requirements for multiple photo-tube placements than would quartz instruments. The obliqueness with which the refracted light beam intersects the focal plane of a quartz spectrograph tends to complicate any direct reading attempt.

The instability of arc and spark light sources commonly used in spectrography requires either an integration or an averaging of light intensity values for proper results. Just as there is a photochemical accumulation in photography, there is required an integration or an averaging of the electrical output when photo-tubes are used. However, when light source conditions are favorable, the integrating period may be limited to a few seconds.

In using groups of photo-tubes for comparative readings, it will be found that these tubes do not all match in luminous sensitivity. The replacement of one photo-tube by another is apt to require complete revision of the analytical working curves involved.

CONCLUSION

Although the results obtained by this method of direct reading have temporarily satisfied our needs in one particular laboratory, it is evident that further refinement of both apparatus and methods is desirable. This experimental application was occasioned only by the lack of commercially built apparatus.

[3] E. A. Boettner and G. P. Brewington, J. Opt. Soc. Am. **34**, 6–11 (1944).
[4] M. F. Hasler and H. W. Dietert, J. Opt. Soc. Am. **43**, 751–758 (1944).

JOURNAL OF THE OPTICAL SOCIETY OF AMERICA VOLUME 35, NUMBER 10 OCTOBER, 1945

Transmission of Light from a Point Source in a Medium Bounded by Diffusely Reflecting Parallel Plane Surfaces*

H. BATEMAN, *California Institute of Technology, Pasadena, California*

AND

C. L. PEKERIS,† *Columbia University, New York, New York*

(Received April 25, 1945)

I. INTRODUCTION

WE consider the transmission of light from a point source in the medium shown in Fig. 1. The point source is at a depth a below the upper surface, and the receiver, which for definiteness is assumed to be a sphere of radius α, is at a depth z, and is at a horizontal distance r from the source. The bounding surfaces are assumed to reflect diffusely according to Lambert's law, with albedos n and m, respectively.

This means that if luminous flux of amount EdA is incident on an elementary area dA of albedo n, the flux reflected in an elementary solid angle $d\Omega$ making an angle θ with the normal to dA is $(n/\pi)EdAd\Omega\cos\theta$ (Fig. 2). The total reflected flux is therefore equal to

$$\frac{n}{\pi}EdA\int_0^{\pi/2}2\pi\sin\theta\cos\theta d\theta=nEdA. \tag{1}$$

The law implies (a) that the elementary area appears of equal luminance when viewed from any direction and (b) this independently of the angular distribution of the incident flux EdA. If the incident light has an angular distribution $I(\theta,\phi)$, then

$$EdA=dA\int_0^{2\pi}d\phi\int_0^{\pi/2}I(\theta,\phi)\sin\theta\cos\theta d\theta, \tag{2}$$

the factor $dA\cos\theta$ representing the area projected normal to the direction of I.

II. FORMAL SOLUTION OF THE PROBLEM

The total luminous flux F received by the sphere is the sum of the flux received from the direct beam plus the flux reflected from the two surfaces. The reflected flux can be computed once the distribution of incident light on the surfaces is known. The latter consists, for each surface, of the direct beam plus the light reflected from the other surface. The procedure is then, first to find the distribution of incident flux on the surfaces, and second to compute the total luminous flux arriving at the receiver. The first step involves the solution of a pair of integral equations arising from multiple interreflections (Eqs. (4) and (5) below), and the second step involves two surface integrations (Eq. (3) below).

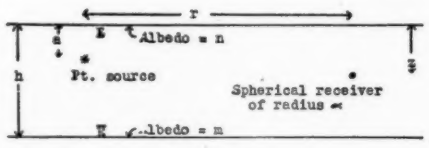

FIG. 1.

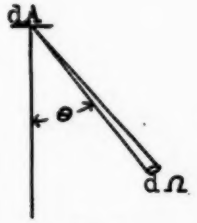

FIG. 2.

* Publication assisted by the Ernest Kempton Adams Fund for Physical Research of Columbia University.

† On leave of absence from Massachusetts Institute of Technology.

If E and $\bar{E}$ denote, respectively, the illuminance on the upper and lower surfaces then we have

$$F=\frac{\pi\alpha^2}{[r^2+(z-a)^2]}+n\alpha^2 z\int\int_{-\infty}^{\infty}\frac{E(x',y')dx'dy'}{R^3}+m\alpha^2(h-z)\int\int_{-\infty}^{\infty}\frac{\bar{E}(x',y')dx'dy'}{R^3}, \tag{3}$$

where R denotes in each case the distance of the elementary area $dx'dy'$ from the receiver, and the integrations are to be carried out over the upper and lower surfaces, respectively. The expressions for the reflected flux originate as follows: $dx'dy'=dA$, $\cos\theta=z/R$ or $(h-z)/R$, $d\Omega=\pi\alpha^2/R^2$. If the receiver were a small horizontal disk sensitive on both sides, the $1/R^3$ factors would be replaced by $1/R^4$.

The quantities E and $\bar{E}$ themselves have to be computed from the following relations

$$E(x,y)=\frac{a}{(r^2+a^2)^{\frac{3}{2}}}+\frac{m}{\pi}\int\int_{-\infty}^{\infty}\frac{\bar{E}(x',y')dx'dy'}{R^2}\left(\frac{h^2}{R^2}\right), \tag{4}$$

$$\bar{E}(x,y)=\frac{(h-a)}{[r^2+(h-a)^2]^{\frac{3}{2}}}+\frac{n}{\pi}\int\int_{-\infty}^{\infty}\frac{E(x',y')dx'dy'}{R^2}\left(\frac{h^2}{R^2}\right), \tag{5}$$

where $R=[(x-x')^2+(y-y')^2+h^2]^{\frac{1}{2}}$.

III. SOLUTION OF THE INTEGRAL EQS. (4) AND (5) FOR THE ILLUMINANCE OF THE SURFACES

In solving Eqs. (4) and (5) we first reduce the double integrations to single integrations; it is then found that the resulting kernel is a Bessel function, so that the equations can be solved directly by a Hankel inversion. The reduction to single integrations is made possible by the fact that both E and $\bar{E}$ have cylindrical symmetry: $E(x,y)=E(r)$, $\bar{E}=E(r)$. We also have

$$\int\int_{-\infty}^{\infty}\frac{E(x',y')dx'dy'}{R^4}=\int_0^{\infty}E(r')r'dr'\int_0^{2\pi}\frac{d\phi'}{[h^2+r^2+r'^2-2rr'\cos(\phi'-\phi)]^2}$$

$$=2\pi\int_0^{\infty}\frac{E(r')r'dr'(h^2+r^2+r'^2)}{[(h^2+r^2+r'^2)^2-4r^2r'^2]^{\frac{3}{2}}}$$

$$=\frac{\pi}{h}\int_0^{\infty}E(r')r'dr'\int_0^{\infty}K_1(hx)J_0(rx)J_0(r'x)x^2dx. \tag{6}$$

Let now

$$F(r)\equiv\int_0^{\infty}J_0(rx)E(x)xdx,\quad \bar{F}(r)\equiv\int_0^{\infty}J_0(rx)\bar{E}(x)xdx,^1 \tag{7}$$

then

$$E(r)=\int_0^{\infty}F(x)J_0(rx)xdx,\quad \bar{E}(r)=\int_0^{\infty}\bar{F}(x)J_0(rx)xdx, \tag{8}$$

[1] No confusion should arise from the use of F in Eqs. (7), and in Eqs. (3), (17), etc., to denote total luminous flux.

and Eqs. (4) and (5) can be written as

$$\int_0^\infty J_0(rx)F(x)xdx=\int_0^\infty e^{-az}J_0(rx)xdx+mh\int_0^\infty xK_1(hx)\bar{F}(x)J_0(rx)xdx, \tag{9}$$

$$\int_0^\infty J_0(rx)F(x)xdx=\int_0^\infty e^{-z(h-a)}J_0(rx)xdx+nh\int_0^\infty xK_1(hx)F(x)J_0(rx)xdx. \tag{10}$$

It follows that

$$F(x)=e^{-az}+mhxK_1(hx)\bar{F}(x), \tag{11}$$

$$\bar{F}(x)=e^{-z(h-a)}+nhxK_1(hx)F(x), \tag{12}$$

or

$$F(x)=\frac{e^{-az}+mhxK_1(hx)e^{-z(h-a)}}{1-nmh^2x^2K_1^2(hx)}, \tag{13}$$

$$\bar{F}(x)=\frac{e^{-z(h-a)}+nhxK_1(hx)e^{-az}}{1-nmh^2x^2K_1^2(hx)}. \tag{14}$$

The solution of the integral Eqs. (4) and (5) is given by (8) with $F(x)$ and $\bar{F}(x)$ substituted from (13) and (14).

IV. TRANSFORMATION OF THE INTEGRALS FOR THE TOTAL LUMINOUS FLUX ARRIVING AT AN INTERIOR POINT

The integrals in (3) can be transformed as follows:

$$\int_{-\infty}^{\infty}\int\frac{E(x'y')dx'dy'}{R^3}=\int_0^\infty r'dr'\int_0^{2\pi}\frac{d\phi'}{[z^2+r^2+r'^2-2rr'\cos(\phi'-\phi)]^{\frac{3}{2}}}\int_0^\infty J_0(r'u)F(u)udu$$

$$=\frac{2\pi}{z}\int_0^\infty e^{-zz}F(x)J_0(rx)xdx. \tag{15}$$

The last equality follows from Gegenbauer's integral

$$\int_0^{2\pi}\frac{d\phi'}{[z^2+r^2+r'^2-2rr'\cos(\phi'-\phi)]^{\frac{3}{2}}}=\frac{2\pi}{z}\int_0^\infty e^{-zz}J_0(rx)J_0(r'x)xdx, \tag{16}$$

and the Hankel identity

$$\int_0^\infty r'dr'J_0(r'x)\int_0^\infty J_0(r'u)F(u)udu=F(x).$$

Substituting in (3) we finally get

$$F=\frac{\pi\alpha^2}{[r^2+(z-a)^2]}+2\pi\alpha^2n\int_0^\infty e^{-zz}F(x)J_0(rx)xdx+2\pi\alpha^2m\int_0^\infty e^{-z(h-z)}\bar{F}(x)J_0(rx)xdx, \tag{17}$$

where $F(x)$ and $\bar{F}(x)$ are given by (13) and (14), respectively.

V. ANALYSIS IN TERMS OF SINGLE AND MULTIPLE REFLECTIONS

If we expand the denominators in (13) and (14) in ascending powers of (nm) we obtain for the first few terms

$$F=\frac{\pi\alpha^2}{[r^2+(z-a)^2]}+2\pi\alpha^2 n\int_0^\infty e^{-xz}J_0(rx)[e^{-ax}+mhxK_1(hx)e^{-x(h-a)}][1+nmh^2x^2K_1^2(hx)+\cdots]xdx$$

$$+2\pi\alpha^2 m\int_0^\infty e^{-x(h-z)}J_0(rx)[e^{-x(h-a)}+nhxK_1(hx)e^{-ax}][1+nmh^2x^2K_1^2(hx)+\cdots]xdx$$

$$=\frac{\pi\alpha^2}{[r^2+(z-a)^2]}+\frac{2\pi\alpha^2 n(z+a)}{[r^2+(z+a)^2]^{\frac{3}{2}}}+\frac{2\pi\alpha^2 m(2h-z-a)}{[r^2+(2h-z-a)^2]^{\frac{3}{2}}}+2\pi\alpha^2 nm\int_0^\infty e^{-x(z+h-a)}hxK_1(hx)J_0(rx)xdx$$

$$+2\pi\alpha^2 nm\int_0^\infty e^{-x(h-z+a)}hxK_1(hx)J_0(rx)xdx+\cdots. \quad (18)$$

The second and third terms in (18) represent first-order reflections from the upper and lower surfaces respectively, the third and fourth terms represent second-order reflections, etc.

VI. A TRANSFORMATION OF THE INTEGRALS IN (17) SUITABLE FOR NUMERICAL INTEGRATION FOR THE CASE WHEN r≫h

The integrals in (17) can be evaluated by numerical integration as long as r/h is not large. In case r/h is large, the numerical integration becomes inaccurate on account of the increasingly oscillatory character of the integrand. This difficulty can be avoided by transforming the path of integration in the x-plane from the real axis to the imaginary axis. The resulting integrals are then found to converge best when r/h is large, and it is also possible to derive from them asymptotic expansions of F for large r/h.

The scheme consists in first writing for $J_0(rx)$ in (17) $\frac{1}{2}[H_0^{(1)}(rx)+H_0^{(2)}(rx)]$. The integral with $H_0^{(1)}(rx)$ is then transformed to one along the positive imaginary axis, while the path of the integral with $H_0^{(2)}(rx)$ is transformed to the negative imaginary axis of x. We shall not give here the justification for the path transformations, nor shall we give the proof that the integrands in (17) have no poles to the right of the imaginary x-axis. Using the relations

$$H_0^{(1)}(iv)=\frac{-2i}{\pi}K_0(v), \quad H_0^{(2)}(-iv)=\frac{2i}{\pi}K_0(v), \quad (19)$$

and with $f(x)$ denoting $e^{-xz}F(x)$ or $e^{-x(h-z)}F(x)$, we thus get

$$\int_0^\infty H_0^{(1)}(rx)f(x)xdx=\int_0^{i\infty} H_0^{(1)}(rx)f(x)xdx=\frac{2i}{\pi}\int_0^\infty K_0(rv)f(iv)vdv, \quad (20)$$

$$\int_0^\infty H_0^{(2)}(rx)f(x)xdx=\int_0^{-i\infty} H_0^{(2)}(rx)f(x)xdx=\frac{-2i}{\pi}\int_0^\infty K_0(rv)f(-iv)vdv, \quad (21)$$

$$\int_0^\infty J_0(rx)f(x)xdx=\frac{i}{\pi}\int_0^\infty K_0(rv)[f(iv)-f(-iv)]vdv. \quad (22)$$

Now on account of the relations

$$K_1(iv)=\frac{-\pi}{2}H_1^{(2)}(v), \quad K_1(-iv)=\frac{-\pi}{2}H_1^{(1)}(v), \quad (23)$$

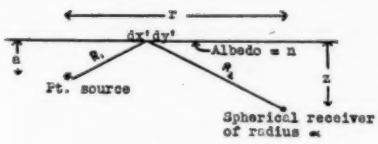

FIG. 3.

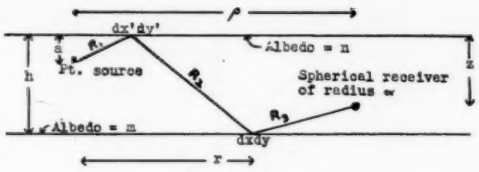

FIG. 4.

$f(iv)$ and $f(-iv)$ are complex conjugates, so that

$$\int_0^\infty J_0(rx)f(x)xdx=\frac{-2}{\pi}I_m\int_0^\infty K_0(rv)f(iv)vdv, \tag{24}$$

where I_m denotes imaginary part. Substituting from (17), (13), (14), and (23) we finally get

$$F=\frac{\pi\alpha^2}{[r^2+(z-a)^2]}-4\alpha^2nI_m\int_0^\infty K_0(rv)e^{-izv}\left[\frac{e^{-iav}(i\pi/2)mhvH_1^{(2)}(hv)e^{-iv(h-a)}}{1+(mn\pi^2/4)h^2v^2H_1^{(2)}(hv)^2}\right]vdv$$
$$-4\alpha^2mI_m\int_0^\infty K_0(rv)e^{-iv(h-z)}\left[\frac{e^{-iv(h-a)}-(i\pi/2)nhvH_1^{(2)}(hv)e^{-iav}}{1+(mn\pi^2/4)h^2v^2H_1^{(2)}(hv)^2}\right]vdv. \tag{25}$$

For large r/h the factor $K_0(rv)$ decreases exponentially in a monotone fashion, and the main contributions to the integral arise from a short range of v at the beginning of the path. This is to be contrasted with the behavior of the original integrals in (17) in which the Bessel function goes through an increasing number of oscillations in the effective range of integration as r increases.

As a check on the transformation of (17) into (25) the integrals were evaluated numerically for the case $n=1$, $m=0.5$, $z=a=0.5h$, and $r=2h$. For the integral

$$\int_0^\infty J_0(2x)xe^{-x}\left[\frac{1.5+xK_1(x)}{1-0.5x^2K_1^2(x)}\right]dx$$

arising from (17), a value of 0.4462 was obtained using the range $0<x<8.0$ and an interval of 0.1; for the corresponding integral arising from (25), using a range $0<v<3.0$ and an interval of 0.1, a value of 0.4470 was obtained.

VII. ASYMPTOTIC EXPANSIONS OF F FOR LARGE RANGES

The asymptotic behavior for large r of an integral of the form

$$Q(r)=\int_0^\infty K_0(rv)P(v)vdv$$

can be obtained by writing

$$x=rv,\quad Q(r)=\frac{1}{r^2}\int_0^\infty K_0(x)P\left(\frac{x}{r}\right)xdx,$$

expanding $P(x/r)$ for small values of the argument, and carrying out the integrations with respect to x for the individual terms. One finds that

$$I_m\left[\frac{e^{-iv(z+a)}-(i\pi/2)mhvH_1^{(2)}(hv)e^{-iv(z+h-a)}}{1+(mn\pi^2/4)h^2v^2H_1^{(2)}(hv)^2}\right]=-\frac{v[(z+a)+m(z+h-a)]}{(1-nm)}$$
$$-\frac{m\pi h^2v^2(1-nm+2n)}{4(1-nm)^2}-0(v^3\ln v). \tag{26}$$

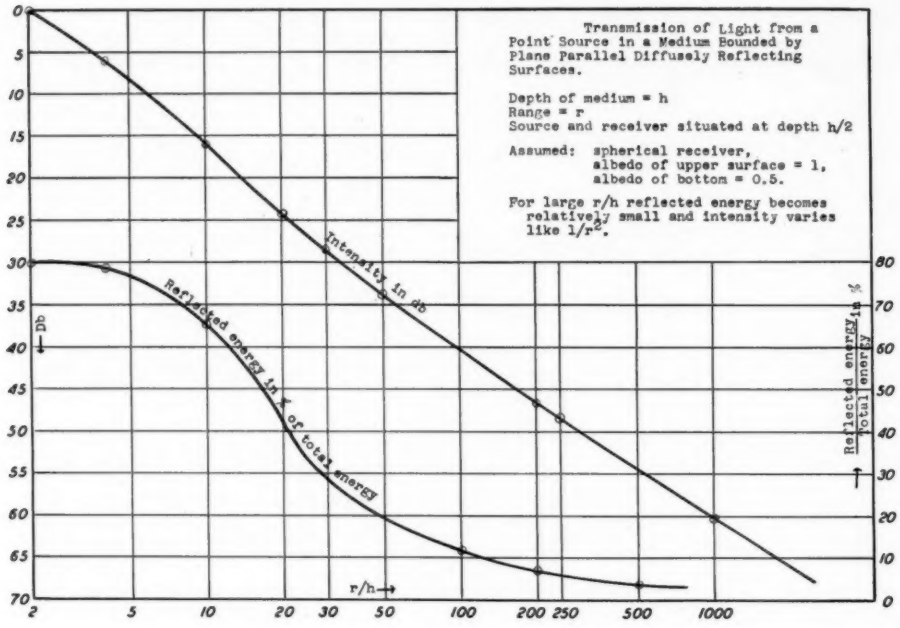
Transmission of Light from a Point Source in a Medium Bounded by Plane Parallel Diffusely Reflecting Surfaces.
Depth of medium = h
Range = r
Source and receiver situated at depth h/2
Assumed: spherical receiver, albedo of upper surface = 1, albedo of bottom = 0.5.
For large r/h reflected energy becomes relatively small and intensity varies like 1/r².
Intensity in db
Reflected energy in % of total energy
db
Reflected energy / total energy in %
r/h
0 5 10 15 20 25 30 35 40 45 50 55 60 65 70
80 70 60 50 40 30 20 10 0
2 5 10 20 30 50 100 200 250 500 1000

FIG. 5.

Substituting in (25) and using the relations

$$\int_0^\infty K_0(rv)v^2dv=\frac{\pi}{2r^3},\quad \int_0^\infty K_0(rv)v^3dv=\frac{4}{r^4}, \tag{27}$$

we obtain the following asymptotic expansion of F:

$$F-\frac{\pi\alpha^2}{[r^2+(z-a)^2]}+\frac{2\pi\alpha^2}{(1-nm)r^3}[n(z+a)+m(2h-a-z)]+\frac{8\pi\alpha^2nmh^2(1-nm+n+m)}{(1-nm)^2r^4}+0\left(\frac{\ln r}{r^5}\right). \tag{28}$$

VIII. ANALYSIS OF THE SINGLE-REFLECTION PROBLEM SHOWN IN FIG. 3 AND OF THE DOUBLE-REFLECTION PROBLEM SHOWN IN FIG. 4

As a check on the preceding analysis we shall treat *ab initio* the case of transmission of light from a point source situated near a plane diffusely reflecting surface (Fig. 3). We have

$$F=\pi\alpha^2\left(\frac{n}{\pi}\right)az\int\int_{-\infty}^{\infty}\frac{dx'dy'}{R_1^3R_2^3}=n\alpha^2az\int_0^\infty\frac{r'dr'}{(r'^2+a^2)^{\frac{3}{2}}}\int_0^{2\pi}\frac{d\phi'}{[z^2+r'^2+r^2-2rr'\cos(\phi'-\phi)]^{\frac{3}{2}}}$$

$$=n\alpha^2az\int_0^\infty\frac{r'dr'}{(r'^2+a^2)^{\frac{1}{2}}}\left(\frac{2\pi}{z}\right)\int_0^\infty e^{-zz}J_0(rx)J_0(r'x)xdx$$

$$=2\pi\alpha^2n\int_0^\infty e^{-zz}J_0(rx)xdxe^{-az}=\frac{2\pi\alpha^2n(a+z)}{[r^2+(a+z)^2]^{\frac{3}{2}}}. \tag{29}$$

The result agrees with the second term in (18).

Similarly in the problem of double reflection shown in Fig. 4, we have

$$F=\left(\frac{nm}{\pi}\right)\alpha^2ah^2(h-z)\int_{-\infty}^{\infty}\int\frac{dxdy}{R_3^3}\int_{-\infty}^{\infty}\int\frac{dx'dy'}{R_1^3R_2^4}, \tag{30}$$

$$\int_{-\infty}^{\infty}\int\frac{dx'dy'}{R_1^3R_2^4}=\int_0^{\infty}\frac{r'dr'}{(a^2+r'^2)^{\frac{1}{2}}}\int_0^{2\pi}\frac{d\phi'}{[h^2+r^2+r'^2-2rr'\cos\phi']^2}$$

$$=\frac{\pi}{h}\int_0^{\infty}\frac{r'dr'}{(a^2+r'^2)^{\frac{1}{2}}}\int_0^{\infty}K_1(hx)J_0(rx)J_0(r'x)x^2dx$$

$$=\frac{\pi}{ah}\int_0^{\infty}e^{-ax}K_1(hx)J_0(rx)x^2dx,$$

$$\int_{-\infty}^{\infty}\int\frac{dxdy}{R_3^3}\int_{-\infty}^{\infty}\int\frac{dx'dy'}{R_1^3R_2^4}=\frac{\pi}{ah}\int_0^{\infty}rdr\int_0^{2\pi}\frac{d\phi}{[(h-z)^2+\rho^2+r^2-2\rho r\cos\phi]^{\frac{1}{2}}}\int_0^{\infty}e^{-ax}K_1(hx)J_0(rx)x^2dx$$

$$=\frac{\pi}{ah}\int_0^{\infty}e^{-ax}K_1(hx)x^2dx\left[\frac{2\pi}{(h-z)}e^{-x(h-z)}J_0(\rho x)\right]$$

$$=\frac{2\pi^2}{ah(h-z)}\int_0^{\infty}e^{-x(a+h-z)}K_1(hx)J_0(\rho x)x^2dx,$$

$$F=2\pi\alpha^2nmh\int_0^{\infty}e^{-x(a+h-z)}K_1(hx)J_0(\rho x)x^2dx. \tag{31}$$

Equation (31) again agrees with the corresponding (fifth) term in Eq. (18).[2]

Figure 5 shows how, in a typical case, the variation in F approaches the inverse square law for ranges greater than several multiples of the depth.

SUMMARY

An *exact* solution is given for the total luminous flux incident on a spherical receiver from a point source situated in a medium bounded by diffusely reflecting parallel plane surfaces. In Section I a definition is given of albedo. In Section II it is shown that the problem of the illuminance of the *plane* surfaces by a point source involves the solution of a pair of simultaneous integral Eqs. (4) and (5). These integral equations are solved exactly in Section III (Eqs. (13), (14), and (8). In Section IV an expression is derived for the illumination of the spherical receiver. This expression is analyzed in terms of multiple reflections in Section V, and is transformed into a form suitable for numerical evaluation at large ranges in Section VI. An asymptotic expression for the illumination of the sphere at large ranges is derived in Section VII, while in Section VIII a direct derivation is given for the previously obtained expressions for single and double reflection from plane surfaces. Our method of solution can also be applied to cases where the reflecting surfaces do not obey the Lambert cos θ law.

ACKNOWLEDGMENT

The authors are indebted to Professor Carl Eckart for the formulation of this problem.

[2] Problems of interreflections have recently been treated by P. Moon in several papers in J. Opt. Soc. Am. **31** (1941), where references to earlier works on the subject will be found.

Zeeman Effect Data for the Spectra of Lanthanum—La I and La II

GEORGE R. HARRISON, NATHAN ROSEN,* AND J. RAND MCNALLY, JR.
George Eastman Research Laboratories of Physics, Massachusetts Institute of Technology, Cambridge, Massachusetts

(Received June 12, 1944)

Zeeman effect data are given for 152 lines of La I and 506 lines of La II in the wave-length range 2257A to 7484A. Spectrograms were made at fields of 81,230, 83,370, and 86,570 oersteds using a Bitter electromagnet, and the 24 plates obtained with three diffraction gratings operating simultaneously were measured with an automatic comparator. g values are given for almost all of the classified terms of La I and La II, and the determinations from various lines agree usually to within 0.004 g unit. This makes available an array of unusually precise data for the evaluation of perturbations in typical rich two-electron and three-electron spectra. The g-sum rule of Pauli is verified in a number of cases to within a few tenths of a percent.

AMONG the most completely analyzed spectra are those of lanthanum (Z-57). Many terms of La I, La II, and La III have been classified by Russell and Meggers.[1] Their analyses are so extensive as to leave little need of additional work from the standpoint of classification,

* Now at University of North Carolina, Chapel Hill, North Carolina.

[1] H. N. Russell and W. F. Meggers, Bur. Stand. J. Research 9, 625 (1932).

TABLE I. Analyzed Zeeman patterns of La I.

Wave-length	Arc int.	Combination	Type	g_1	g_2
7382.72	5	$a^2P_{1\frac{1}{2}} - z^2S^\circ_{\frac{1}{2}}$	7*b*?	(1.23)	1.91
7379.71	10	$a^3G_{4\frac{1}{2}} - 2^\circ_{4\frac{1}{2}}$	7*b*	1.12	1.12
7345.31	125	$a^3F_{2\frac{1}{2}} - x^3F^\circ_{2\frac{1}{2}}$	6	1.143	0.995
7334.17	100	$a^2D_{1\frac{1}{2}} - z^4F^\circ_{2\frac{1}{2}}$	5	0.794	1.096
7270.11	15	$a^2F_{2\frac{1}{2}} - y^4F^\circ_{3\frac{1}{2}}$	5	0.892	1.168
7219.90	20	$a^4F_{2\frac{1}{2}} - y^2F^\circ_{2\frac{1}{2}}$	6	(1.030)	0.809
7161.25	100	$a^2F_{2\frac{1}{2}} - x^2F^\circ_{2\frac{1}{2}}$	7*b*	0.896	0.896
7158.05	125	$a^2D_{2\frac{1}{2}} - z^4F^\circ_{3\frac{1}{2}}$	5	(1.198)	1.23
7068.36	100	$a^2D_{2\frac{1}{2}} - z^2F^\circ_{2\frac{1}{2}}$	6	1.198	0.904
7045.96	125	$a^4F_{1\frac{1}{2}} - y^2F^\circ_{2\frac{1}{2}}$	5	0.409	0.811
7032.03	40	$a^2P_{\frac{1}{2}} - z^2S^\circ_{\frac{1}{2}}$	6	(0.690)	1.89
7023.67	100*h*	$a^2F_{3\frac{1}{2}} - z^2G^\circ_{4\frac{1}{2}}$	7*b*	(1.137)	1.15
6925.21	100	$a^2F_{3\frac{1}{2}} - z^2G^\circ_{3\frac{1}{2}}$	5	0.898	1.103
6709.496	150	$a^4F_{2\frac{1}{2}} - y^4F^\circ_{3\frac{1}{2}}$	5	(1.030)	1.08
6692.87	50	$a^4F_{2\frac{1}{2}} - z^4G^\circ_{2\frac{1}{2}}$	6	1.03	1.03
6661.399	70	$a^4F_{4\frac{1}{2}} - z^4G^\circ_{4\frac{1}{2}}$	6	1.335	1.174
6650.801	100	$a^2D_{1\frac{1}{2}} - z^2D^\circ_{1\frac{1}{2}}$	6	0.795	0.917
6616.577	125	$a^4F_{3\frac{1}{2}} - z^4G^\circ_{3\frac{1}{2}}$	6	1.238	1.052
6608.257	50	$a^2G_{3\frac{1}{2}} - z^2H^\circ_{4\frac{1}{2}}$	5	0.92	0.94
6600.168	40	$a^4F_{3\frac{1}{2}} - z^4F^\circ_{2\frac{1}{2}}$	6	1.029	1.174
6593.467	25	$a^4F_{2\frac{1}{2}} - y^2D^\circ_{1\frac{1}{2}}$	5	1.031	0.802
6578.513	100	$a^2D_{1\frac{1}{2}} - z^2F^\circ_{2\frac{1}{2}}$	5	0.808	0.909
6565.434	15	$a^2D_{2\frac{1}{2}} - z^2P^\circ_{1\frac{1}{2}}$	4	1.201	1.329
6543.151	125	$a^4F_{1\frac{1}{2}} - z^4G^\circ_{2\frac{1}{2}}$	5	0.405	1.064
6485.549	50	$a^2F_{3\frac{1}{2}} - 2^\circ_{4\frac{1}{2}}$	7*b*	(1.137)	1.13
6468.434	25	$b^2D_{2\frac{1}{2}} - z^4S^\circ_{1\frac{1}{2}}$	4	1.246	1.774
6455.988	100	$a^2D_{2\frac{1}{2}} - z^2F^\circ_{2\frac{1}{2}}$	7*b*	(1.198)	1.19
6454.531	125	$a^4F_{1\frac{1}{2}} - z^4P^\circ_{2\frac{1}{2}}$	5	0.406	1.175
6410.995	100	$a^4F_{3\frac{1}{2}} - z^4G^\circ_{3\frac{1}{2}}$	7*b*	(1.030)	1.04
6394.234	150	$a^4F_{3\frac{1}{2}} - z^4G^\circ_{4\frac{1}{2}}$	4	(1.239)	1.17
6360.238	15	$a^2P_{\frac{1}{2}} - x^2D^\circ_{1\frac{1}{2}}$	5	0.690	0.855
6325.923	30	$a^2D_{2\frac{1}{2}} - y^2F^\circ_{3\frac{1}{2}}$	6	1.199	0.809
6293.565	30	$a^4F_{3\frac{1}{2}} - y^2D^\circ_{2\frac{1}{2}}$	5	1.24	1.20
6266.030	80	$a^2G_{4\frac{1}{2}} - z^2H^\circ_{5\frac{1}{2}}$	7*b*?	(1.12)	1.11
6249.929	300	$a^4F_{4\frac{1}{2}} - z^4G^\circ_{5\frac{1}{2}}$	4	(1.338)	1.29
6238.587	25	$a^4P_{2\frac{1}{2}} - x^4D^\circ_{1\frac{1}{2}}$	5	1.496	1.119
6165.699	100	$a^4P_{1\frac{1}{2}} - x^4D^\circ_{1\frac{1}{2}}$	6	1.703	1.134
6134.39	70*R*	$a^4P_{\frac{1}{2}} - x^4D^\circ_{\frac{1}{2}}$	6	2.660	0.152
6111.723	50	$a^2F_{3\frac{1}{2}} - w^2F^\circ_{2\frac{1}{2}}$	6	1.16	1.19
6108.492	70	$a^4P_{2\frac{1}{2}} - x^4D^\circ_{2\frac{1}{2}}$	6	1.505	1.274
6068.663	10	$a^4P_{\frac{1}{2}} - x^4D^\circ_{1\frac{1}{2}}$	4	2.654	1.154
6038.606	50	$a^4P_{1\frac{1}{2}} - x^4D^\circ_{2\frac{1}{2}}$	4	1.703	1.273
6007.381	70	$a^4F_{4\frac{1}{2}} - y^4F^\circ_{3\frac{1}{2}}$	5	1.341	1.185
5982.357	10	$a^4F_{1\frac{1}{2}} - y^2D^\circ_{2\frac{1}{2}}$	5	0.397	1.174
5960.586	10	$b^2D_{1\frac{1}{2}} - x^2D^\circ_{2\frac{1}{2}}$	5	0.929	1.241
5935.288	20	$a^4F_{3\frac{1}{2}} - y^4F^\circ_{2\frac{1}{2}}$	5	1.244	1.014
5930.667	100	$a^2D_{1\frac{1}{2}} - y^2F^\circ_{2\frac{1}{2}}$	5	(0.798)	0.81
5930.628	200	$a^2D_{2\frac{1}{2}} - y^2F^\circ_{3\frac{1}{2}}$	4	(1.198)	1.086
5917.629	25	$a^2D_{2\frac{1}{2}} - z^4G^\circ_{2\frac{1}{2}}$	6	1.195	1.062
5904.308	6	$a^2F_{2\frac{1}{2}} - x^4F^\circ_{2\frac{1}{2}}$	5	1.14	1.09
5894.847	25	$a^4P_{2\frac{1}{2}} - z^4S^\circ_{1\frac{1}{2}}$	4	1.506	1.788
5874.736	20	$a^4P_{1\frac{1}{2}} - v^2F^\circ_{2\frac{1}{2}}$	4	1.705	1.158
5855.591	30	$a^4F_{3\frac{1}{2}} - y^4F^\circ_{1\frac{1}{2}}$	5	1.030	0.731
5848.385	20	$z^4F^\circ_{1\frac{1}{2}} - e^4F_{2\frac{1}{2}}$	7*b*	0.93	0.93
5845.040	15	$a^2D_{2\frac{1}{2}} - z^4P^\circ_{2\frac{1}{2}}$	6	1.198	1.184
5829.726	25	$a^4P_{1\frac{1}{2}} - z^4S^\circ_{1\frac{1}{2}}$	6	1.70	1.78
5827.556	15	$b^2D_{2\frac{1}{2}} - y^4P^\circ_{2\frac{1}{2}}$	6	1.255	1.524
5823.827	15	$a^2F_{3\frac{1}{2}} - x^2D^\circ_{2\frac{1}{2}}$	4	1.130	1.240
5821.998	40	$a^2G_{3\frac{1}{2}} - y^2G^\circ_{3\frac{1}{2}}$	6	0.93	0.91
5791.345	200	$a^4F_{4\frac{1}{2}} - y^4F^\circ_{4\frac{1}{2}}$	6	1.33	1.28
5789.248	125	$a^4F_{3\frac{1}{2}} - y^4F^\circ_{3\frac{1}{2}}$	6	1.26	1.20
5761.845	60	$a^4F_{1\frac{1}{2}} - y^2P^\circ_{1\frac{1}{2}}$	6	0.404	1.020
5744.412	80	$a^4P_{2\frac{1}{2}} - x^4D^\circ_{3\frac{1}{2}}$	4	1.491	1.379
5734.959	15	$a^2G_{3\frac{1}{2}} - u^2F^\circ_{2\frac{1}{2}}$	7*b*?	(0.91)	0.92
5696.193	50	$a^2D_{2\frac{1}{2}} - z^4G^\circ_{3\frac{1}{2}}$	4	1.189	1.051
5657.731	50	$a^4F_{1\frac{1}{2}} - y^4F^\circ_{2\frac{1}{2}}$	5	0.414	1.012
5648.254	150	$a^2G_{4\frac{1}{2}} - y^2G^\circ_{4\frac{1}{2}}$	7*b*	1.117	1.117
5639.301	15	$a^4P_{1\frac{1}{2}} - x^2D^\circ_{2\frac{1}{2}}$	4	1.708	1.249
5632.025	20	$a^2F_{2\frac{1}{2}} - x^2D^\circ_{1\frac{1}{2}}$	5	0.887	(0.855)
5631.214	50	$a^4F_{2\frac{1}{2}} - y^4F^\circ_{3\frac{1}{2}}$	5	1.036	1.181
5588.342	40	$a^4F_{3\frac{1}{2}} - y^4F^\circ_{4\frac{1}{2}}$	5	(1.239)	1.27
5541.258	50*w*	$b^2D_{2\frac{1}{2}} - w^2P^\circ_{1\frac{1}{2}}$	4	(1.250)	1.27
5517.342	30	$a^2G_{4\frac{1}{2}} - u^2F^\circ_{3\frac{1}{2}}$	4?	(1.12)	1.13
5429.864	10	$a^4P_{\frac{1}{2}} - y^4P^\circ_{1\frac{1}{2}}$	4	2.630	1.590
5365.897	5	$a^2F_{2\frac{1}{2}} - y^4P^\circ_{1\frac{1}{2}}$	4	0.896	1.609
5357.873	40	$a^4P_{2\frac{1}{2}} - y^4P^\circ_{2\frac{1}{2}}$	6	(1.498)	1.53

TABLE I.—*Continued.*

Wave-length	Arc int.	Combination	Type	g_1	g_2
5323.573	3	$b^2D_{1\frac{1}{2}} - w^2P^\circ_{1\frac{1}{2}}$	6	0.953	1.335
5321.380	—	$a^2P_{1\frac{1}{2}} - w^2D^\circ_{2\frac{1}{2}}$	7*b*	1.23	1.23
5276.43	20	$b^2D_{1\frac{1}{2}} - w^2F^\circ_{2\frac{1}{2}}$	7*b*	(0.934)	0.90
5253.458	100	$a^2D_{2\frac{1}{2}} - y^4F^\circ_{1\frac{1}{2}}$	5	1.201	0.731
5234.274	200*r*	$a^4F_{4\frac{1}{2}} - 1^\circ_{2\frac{1}{2}}$	5	1.333	1.078
5211.870	300*r*	$a^4F_{4\frac{1}{2}} - y^4D^\circ_{2\frac{1}{2}}$	5	1.338	1.183
5177.311	150	$a^4F_{3\frac{1}{2}} - y^4D^\circ_{2\frac{1}{2}}$	4	1.240	1.363
5158.693	50	$a^2D_{1\frac{1}{2}} - y^2D^\circ_{2\frac{1}{2}}$	5	0.802	1.186
5145.422	100	$a^4F_{2\frac{1}{2}} - y^4D^\circ_{1\frac{1}{2}}$	4	1.025	1.191
5056.461	80	$a^4F_{1\frac{1}{2}} - y^4D^\circ_{1\frac{1}{2}}$	6	0.404	1.193
5050.569	80	$a^4F_{2\frac{1}{2}} - y^4D^\circ_{2\frac{1}{2}}$	6	1.031	1.362
5046.884	80	$a^4F_{3\frac{1}{2}} - y^4D^\circ_{2\frac{1}{2}}$	6?	(1.239)	1.18
4905.126	8	$a^2F_{2\frac{1}{2}} - u^2F^\circ_{2\frac{1}{2}}$	7*b*	0.89	0.89
4770.433	25	$a^2F_{2\frac{1}{2}} - w^2D^\circ_{1\frac{1}{2}}$	5	(0.893)	0.85
4766.894	100	$a^2D_{1\frac{1}{2}} - x^2F^\circ_{2\frac{1}{2}}$	5	0.807	0.894
4652.084	5	$a^4F_{3\frac{1}{2}} - x^4F^\circ_{2\frac{1}{2}}$	5	1.236	1.063
4650.331	8	$a^4F_{2\frac{1}{2}} - v^2F^\circ_{2\frac{1}{2}}$	6	(1.030)	1.16
4570.027	80	$a^4F_{4\frac{1}{2}} - x^4F^\circ_{4\frac{1}{2}}$	6	(1.338)	1.31
4567.909	100	$a^4F_{3\frac{1}{2}} - x^4F^\circ_{3\frac{1}{2}}$	–	(1.23)	1.23
4549.502	15	$a^4F_{2\frac{1}{2}} - x^4F^\circ_{2\frac{1}{2}}$	6	1.03	1.06
4541.788	30	$a^4P_{1\frac{1}{2}} - w^4D^\circ_{2\frac{1}{2}}$	4	1.701	1.261
4501.577	5	$a^4F_{2\frac{1}{2}} - x^2D^\circ_{2\frac{1}{2}}$	6	1.030	1.247
4500.219	15	$a^4P_{2\frac{1}{2}} - w^4D^\circ_{3\frac{1}{2}}$	4	1.491	1.352
4494.706	10	$a^4F_{1\frac{1}{2}} - x^4F^\circ_{1\frac{1}{2}}$	6	0.402	0.724
4491.756	8	$a^4P_{2\frac{1}{2}} - 7^\circ_{1\frac{1}{2}}$	7*b*?	(1.498)	1.49
4486.056	15	$a^4P_{1\frac{1}{2}} - v^2D^\circ_{2\frac{1}{2}}$	4	1.702	1.251
4468.964	10	$a^4F_{2\frac{1}{2}} - x^4F^\circ_{2\frac{1}{2}}$	5	1.027	1.228
4452.153	15	$a^2G_{3\frac{1}{2}} - y^2H^\circ_{4\frac{1}{2}}$	5	(0.91)	0.92
4443.949	3	$a^2D_{2\frac{1}{2}} - 3^\circ_{2\frac{1}{2}}$	6	1.15?	1.12?
4423.898	5	$a^2G_{4\frac{1}{2}} - y^2H^\circ_{5\frac{1}{2}}$	4	(1.12)	1.11
4402.649	5	$a^2P_{\frac{1}{2}} - u^2D^\circ_{1\frac{1}{2}}$	5	0.704	0.826
4389.868	5	$a^2P_{1\frac{1}{2}} - u^2D^\circ_{2\frac{1}{2}}$	4	(1.23)	1.18
4380.555	4	$a^2D_{2\frac{1}{2}} - w^2F^\circ_{2\frac{1}{2}}$	6	1.205	0.960
4340.727	50	$b^2D_{1\frac{1}{2}} - r^2F^\circ_{2\frac{1}{2}}$	7*b*?	(0.942)	0.92
4311.743	15	$a^4P_{\frac{1}{2}} - 8^\circ_{1\frac{1}{2}}$	4	2.647	1.537
4280.261	50	$a^2D_{2\frac{1}{2}} - w^2F^\circ_{3\frac{1}{2}}$	7*b*?	(1.198)	1.18
4271.157	30	$a^4P_{1\frac{1}{2}} - 9^\circ_{2\frac{1}{2}}$	4	(1.704)	1.428
4187.316	50	$a^2D_{1\frac{1}{2}} - w^2F^\circ_{2\frac{1}{2}}$	5	0.798	0.954
4172.316	8	$a^4F_{3\frac{1}{2}} - y^4G^\circ_{3\frac{1}{2}}$	6	1.234	0.976
4171.132	8	$a^4F_{4\frac{1}{2}} - y^4G^\circ_{4\frac{1}{2}}$	6	(1.338)	1.145
4157.513	10	$a^2D_{1\frac{1}{2}} - x^4D^\circ_{2\frac{1}{2}}$	5	0.791	1.268
4144.354	3	$a^4F_{2\frac{1}{2}} - y^6G^\circ_{3\frac{1}{2}}$	4	(1.030)	0.94
4137.025	15	$a^2D_{2\frac{1}{2}} - x^2D^\circ_{2\frac{1}{2}}$	6	1.198	1.242
4109.805	15	$a^2D_{2\frac{1}{2}} - v^2F^\circ_{3\frac{1}{2}}$	4	(1.198)	1.13
4089.612	40	$a^4F_{2\frac{1}{2}} - y^4G^\circ_{3\frac{1}{2}}$	4	(1.030)	0.99
4079.178	25	$a^2D_{1\frac{1}{2}} - v^2F^\circ_{2\frac{1}{2}}$	5	(0.798)	1.16
4065.580	30	$a^2D_{2\frac{1}{2}} - y^4P^\circ_{1\frac{1}{2}}$	4	1.198	1.600
4064.783	40	$a^4F_{3\frac{1}{2}} - y^4G^\circ_{4\frac{1}{2}}$	4	1.243	1.173
4060.321	80	$a^4F_{4\frac{1}{2}} - y^4G^\circ_{5\frac{1}{2}}$	4	(1.338)	1.28
4037.214	50	$a^2D_{1\frac{1}{2}} - x^2D^\circ_{1\frac{1}{2}}$	6	0.792	0.847
4015.393	100	$a^2D_{2\frac{1}{2}} - x^2P^\circ_{1\frac{1}{2}}$	4	1.195	1.433
3953.680	30	$a^2D_{2\frac{1}{2}} - y^4P^\circ_{2\frac{1}{2}}$	6	1.200	1.524
3927.558	40	$a^2D_{1\frac{1}{2}} - x^2P^\circ_{\frac{1}{2}}$	4	0.801	0.985
3704.531	25	$a^2D_{2\frac{1}{2}} - u^2F^\circ_{3\frac{1}{2}}$	4	(1.198)	1.13
3649.509	40	$a^2D_{1\frac{1}{2}} - u^2F^\circ_{2\frac{1}{2}}$	5	0.786	0.888
3641.522	25	$a^2D_{2\frac{1}{2}} - w^2D^\circ_{2\frac{1}{2}}$	7*b*	1.20	1.20
3613.077	12	$a^2D_{1\frac{1}{2}} - t^2F^\circ_{2\frac{1}{2}}$	5	(0.798)	0.87
3574.426	30	$a^2D_{1\frac{1}{2}} - w^2D^\circ_{1\frac{1}{2}}$	6	0.800	0.836
3514.063	8	$a^2D_{2\frac{1}{2}} - w^4D^\circ_{2\frac{1}{2}}$	6	1.17	1.24
3480.607	7	$a^2D_{2\frac{1}{2}} - v^2D^\circ_{2\frac{1}{2}}$	6	1.21	1.26
3461.184	10	$a^2D_{2\frac{1}{2}} - 7^\circ_{1\frac{1}{2}}$	4	(1.198)	1.492
3450.641	10	$a^2D_{1\frac{1}{2}} - v^2D^\circ_{1\frac{1}{2}}$	6	0.80	0.71
3404.52	9	$a^2D_{2\frac{1}{2}} - 8^\circ_{1\frac{1}{2}}$	4	1.190	1.528
3388.612	10	$a^2D_{1\frac{1}{2}} - w^4D^\circ_{2\frac{1}{2}}$	5	0.793	1.266
3362.040	10	$a^2D_{2\frac{1}{2}} - s^2F^\circ_{2\frac{1}{2}}$	6	1.194	1.036
3357.49	7	$a^2D_{1\frac{1}{2}} - v^2D^\circ_{2\frac{1}{2}}$	5	0.802	1.253
3342.224	80	$a^2D_{2\frac{1}{2}} - s^2F^\circ_{3\frac{1}{2}}$	4	(1.198)	1.16
3247.04	8	$a^2D_{1\frac{1}{2}} - s^2F^\circ_{2\frac{1}{2}}$	5	(0.798)	1.049
3235.65	8	$a^2D_{1\frac{1}{2}} - 9^\circ_{2\frac{1}{2}}$	5	0.788	1.420
3215.813	10	$a^2D_{2\frac{1}{2}} - r^2F^\circ_{3\frac{1}{2}}$	4	(1.198)	1.16
3179.78	8	$a^2D_{2\frac{1}{2}} - u^2D^\circ_{2\frac{1}{2}}$	6	1.197	1.145
3148.51	6	$a^2D_{1\frac{1}{2}} - u^2D^\circ_{1\frac{1}{2}}$	7*b*	0.80	0.80
3109.436	25	$a^2D_{2\frac{1}{2}} - v^2P^\circ_{1\frac{1}{2}}$	–	(1.198)	1.27
3096.023	15	$a^2D_{1\frac{1}{2}} - v^2P^\circ_{\frac{1}{2}}$	5	(0.798)	0.71
2725.586	10	$a^2D_{2\frac{1}{2}} - 11^\circ_{3\frac{1}{2}}$?	5	(1.198)	1.18?

and these spectra are excellent subjects for detailed examination of perturbations by Zeeman-effect and intensity studies.

Rybar[2] in 1911 studied Zeeman effects in lanthanum, using fields of 25,000 to 28,000 oersteds. He lists 42 resolved patterns and 24 unresolved patterns of symmetrical type. He states also that he measured 160 unresolved triplets, but data on these are not given in his article.

Meggers[3] in 1932 studied the magnetic resolution of 476 lanthanum lines in the range 2791 to 7484A, at fields of 33,000 oersteds, and his results were used by Russell and Meggers[1] in their lanthanum classification. Accuracy for a single determination is claimed to ± 0.02 units only, and evidence is presented there that Megger's g values might well be diminished by 0.78 percent on the average.

The exact determination of g values in complex spectra is so useful in determining the degree of perturbation between terms that it now seems worthwhile to publish new Zeeman data for La I and La II, obtained with much greater magnetic and spectrographic resolution than was available to Meggers. The g values he obtained were sufficiently precise for classification purposes and for initial tests of the Pauli g-sum rule, but are inadequate for closely approximate perturbation calculations. The spectrum of La I is of especial interest because, as pointed out by Russell and Meggers, it is representative of a typical three-electron spectrum, while at the same time it occupies a position in the Periodic System preceding the rare earths, and anticipates the addition of f-type electrons in their electron configurations.

[2] S. Rybar, Physik. Zeits. **12**, 889 (1911).
[3] W. F. Meggers, Bur. Stand. J. Research **9**, 239 (1932).

TABLE II. g values of terms in La I.

Level	Wave number	g LS	g RM	g Meas.	Number resolved patterns
$a^2D_{1\frac{1}{2}}$	0.00	.800	.790	.798	16
$a^2D_{2\frac{1}{2}}$	1,053.20	1.200	1.203	1.198	17
$a^4F_{1\frac{1}{2}}$	2,668.20	.400	.411	.405	8
$a^4F_{2\frac{1}{2}}$	3,010.01	1.029	1.032	1.030	12
$a^4F_{3\frac{1}{2}}$	3,494.58	1.238	1.222	1.239	8
$a^4F_{4\frac{1}{2}}$	4,121.61	1.333	1.327	1.338	4
$a^4P_{\frac{1}{2}}$	7,231.36	2.667	2.706	2.648	4
$a^4P_{1\frac{1}{2}}$	7,490.46	1.733	1.69	1.704	7
$a^4P_{2\frac{1}{2}}$	7,679.94	1.600	1.54	1.498	5
$a^2F_{2\frac{1}{2}}$	7,011.90	.857	.90	.893	3
$a^2F_{3\frac{1}{2}}$	8,052.15	1.143	1.13	1.137	2
$b^2D_{1\frac{1}{2}}$	8,446.03	.800	.89	0.942	2
$b^2D_{2\frac{1}{2}}$	9,183.77	1.200	1.29	1.250	2
$a^2P_{\frac{1}{2}}$	9,044.21	.667	.67	.690	1
$a^2P_{1\frac{1}{2}}$	9,719.44	1.333	1.32	1.23	0
$a^2G_{4\frac{1}{2}}$	9,919.94	1.111	1.12	1.12	0
$a^2G_{2\frac{1}{2}}$	9,960.96	.889	.91	.91	0
$z^4F^\circ_{1\frac{1}{2}}$	13,260.36	.400	—	.93	0
$z^4F^\circ_{2\frac{1}{2}}$	13,631.08	1.029	1.08	1.096	1
$z^4F^\circ_{3\frac{1}{2}}$	15,019.55	1.238	1.21	1.23	0
$z^2D^\circ_{1\frac{1}{2}}$	15,031.65	.800	.97	.917	1
$z^2F^\circ_{2\frac{1}{2}}$	15,196.80	.857	.90	.906	2
$z^2F^\circ_{3\frac{1}{2}}$	16,538.44	1.143	1.19	1.19	0
$z^2P^\circ_{1\frac{1}{2}}$	16,280.20	1.333	—	1.329	1
$y^2F^\circ_{2\frac{1}{2}}$	16,856.82	.857	.83	.810	3
$y^2F^\circ_{3\frac{1}{2}}$	17,910.18	1.143	1.08	1.086	1
$z^2P^\circ_{2\frac{1}{2}}$	18,157.00	1.600	1.20	1.175	2
$z^4G^\circ_{2\frac{1}{2}}$	17,947.16	.571	1.07	1.063	2
$z^4G^\circ_{3\frac{1}{2}}$	18,603.95	.984	1.06	1.051	2
$z^4G^\circ_{4\frac{1}{2}}$	19,129.34	1.172	1.15	1.173	2
$z^4G^\circ_{5\frac{1}{2}}$	20,117.40	1.273	1.27	1.290	1
$y^2D^\circ_{1\frac{1}{2}}$	18,172.39	.800	.83	.802	1
$y^2D^\circ_{2\frac{1}{2}}$	19,379.44	1.200	1.19	1.186	3
$y^2P^\circ_{1\frac{1}{2}}$	20,019.00	1.333	1.05	1.020	1
$y^4F^\circ_{1\frac{1}{2}}$	20,083.02	.400	.78	.731	2
$y^4F^\circ_{2\frac{1}{2}}$	20,338.30	1.029	1.01	1.013	2
$y^4F^\circ_{3\frac{1}{2}}$	20,763.31	1.238	1.18	1.178	3
$y^4F^\circ_{4\frac{1}{2}}$	21,384.06	1.333	1.28	1.278	1
$x^2F^\circ_{2\frac{1}{2}}$	20,972.22	.857	.90	.894	1
$x^2F^\circ_{3\frac{1}{2}}$	21,662.61	1.143	1.13	.995	1
$z^2G^\circ_{3\frac{1}{2}}$	21,447.92	.889	1.08	1.103	1
$z^2G^\circ_{4\frac{1}{2}}$	22,285.85	1.111	1.13	1.15	0
$y^4D^\circ_{\frac{1}{2}}$	22,246.64	.000	.03	−.22?	0
$y^4D^\circ_{1\frac{1}{2}}$	22,439.37	1.200	1.21	1.192	2
$y^4D^\circ_{2\frac{1}{2}}$	22,804.26	1.371	1.35	1.362	2
$y^4D^\circ_{3\frac{1}{2}}$	23,303.31	1.429	1.22	1.183	1
$1^\circ_{2\frac{1}{2}}$	23,221.16	—	1.11	1.078	1
$z^2S^\circ_{\frac{1}{2}}$	23,260.90	2.000	1.87	1.89	0
$2^\circ_{4\frac{1}{2}}$	23,466.85	—	1.12	1.12	0
$x^4D^\circ_{\frac{1}{2}}$	23,528.38	.000	.00	.152	1
$z^4D^\circ_{1\frac{1}{2}}$	23,704.76	1.200	1.15	1.135	3
$x^4D^\circ_{2\frac{1}{2}}$	24,046.06	1.371	1.22	1.272	3
$x^4D^\circ_{3\frac{1}{2}}$	25,083.42	1.429	1.41	1.379	1
$3^\circ_{2\frac{1}{2}}$	23,549.42	—	—	1.16	0
$w^2F^\circ_{2\frac{1}{2}}$	23,875.00	.857	.94	.957	2
$w^2F^\circ_{3\frac{1}{2}}$	24,409.70	1.143	1.17	1.17	0
$v^2F^\circ_{2\frac{1}{2}}$(?)	24,507.89	.857	1.20	1.159	3
$v^2F^\circ_{3\frac{1}{2}}$(?)	25,378.46	1.143	1.13	1.13	0
$z^4S^\circ_{1\frac{1}{2}}$	24,639.27	2.000	1.81	1.781	2
$x^2D^\circ_{1\frac{1}{2}}$	24,762.62	.800	.88	.855	1
$x^2D^\circ_{2\frac{1}{2}}$	25,218.25	1.200	1.25	1.244	5
$x^4F^\circ_{1\frac{1}{2}}$	24,910.39	.400	.73	.724	1
$x^4F^\circ_{2\frac{1}{2}}$	24,984.33	1.029	1.11	1.063	1
$x^4F^\circ_{3\frac{1}{2}}$	25,380.33	1.238	1.23	1.228	1
$x^4F^\circ_{4\frac{1}{2}}$	25,997.27	1.333	1.36	1.319	0
$z^2H^\circ_{4\frac{1}{2}}$	25,089.50	.909	.94	.94	0
$z^2H^\circ_{5\frac{1}{2}}$	25,874.68	1.091	—	1.11	0
$x^2P^\circ_{\frac{1}{2}}$	25,453.92	.667	.92	.985	1
$x^2P^\circ_{1\frac{1}{2}}$	25,950.39	1.333	1.41	1.433	1
$y^4P^\circ_{\frac{1}{2}}$	25,643.02	1.733	1.61	1.600	3
$y^4P^\circ_{2\frac{1}{2}}$	26,338.90	1.600	1.54	1.524	2
$y^4G^\circ_{3\frac{1}{2}}$	27,455.34	.984	.99	.976	1
$y^4G^\circ_{4\frac{1}{2}}$	28,089.18	1.172	1.16	1.159	2
$y^4G^\circ_{5\frac{1}{2}}$	28,743.21	1.273	1.29	1.28	0
$y^2G^\circ_{3\frac{1}{2}}$	27,132.50	.889	.95	.94	1
$y^2G^\circ_{4\frac{1}{2}}$	27,619.69	1.111	1.12	1.12	0
$w^2P^\circ_{1\frac{1}{2}}$	27,225.27	1.333	1.34	1.335	1
$u^2F^\circ_{2\frac{1}{2}}$	27,393.00	.857	.90	.888	1
$u^2F^\circ_{3\frac{1}{2}}$	28,039.54	1.143	1.13	1.13	0
$t^2F^\circ_{2\frac{1}{2}}$	27,669.38	.857	.88	.87	0
$w^2D^\circ_{1\frac{1}{2}}$	27,968.53	.800	.91	.836	1
$w^2D^\circ_{2\frac{1}{2}}$	28,506.39	1.200	1.15	1.20	0
$w^4D^\circ_{2\frac{1}{2}}$	29,502.17	1.371	—	1.263	2
$w^4D^\circ_{3\frac{1}{2}}$	29,894.91	1.429	1.29	1.352	1
$v^2D^\circ_{1\frac{1}{2}}$	28,971.82	.800	.94	.71	0
$v^2D^\circ_{2\frac{1}{2}}$	29,775.57	1.200	1.13	1.253	3
$7^\circ_{1\frac{1}{2}}$	29,936.73	—	1.54	1.492	1
$8^\circ_{1\frac{1}{2}}$	30,417.47	—	1.54	1.533	2
$e^4F_{2\frac{1}{2}}$	30,354.32	1.029	—	.93	0
$s^2F^\circ_{2\frac{1}{2}}$	30,788.40	.857	—	1.043	2
$s^2F^\circ_{2\frac{1}{2}}$	30,964.82	1.143	1.18	1.16	0
$9^\circ_{2\frac{1}{2}}$	30,896.88	—	1.45	1.424	2
$r^2F^\circ_{2\frac{1}{2}}$	31,477.16	.857	.88	.92	0
$r^2F^\circ_{3\frac{1}{2}}$	32,140.60	1.143	1.18	1.16	1
$u^2D^\circ_{1\frac{1}{2}}$	31,751.68	.800	.82	.80	0
$u^2D^\circ_{2\frac{1}{2}}$	32,492.80	1.200	1.17	1.145	1
$v^2P^\circ_{\frac{1}{2}}$	32,290.25	.667	—	.70	0
$v^2P^\circ_{1\frac{1}{2}}$	33,204.20	1.333	1.26	1.27	0
$y^2H^\circ_{4\frac{1}{2}}$	32,410.76	.909	.93	.92	0
$y^2H^\circ_{5\frac{1}{2}}$	32,518.12	1.091	1.11	1.11	0
$11^\circ_{3\frac{1}{2}}$?	37,731.90	—	—	1.18?	0

In this paper we give results obtained from Zeeman patterns of 152 lines of La I and 506 lines of La II in the range 2257 to 7484A. These data were obtained by measuring with an automatic comparator[4] two sets of spectrum photographs, each consisting of twelve 2×20 inch plates. These were obtained with a Bitter electromagnet,[5] using the technique described in previous papers.[6] Exposure Z 98 was taken with a

[4] G. R. Harrison, J. Opt. Soc. Am. **25**, 169 (1935); G. R. Harrison and J. P. Molnar, J. Opt. Soc. Am. **30**, 343 (1940).

[5] G. R. Harrison and F. Bitter, Phys. Rev. **57**, 15 (1940).

[6] G. R. Harrison and J. R. McNally, Jr., Phys. Rev. **58**, 703 (1940)—Ru.
J. P. Molnar and W. J. Hitchcock, J. Opt. Soc. Am. **30**, 523 (1940)—Rh I.
G. R. Harrison, W. E. Albertson, and N. F. Hosford, J. Opt. Soc. Am. **31**, 439 (1941)—Ce II.
N. Rosen, G. R. Harrison, and J. R. McNally, Jr., Phys. Rev. **60**, 722 (1941)—Pr II.
W. E. Albertson, G. R. Harrison, and J. R. McNally, Jr., Phys. Rev. **61**, 167 (1942)—Nd II.
J. R. McNally, Jr., G. R. Harrison, and H. B. Park, J. Opt. Soc. Am. **32**, 334 (1942)—Th II.
J. R. McNally, Jr., and G. R. Harrison, J. Opt. Soc. Am. **35**, 584 (1945)—Yt I, Yt II, Yt III.

TABLE III. Analyzed Zeeman patterns of La II.

Wave-length	Spk. int.	Combination	Type	g_1	g_2
7483.52	15	$a^3F_3 - z^3F^\circ_3$	7b	1.08	1.08
7297.99	2	$y^1F^\circ_3 - e^3D_2$	7b	(1.034)	1.06
7282.34	125	$a^3F_4 - z^3F^\circ_4$	7b(3)	1.26	1.24
7266.13	2	$y^1D^\circ_2 - e^3D_2$	3	0.894	1.070
7118.6	2	$x^3F^\circ_2 - e^1D_2$	3	0.821	1.032
7116.8	2	$a^1S_0 - z^3D^\circ_1$	7a	0/0	0.543
7104.7	2	$y^1D^\circ_2 - e^3D_1$	2	0.888	0.499
7066.21	150	$a^3F_2 - z^3F^\circ_2$	3	0.720	0.669
6968.73	12	$z^3D^\circ_1 - e^3F_2$	2	0.552	0.723
6958.08	50	$b^1D_2 - y^1D^\circ_2$	3	0.999	0.882
6954.50	10	$a^3F_2 - z^3F^\circ_3$	2	0.718	1.051
6952.49	5	$a^1D_2 - z^1F^\circ_3$	7b	(0.977)	1.00
6834.02	10	$a^3F_4 - z^1G^\circ_4$	3	1.248	0.976
6813.64	25	$z^3D^\circ_3 - e^1F_3$	3	1.287	0.946
6808.84	15	$a^3F_3 - z^3F^\circ_4$	2	(1.083)	1.259
6774.23	120	$a^3F_3 - z^1F^\circ_3$	3	1.08	1.03
6732.78	20	$z^3D^\circ_2 - e^3F_3$	1	1.149	1.049
6718.67	30	$y^1F^\circ_3 - e^3D_3$	3	1.038	1.279
6714.09	40	$z^3G^\circ_5 - e^3G_4$	2	(1.197)	1.14
6671.382	25	$a^3D_3 - y^3F^\circ_3$	3	1.341	1.086
6642.787	25	$z^3G^\circ_3 - e^3G_3$	3	0.757	0.872
6554.162	—	$z^3D^\circ_3 - e^3F_4$	1	1.293	1.118
6526.986	100	$a^3D_1 - y^3F^\circ_2$	2	0.503	0.755
6498.188	125	$z^3G^\circ_3 - e^3F_2$	2	(0.76)	0.72
6446.604	100	$z^3G^\circ_5 - e^3F_4$	2	1.18	(1.113)
6443.05	25h	$z^3P^\circ_1 - e^3D_2$	1	1.438	1.070
6390.484	100	$a^3D_2 - y^3F^\circ_3$	1	1.12	(1.086)
6374.107	15	$z^3D^\circ_3 - e^3D_2$	2	1.293	1.078
6358.137	15	$a^3P_1 - z^3D^\circ_1$	3	1.500	0.541
6337.88	2	$a^3F_2 - z^1F^\circ_3$	2	0.712	1.013
6320.392	100	$a^1D_2 - y^3F^\circ_2$	3	0.981	0.752
6315.817	25	$z^3P^\circ_1 - e^3D_1$	3	1.438	0.497
6310.926	100	$z^3G^\circ_4 - e^3G_4$	3	1.07	1.11
6307.266	10h	$z^3P^\circ_0 - e^3D_1$	7a	0/0	0.499
6305.45	5	$a^3F_4 - z^3H^\circ_4$	3	1.249	0.843
6296.096	150	$b^1D_2 - y^3D^\circ_1$	2	1.009	0.788
6273.763	50	$y^1F^\circ_3 - e^1D_2$	7b	1.03	1.03
6262.296	150	$a^3D_3 - y^3F^\circ_4$	1	(1.334)	1.239
6203.510	25	$z^3D^\circ_2 - e^3D_2$	3	1.162	1.071
6188.091	50	$z^3P^\circ_2 - e^3D_3$	1	1.446	1.268
6174.194	3	$a^3P_0 - z^3D^\circ_1$	7a	0/0	0.539
6172.730	5	$a^3F_3 - y^3F^\circ_2$	2	1.084	0.754
6146.531	8	$a^3F_4 - y^3F^\circ_3$	2	1.248	1.084
6129.554	25	$a^3P_2 - z^3D^\circ_3$	1	1.475	1.282
6126.086	25	$b^1D_2 - x^3F^\circ_2$	3	1.005	0.823
6100.379	15	$a^3P_1 - z^3D^\circ_2$	1	1.496	1.170
6085.485	5	$z^3D^\circ_2 - e^3D_1$	2	1.169	0.496
6074.045	—	$z^3G^\circ_4 - e^3F_4$	3	1.050	1.110
5991.98	4h	$z^3D^\circ_3 - e^1G_4$	1	1.287	1.057
5973.527	120	$z^3G^\circ_5 - e^3G_5$	7b	1.20	1.20
5971.09	8	$b^1D_2 - x^3F^\circ_2$	2	(1.005)	1.08
5957.90	4	$z^3D^\circ_1 - e^3D_2$	2	0.546	1.070
5948.236	20	$z^3G^\circ_3 - e^1F_3$	3	0.759	0.949
5936.218	20	$a^1D_2 - y^3F^\circ_2$	2	0.99	(1.086)
5927.71	30	$z^3D^\circ_2 - e^3D_2$	7b	(1.288)	1.27
5918.26	4	$z^1D^\circ_2 - e^3F_2$	3	0.924	0.721
5901.953	40	$z^3G^\circ_5 - e^1G_4$	2	1.205	1.068
5880.647	50	$a^3D_1 - z^1D^\circ_2$	2	0.502	0.925
5874.003	6	$a^3P_2 - z^3P^\circ_2$	7b	(1.481)	1.46
5863.709	80	$a^1G_4 - y^1F^\circ_3$	1	1.01	(1.03)
5848.949	3	$z^3D^\circ_1 - e^3D_1$	3	0.54	0.50
5808.332	60	$a^3F_2 - y^3F^\circ_3$	3	0.73	0.75
5805.783	120	$a^3F_3 - y^3F^\circ_3$	7b	(1.083)	1.09
5797.587	150	$a^3F_4 - y^3F^\circ_4$	3	1.25	1.23
5781.02	3	$b^1D_2 - y^3D^\circ_2$	3	(1.005)	1.166
5779.91	4	$z^3D^\circ_2 - e^3D_3$	2	1.170	1.269
5712.402	40	$a^1D_2 - z^1D^\circ_2$	3	0.970	0.924
5703.327	20	$a^3P_1 - z^3P^\circ_2$	1	(1.497)	1.47
5671.550	100	$z^3H^\circ_4 - e^3G_3$	1	(0.846)	0.87
5566.943	20	$y^3F^\circ_4 - e^3G_4$	3	1.239	1.141
5535.671	100	$b^1D_2 - y^3P^\circ_1$	1	1.004	1.265
5493.452	20	$a^3F_3 - y^3F^\circ_4$	2	(1.083)	1.230
5482.270	50	$a^3F_3 - y^3F^\circ_2$	2	0.724	1.084
5480.739	40	$y^3F^\circ_2 - e^3G_3$	2	0.767	0.886
5464.381	30	$a^3P_2 - y^1F^\circ_3$	1	1.479	1.032
5458.687	50	$z^1D^\circ_2 - e^1F_3$	2	(0.923)	0.94
5447.59	10	$z^3D^\circ_2 - e^1D_2$	3	1.165	1.042
5381.925	100	$y^3F^\circ_2 - e^3F_2$	3	(0.754)	0.72
5381.77	20	$y^3F^\circ_4 - e^3F_4$	3	1.230	1.115
5380.997	100	$a^1S_0 - y^3D^\circ_1$	7a	0/0	0.783
5377.095	200	$z^3H^\circ_5 - e^3G_4$	1	1.017	1.122
5340.67	100	$y^3F^\circ_3 - e^3F_3$	3	1.07	1.07
5303.556	125	$a^3D_2 - z^3D^\circ_1$	2	1.137	0.548
5301.984	200	$a^3D_3 - z^3D^\circ_2$	2	1.336	1.173
5290.836	100	$a^3F_2 - z^1D^\circ_2$	3	0.722	0.924
5279.15	15	$y^3F^\circ_3 - e^3G_4$	2	(1.086)	1.11
5259.389	50	$a^1D_2 - z^3G^\circ_3$	1	0.976	0.754
5226.216	20l	$z^3H^\circ_4 - e^3F_3$	1	0.840	1.059
5222.48	3h	$e^3D_2 - 1^\circ_3$	7b?	(1.071)	1.066
5188.229	500	$z^3H^\circ_6 - e^3G_5$	1?	(1.178)	1.20
5183.422	400	$a^3D_3 - z^3D^\circ_3$	3	(1.334)	1.28
5173.854	25h	$x^1F^\circ_3 - f^1D_2$	7b	(1.005)	1.02
5172.924	20l	$z^1D^\circ_2 - e^3D_2$	3	0.925	1.070
5167.28	10	$z^3H^\circ_4 - e^3G_4$	3	0.852	1.132
5163.615	40	$a^3F_4 - z^3G^\circ_4$	3	1.248	1.049
5156.741	40	$a^3F_3 - z^3G^\circ_3$	3	1.084	0.755
5122.990	200	$a^3D_2 - z^3D^\circ_2$	3	1.16	1.19
5114.573	200	$a^3D_1 - z^3D^\circ_1$	7b	0.50	0.50
5090.58	2h	$z^1D^\circ_2 - e^3D_1$	2	0.924	0.496
5080.21	10h	$z^1F^\circ_3 - e^3G_3$	3	1.019	0.877
5062.925	20	$a^3P_2 - y^3D^\circ_1$	2	1.482	0.780
5014.45	30hl	$x^1F^\circ_3 - f^1F_3$	3	(1.005)	0.98
5002.133	15	$y^3F^\circ_3 - e^3D_2$	2	(1.086)	1.08
4996.823	30	$y^3F^\circ_4 - e^1G_4$	3	1.236	1.061
4991.284	80	$a^1S_0 - z^1P^\circ_1$	7a	0/0	0.878
4986.834	100	$a^1D_2 - z^3D^\circ_1$	2	0.979	0.544
4970.392	100	$a^3D_2 - z^3P^\circ_1$	1	1.129	1.427
4952.069	40	$y^3F^\circ_4 - e^3D_3$	1	(1.232)	1.267
4946.466	50	$a^3D_1 - z^3D^\circ_2$	2	0.496	1.169
4934.825	100	$b^1D_2 - y^1P^\circ_1$	1	(1.005)	1.05
4921.783	400	$a^3F_4 - z^3G^\circ_5$	1	(1.248)	1.21
4911.337	20	$z^1G^\circ_4 - e^3F_3$	1	.98	(1.061)
4904.43	2h	$x^3P^\circ_0 - g^3D_1$	7a	0/0	0.630
4899.924	200	$a^3F_2 - z^3G^\circ_3$	7b	(0.721)	0.75
4860.908	100	$a^3F_4 - z^3D^\circ_3$	1	(1.248)	1.28
4850.584	20	$z^1G^\circ_4 - e^1F_3$	2	(0.969)	0.95
4824.066	150	$a^3P_0 - y^3D^\circ_1$	7a	0/0	0.782
4809.015	150	$a^3D_1 - z^3P^\circ_0$	7a	0.499	0/0
4796.688	10	$a^1G_4 - y^3D^\circ_3$	1	1.000	1.313
4748.729	200	$a^1G_4 - z^1H^\circ_5$	7b	1.00	1.00
4743.085	300	$z^3F^\circ_3 - e^3G_3$	3	1.055	0.872
4740.277	300	$a^3F_3 - z^3D^\circ_2$	1	1.074?	1.161?
4728.417	300	$a^1D_2 - z^3D^\circ_2$	2	0.978	1.286
4724.426	20	$a^3P_2 - y^3D^\circ_2$	3	1.483	1.167
4719.947	300	$z^1F^\circ_3 - e^3F_3$	3	1.03	1.06
4717.586	25	$z^1G^\circ_4 - e^3F_4$	3	0.969	1.108
4716.443	200	$a^3P_2 - z^1P^\circ_1$	2	1.480	0.876
4712.934	150	$a^3D_3 - y^1D^\circ_2$	2	1.331	0.883
4703.278	300r	$z^3F^\circ_4 - e^3F_3$	2	1.251	1.062
4699.627	200r	$a^3D_3 - y^1F^\circ_3$	3	1.333	1.033
4692.502	300	$z^3F^\circ_2 - e^3G_3$	2	0.668	0.878
4688.656	20	$y^3F^\circ_2 - e^3D_1$	2	0.749	0.496
4671.833	150	$z^1F^\circ_3 - e^3G_4$	2	(1.017)	1.12
4668.914	300r	$z^3F^\circ_3 - e^3F_2$	2	1.055	0.716
4663.765	200	$z^1F^\circ_3 - e^1F_3$	3	1.015	0.943
4662.511	200	$a^3F_2 - z^3D^\circ_1$	2	0.721	0.543
4655.497	300	$z^3F^\circ_4 - e^3G_4$	3	1.249	1.125
4647.509	50	$z^3F^\circ_4 - e^1F_3$	2	1.242	0.938

TABLE III.—*Continued.*

Wave-length	Spk. int.	Combination	Type	g_1	g_2
4645.281	40	$a^3F_3 - z^3D^\circ_3$	3	1.080	1.286
4636.425	20	$z^1D^\circ_2 - e^1D_2$	3	0.922	1.033
4634.971	5	$y^3D^\circ_3 - f^3D_2$	2	1.339	1.154
4619.882	200	$z^3F^\circ_2 - e^3F_3$	3	0.66	0.71
4613.393	100	$a^3P_1 - y^3D^\circ_2$	1	1.498	1.166
4605.782	100	$a^3P_1 - z^1P^\circ_1$	3	1.495	0.877
4580.057	100	$a^3P_1 - y^3P^\circ_0$	7*a*	1.498	0/0
4574.875	300	$a^1D_2 - z^3P^\circ_2$	3	0.975	1.457
4570.971	10	$a^3D_2 - y^1D^\circ_2$	3	1.136	0.885
4559.295	150	$a^3P_2 - y^3P^\circ_1$	2	1.483	1.270
4558.464	200	$a^3D_2 - y^1F^\circ_3$	1	1.134	1.034
4540.707	25	$z^1F^\circ_3 - e^3F_4$	2	(1.017)	1.091
4530.562	25	$b^1D_2 - x^3P^\circ_1$	1	1.007	1.496
4526.109	150	$a^3P_2 - y^3D^\circ_3$	1	1.484	1.311
4525.303	100	$z^3F^\circ_4 - e^3F_4$	3	1.248	1.113
4522.372	400	$a^3F_3 - z^3D^\circ_3$	3	0.721	1.169
4508.478	2	$a^3P_0 - z^1P^\circ_1$	7*a*	0/0	0.877
4502.16	10*hl*	$x^3P^\circ_1 - e^3S_1$	7*b*	(1.492)	1.48
4498.751	4*h*	$y^3F^\circ_3 - e^1D_2$	2	(1.086)	1.05
4481.198	2*h*	$z^1P^\circ_1 - f^3D_1$	3	0.874	0.498
4474.029	20	$y^3D^\circ_2 - f^3D_1$	2	1.165	0.498
4455.795	25	$a^3P_1 - y^3P^\circ_1$	3	1.498	1.270
4435.847	3	$a^3F_2 - z^3D^\circ_3$	2	0.726	1.293
4432.949	5	$a^3F_4 - y^1F^\circ_3$	2	1.249	1.035
4429.904	300	$a^3D_1 - y^1D^\circ_2$	2	0.494	0.887
4427.567	50	$z^3F^\circ_3 - e^3F_3$	–	1.06?	1.06?
4411.204	10*h*	$x^3F^\circ_4 - f^3D_3$	1	(1.245)	1.32
4385.204	10	$z^3F^\circ_3 - e^3G_4$	2	(1.056)	1.12
4383.45	50	$z^3F^\circ_2 - e^3F_3$	2	0.664	1.061
4378.097	30	$z^3F^\circ_3 - e^1F_3$	3	1.061	0.947
4364.666	50	$a^3P_0 - y^3P^\circ_1$	7*a*	0/0	1.271
4363.062	3	$y^3D^\circ_3 - f^3D_3$	7*b*?	(1.308)	1.33
4354.399	100	$a^1S_0 - y^1P^\circ_1$	7*a*	0/0	1.076
4337.777	3*h*	$x^3F^\circ_3 - f^3D_2$	1	(1.088)	1.09
4334.964	50	$z^3F^\circ_2 - e^1F_3$	2	0.658	0.941
4333.734	500	$a^1D_2 - y^1D^\circ_2$	3	0.980	0.884
4322.503	150	$a^1D_2 - y^1F^\circ_3$	2	(0.977)	1.02
4315.902	3*h*	$a^3D_3 - x^3F^\circ_2$	2	1.332	0.823
4300.435	20	$a^3F_2 - z^3P^\circ_2$	3	0.726	1.462
4296.048	200	$a^3P_2 - y^3P^\circ_2$	3?	1.48	1.48
4286.973	300	$z^3F^\circ_4 - e^3G_5$	1	(1.247)	1.21
4269.494	150	$z^3F^\circ_3 - e^3F_4$	2	(1.056)	1.09
4263.580	150	$z^1F^\circ_3 - e^1G_4$	7*b*?	(1.017)	1.04
4249.991	50	$z^3F^\circ_4 - e^1G_4$	3	1.246	1.053
4241.20	15*hl*	$e^3G_4 - 4^\circ_4$	3	1.14	1.26
4238.379	300	$a^3D_3 - x^3F^\circ_3$	3	1.333	1.089
4230.953	50	$z^1F^\circ_3 - e^3D_3$	3	1.020	1.275
4207.617	3*h*	$y^3D^\circ_1 - f^3D_1$	3	0.780	0.498
4204.038	25	$a^3P_1 - y^3P^\circ_2$	1	(1.497)	1.48
4196.547	150	$a^3D_2 - x^3F^\circ_2$	3	1.134	0.821
4194.354	15	$x^1F^\circ_3 - f^1G_4$	7*b*	(1.005)	1.01
4193.371	10	$y^3D^\circ_2 - f^3D_3$	2	(1.167)	1.32
4192.358	50	$z^3F^\circ_3 - e^3D_2$	2?	1.05	1.05
4180.97	10*h*	$y^3D^\circ_1 - f^3D_2$	2	0.792	1.123
4152.775	50	$z^3F^\circ_2 - e^3D_2$	3	0.661	1.069
4151.955	300	$a^3D_1 - y^3D^\circ_1$	3	0.499	0.782
4148.155	4	$z^1P^\circ_1 - f^1D_2$	2	(0.876)	1.037
4143.742	10*h*	$a^3P_2 - y^1P^\circ_1$	2	(1.482)	1.071
4141.740	200	$a^3D_3 - y^3D^\circ_2$	2	1.338	1.168
4132.501	10*h*	$y^3P^\circ_2 - g^3D_3$	1	1.464	1.219
4131.74	3	$e^3D_3 - 7^\circ_4$	1	(1.274)	1.23
4123.228	500	$a^3D_2 - x^3F^\circ_3$	1	(1.133)	1.099
4113.28	20	$e^1F_3 - 6^\circ_4$	1	(0.944)	0.97?
4099.542	100	$z^3F^\circ_2 - e^3D_1$	2	0.664	0.494
4086.714	500	$a^3F_2 - y^1D^\circ_2$	3	0.723	0.884
4077.340	400	$a^3D_1 - x^3F^\circ_2$	2	0.496	0.822
4076.711	5	$a^3F_2 - y^1F^\circ_3$	2	(0.721)	1.03
4067.392	80	$a^1D_2 - y^3D^\circ_1$	2	0.978	0.778
4058.085	—	$a^3P_1 - y^1P^\circ_1$	3	1.496	1.074
4050.079	60	$z^1F^\circ_3 - e^1D_2$	7*b*	1.02	1.02
4042.911	300	$a^1G_4 - x^1F^\circ_3$	7*b*	0.99	0.99
4036.596	15	$a^1S_0 - x^3P^\circ_1$	7*a*	0/0	1.494
4031.692	300	$a^3D_2 - y^3D^\circ_2$	3	1.13	1.16
4025.882	50	$a^3D_3 - z^1P^\circ_1$	2	1.133	0.878
4023.588	15	$z^3F^\circ_3 - e^1G_4$	7*b*	1.05	1.05
4020.19	2*h*	$y^3P^\circ_2 - e^3S_1$	–	1.47	1.47
3995.750	300	$a^1D_2 - x^3F^\circ_2$	3	0.983	0.821
3994.474	5	$z^3F^\circ_3 - e^3D_3$	3	(1.056)	1.276
3988.518	800	$a^3D_3 - y^3D^\circ_3$	3	(1.334)	1.29
3981.35	10*l*	$x^3F^\circ_2 - f^1D_2$	3	0.826	1.035
3979.08	2	$x^3F^\circ_4 - g^3D_3$	–	(1.245)	1.23
3958.54	2*h*	$z^3F^\circ_2 - e^3D_3$	2	(0.664)	1.284
3956.07	4	$y^1D^\circ_2 - f^3D_1$	2	0.884	0.501
3951.43	2*h*	$x^3F^\circ_3 - f^1F_3$	3	(1.088)	0.998
3944.15	2	$y^3D^\circ_2 - g^3D_2$	7*b*	1.16	1.16
3939.85	3*h*	$y^3D^\circ_3 - g^3D_3$	3	1.29	1.22
3936.221	50	$a^3F_3 - x^3F^\circ_2$	2	1.082	0.825
3932.523	2*h*	$y^1D^\circ_2 - f^3D_2$	3	(0.887)	1.121
3929.216	300	$a^1D_2 - x^3F^\circ_2$	2	0.980	1.093
3921.535	200	$a^3D_1 - y^3D^\circ_2$	2	0.500	1.166
3916.045	400	$a^3D_1 - z^1P^\circ_1$	3	0.491	0.877
3910.806	5*h*	$a^3D_2 - y^3P^\circ_1$	1	1.130	1.260
3886.368	200	$a^3D_2 - y^3D^\circ_3$	2	1.134	1.308
3871.631	15	$a^3F_3 - x^3F^\circ_3$	7*b*	1.085	1.085
3860.31	2	$x^3F^\circ_3 - g^3D_2$	1	(1.088)	1.14
3854.910	40	$a^3P_2 - x^3P^\circ_1$	7*b*	1.48	1.48
3849.013	150	$a^3F_2 - y^3D^\circ_1$	1	(0.721)	0.76
3845.997	50	$a^1D_2 - y^3D^\circ_2$	3	0.980	1.165
3840.709	70	$a^1D_2 - z^1P^\circ_1$	2	0.974	0.880
3836.4	—	$x^1F^\circ_3 - g^3F_4$	2	(1.008)	1.196
3835.074	15	$a^3P_1 - x^3P^\circ_0$	7*a*	1.500	0/0
3817.224	5	$e^3D_2 - 8^\circ_3$	1	(1.071)	0.97
3816.168	10*h*	$y^3D^\circ_1 - g^3D_1$	3	(0.782)	0.630
3814.02	2	$y^3P^\circ_1 - e^3S_1$	3	(1.278)	1.464
3808.781	10	$a^3D_3 - y^3P^\circ_2$	1	1.332	1.467
3807.1	1	$a^3D_1 - y^3P^\circ_1$	3	0.497	1.272
3801.009	1	$y^3D^\circ_2 - g^3D_3$	2	(1.167)	1.21
3798.19	2	$x^3F^\circ_2 - g^3D_2$	3	0.817	1.159
3794.773	200	$a^3F_4 - y^3D^\circ_3$	1	(1.248)	1.30
3790.822	300	$a^3F_3 - y^3D^\circ_2$	1	(1.083)	1.17
3784.797	2	$a^3F_2 - x^3F^\circ_2$	3	0.730	0.830
3783.06	1	$e^3G_4 - 7^\circ_4$	3	1.122	1.202
3780.674	50	$a^3P_1 - x^3P^\circ_1$	3?	1.494	1.494
3780.515	20	$x^3F^\circ_2 - f^3G_3$	2	(0.825)	0.86
3773.117	20*l*	$x^3F^\circ_3 - f^3G_4$	1	(1.088)	1.06
3768.98	2	$y^3D^\circ_3 - f^3F_3$	3	1.314	1.088
3767.05	10*h*	$y^3P^\circ_2 - e^3P_2$	3	(1.471)	1.200
3766.56	3*h*	$x^3F^\circ_4 - e^3H_4$	3	1.245	0.874
3759.080	150	$a^3F_4 - x^3F^\circ_4$	7*b*	1.24	1.24
3736.415	6	$x^3F^\circ_4 - f^3F_4$	3	1.30	1.20
3735.851	10	$a^1D_2 - y^3P^\circ_1$	1	0.976	1.269
3731.42	8	$y^3D^\circ_3 - e^3H_4$	1	1.305	0.876
3725.052	15	$a^3F_2 - x^3F^\circ_2$	2	0.725	1.092
3717.98	3	$x^3F^\circ_2 - e^1P_1$	1	0.818	1.335
3715.524	50	$a^3D_2 - y^3P^\circ_2$	3	1.131	1.472
3714.858	40	$a^3P_0 - x^3P^\circ_1$	7*a*	0/0	1.487
3713.544	60	$a^1D_2 - y^3D^\circ_3$	2	0.975	1.307
3705.818	80*h*	$a^3P_2 - x^3P^\circ_2$	3	(1.481)	1.50
3701.807	10	$y^3D^\circ_3 - f^3F_4$	1	(1.308)	1.146
3694.27	10	$y^1D^\circ_2 - f^1D_2$	3	(0.887)	1.031
3665.22	4	$x^3F^\circ_2 - g^3D_3$	2	0.853?	1.248?
3662.073	40	$a^3F_3 - y^3D^\circ_3$	3	1.080	1.310
3658.41	3	$x^1F^\circ_3 - g^1G_4$	2	(1.005)	1.03
3650.174	60	$a^3F_2 - y^3D^\circ_2$	3	0.715	1.163
3645.414	60	$a^3F_2 - z^1P^\circ_1$	1	0.717	0.874
3641.656	4	$y^3D^\circ_2 - f^3F_3$	1	(1.164)	1.09
3637.148	40	$a^3P_1 - x^3P^\circ_2$	7*b*	1.49	1.49
3628.822	40*h*	$a^3F_3 - x^3F^\circ_4$	2	1.082	1.249

TABLE III.—*Continued.*

Wave-length	Spk. int.	Combination	Type	g_1	g_2
3621.77	8	$a^3D_1 - y^3P^\circ_2$	2	0.498	1.473
3620.16	1	$y^1F^\circ_3 - f^1F_3$	3	1.02	0.99
3618.602	1	$z^3D^\circ_2 - f^3D_1$	2	1.174	(0.500)
3612.334	15*h*	$y^1D^\circ_2 - f^1F_3$	2	(0.887)	1.01
3611.09	3	$y^3P^\circ_0 - e^3P_1$	7*a*	0/0	1.495
3609.23	3	$x^1F^\circ_3 - h^1D_2$	7*b*	(1.005)	0.99
3608.16	6	$y^1D^\circ_2 - g^3D_1$	2	0.880	0.644
3606.432	3*h*	$y^3D^\circ_3 - f^1G_4$	1	1.301	1.024
3601.054	15	$a^3D_2 - y^1P^\circ_1$	7*b*	(1.133)	1.09
3598.927	3*hl*	$z^3D^\circ_2 - f^3D_2$	7*b*	(1.167)	1.13
3596.65	3	$y^3D^\circ_2 - g^1D_2$	7*b*	(1.164)	1.18
3590.66	1*h*	$y^3D^\circ_2 - e^3P_1$	1	1.160	1.545
3585.523	6*h*	$y^3P^\circ_1 - e^3P_2$	7*b*	(1.267)	1.24
3581.68	20*hl*	$y^3D^\circ_1 - f^3F_2$	7*b*	(0.782)	0.75
3580.099	3*h*	$x^3P^\circ_2 - f^3P_1$	7*b*	(1.494)	1.51
3578.89	3*h*	$x^3P^\circ_1 - f^3P_0$	7*a*	1.494	0/0
3576.581	3*d*	$x^3F^\circ_2 - e^3S_1$	1	0.826	1.458
3570.095	10	$x^3F^\circ_3 - f^3F_3$	7*b*	(1.088)	1.06
3557.251	8	$a^1D_2 - y^3P^\circ_2$	3	0.978	1.475
3550.815	4	$a^3F_2 - y^3P^\circ_1$	1	0.721	1.272
3536.37	3	$x^3F^\circ_3 - e^3H_4$	1	1.092	0.886
3533.67	3*h*	$z^3D^\circ_1 - f^3D_1$	7*b*	(0.542)	0.49
3530.661	6	$a^3F_2 - y^3D^\circ_3$	2	0.712	1.305
3526.77	2*h*	$x^3F^\circ_3 - g^1D_2$	7*b*	(1.088)	1.16
3520.711	4	$y^1D^\circ_2 - f^3G_3$	7*b*	(0.887)	0.87
3514.87	2	$z^3D^\circ_1 - f^3D_2$	2	0.534	1.104
3512.917	15	$a^3D_1 - y^1P^\circ_1$	3	0.496	1.076
3509.989	10	$a^3F_3 - y^3P^\circ_2$	1	1.083	1.476
3493.97	2	$z^1P^\circ_1 - e^3P_2$	2	0.959?	1.268?
3484.38	5	$z^3D^\circ_3 - f^3D_3$	7*b*	(1.288)	1.32
3474.84	8	$x^3F^\circ_2 - g^1D_2$	3	824	1.180
3460.31	3	$z^3P^\circ_2 - f^1F_3$	1	1.456	0.983
3453.168	40	$a^3D_3 - x^1F^\circ_3$	3	1.329	1.005
3452.184	40	$a^1D_2 - y^1P^\circ_1$	7*b*	(0.977)	1.06
3451.12	4*h*	$x^3P^\circ_1 - f^3P_1$	7*b*?	1.48?	1.48?
3432.81	3	$z^3D^\circ_2 - f^3D_3$	2	(1.167)	1.30
3427.57	3	$y^1F^\circ_3 - g^3D_3$	3	1.034	1.224
3423.9	2	$x^3F^\circ_3 - f^1G_4$	7*b*	(1.088)	1.04
3422.44	2*h*	$y^3D^\circ_1 - g^1D_2$	2	0.783	1.178
3420.54	2	$y^1D^\circ_2 - g^3D_3$	2	0.902	1.238
3411.76	25*hl*	$x^3P^\circ_2 - f^3P_2$	3	(1.494)	1.41
3407.00	4	$x^3P^\circ_0 - f^3P_1$	7*a*	0/0	1.531
3397.76	8	$y^1D^\circ_2 - f^3F_2$	3	0.89	0.76
3392.94	3	$z^3P^\circ_1 - g^3D_1$	3	1.435	0.621
3390.40	2	$z^3P^\circ_0 - g^3D_1$	7*a*	0/0	0.616
3380.910	100*h*	$a^3D_2 - x^3P^\circ_1$	1	1.133	1.495
3376.329	50	$a^3D_2 - x^1F^\circ_3$	1	(1.133)	0.999
3351.89	2	$x^1F^\circ_3 - i^1D_2$	1	(1.005)	1.03
3344.560	200*wh*	$a^3D_1 - x^3P^\circ_0$	7*a*	0.500	0/0
3337.488	300*wh*	$a^3D_3 - x^3P^\circ_2$	1	1.35	1.52
3326.21	3	$z^3P^\circ_2 - e^1P_1$	2	(1.460)	1.39
3325.33	2	$z^3D^\circ_2 - g^3D_1$	2	1.166	0.611
3310.62	3	$z^3D^\circ_3 - g^3D_2$	2	(1.288)	1.20
3306.98	8	$a^3F_4 - x^1F^\circ_3$	2	1.245	1.008
3303.11	150	$a^3D_1 - x^3P^\circ_1$	3	0.499	1.486
3294.44	5	$x^3P^\circ_1 - f^3P_2$	1	(1.492)	1.43
3277.83	3*h*	$x^3P^\circ_2 - g^3P_1$	7*b*	1.49	1.49
3267.31	3	$z^3P^\circ_1 - e^1P_1$	3	(1.437)	1.39
3265.67	200	$a^3D_2 - x^3P^\circ_2$	3	1.133	1.502
3263.99	4	$z^3D^\circ_2 - g^3D_2$	3	(1.167)	1.15
3253.42	4	$z^3D^\circ_1 - g^3D_1$	3	—	0.596
3249.351	80	$a^1D_2 - x^3P^\circ_1$	1	0.969	1.486
3245.120	300	$a^1D_2 - x^1F^\circ_3$	2	(0.977)	1.00
3226.008	2	$z^1D^\circ_2 - f^3D_2$	3	0.91	1.09
3224.770?	—	$z^1H^\circ_5 - g^1G_4$	1	1.01	(1.040)
3217.12	10*h*	$x^3P^\circ_2 - g^3P_2$	3	1.50	1.43
3212.56	2	$z^3P^\circ_2 - e^3S_1$	2	(1.460)	1.47
3209.13	3	$z^3D^\circ_3 - g^3D_3$	3	1.265	1.216
3205.76	5	$a^3F_3 - x^1F^\circ_3$	3	1.092	1.026
3204.55	2	$z^3D^\circ_2 - e^1P_1$	1	(1.167)	1.31
3194.70	2	$z^3D^\circ_1 - g^3D_2$	2	0.538	1.150
3193.02	60	$a^3D_1 - x^3P^\circ_2$	2	0.495	1.493
3191.39	8*hl*	$x^3P^\circ_2 - h^3D_2$	3	1.488	1.213
3165.19	4	$y^3D^\circ_3 - h^1D_2$	2	1.310	1.030
3160.56	3*h*	$y^3P^\circ_2 - f^3P_1$	1	(1.471)	1.51
3157.58	2	$z^3P^\circ_1 - e^3S_1$	3	(1.432)	1.47
3156.35	2*h*	$y^1P^\circ_1 - i^1D_2$	1	(1.074)	1.06
3145.7	2*h*	$z^3D^\circ_2 - f^3F_2$	3	(1.167)	0.741
3142.762	50	$a^1D_2 - x^3P^\circ_2$	3	0.973	1.490
3132.14	3*h*	$x^3P^\circ_0 - g^3P_1$	7*a*	0/0	1.494
3130.25	4	$z^3P^\circ_2 - g^1D_2$	3	1.461	1.189
3125.72	3	$z^3P^\circ_2 - e^3P_1$	1	(1.460)	1.52
3112.63	10*hl*	$x^3P^\circ_1 - g^3P_2$	1	(1.492)	1.43
3108.462	8	$a^3F_2 - x^3P^\circ_1$	1	0.720	1.495
3104.589	50	$a^3F_2 - x^1F^\circ_3$	2	0.721	1.008
3088.53	3*h*	$x^3P^\circ_1 - h^3D_2$	1	1.464?	1.210?
3081.42	7	$z^3D^\circ_1 - f^3F_2$	2	(0.543)	0.712
3075.51	2	$y^3P^\circ_1 - f^3S_1$	3	1.265	1.955
3069.45	3	$z^3D^\circ_3 - e^3H_4$	–	1.285	0.881
3068.96	3	$x^3P^\circ_0 - h^3D_1$	7*a*	0/0	0.506
3059.91	7	$z^1P^\circ_1 - f^3P_0$	7*a*	0.877	0/0
3054.02	6	$z^3D^\circ_2 - f^3F_3$	1	(1.167)	1.10
3049.39	3	$z^3D^\circ_3 - f^3F_4$	1	(1.288)	1.157
3045.63	1	$z^3G^\circ_5 - e^3H_4$	2	1.197	(0.883)
3036.43	2	$z^3D^\circ_1 - e^3S_1$	3	0.540	1.457
3035.80	1	$z^3G^\circ_4 - f^3G_4$	2	(0.757)	1.034
3028.64	2*h*	$y^3P^\circ_2 - f^3P_2$	3	1.46	1.42
3025.88	3	$z^3G^\circ_5 - f^3F_4$	2	(1.197)	1.15
3022.26	3	$z^3D^\circ_2 - g^1D_2$	3	(1.167)	1.19
3010.78	—	$a^3F_2 - x^3P^\circ_2$	3	0.719	1.492
3007.32	4	$z^1D^\circ_2 - f^1F_3$	2	(0.923)	0.97
2985.75	2	$z^3G^\circ_3 - f^3F_2$	7*b*	0.75	0.75
2985.432	3	$x^3F^\circ_2 - h^1D_2$	3	0.817	1.032
2984.336	2	$z^3D^\circ_3 - f^1G_4$	1	(1.288)	1.039
2983.45	2	$z^3G^\circ_4 - f^3F_3$	1	(1.049)	1.07
2976.83	3	$y^3P^\circ_0 - f^3P_1$	7*a*	0/0	1.530
2971.48	1	$y^3F^\circ_4 - f^3G_5$	2	(1.232)	0.868
2966.57	4	$z^3G^\circ_5 - e^3H_5$	3	1.191	1.027
2966.05	2	$z^1P^\circ_1 - f^3P_1$	3	0.861	1.529
2962.910	15	$y^3D^\circ_2 - f^3P_1$	1	1.160	1.524
2959.850	5	$z^3G^\circ_4 - e^3H_4$	3	1.042	0.887
2958.71	1	$z^3D^\circ_1 - e^3P_1$	3	(0.542)	1.559
2951.45	3	$y^3P^\circ_1 - i^1D_2$	1	1.254	1.054
2950.492	50	$z^1H^\circ_5 - e^1I_6$	7*b*	0.996	0.996
2943.551	6*hl*	$z^1D^\circ_2 - f^3G_3$	1	(0.923)	0.88
2939.618	3*h*	$y^1P^\circ_1 - h^3D_1$	3	1.073	0.494
2929.88	7	$y^3D^\circ_1 - f^3P_0$	7*a*	0.781	0/0
2925.148	5*h*	$y^1P^\circ_1 - h^3D_2$	2	(1.074)	1.20
2923.90	20	$y^3D^\circ_3 - f^3P_2$	1	(1.308)	1.42
2913.61	2	$y^3F^\circ_2 - f^1D_2$	3	0.762	1.027
2905.52	4*hl*	$z^1D^\circ_2 - e^1P_1$	1	0.915	1.335
2899.80	4*hl*	$y^3F^\circ_4 - g^3D_3$	7*b*	1.23	1.23
2897.76	5*hl*	$y^3F^\circ_3 - g^3D_2$	1	(1.086)	1.13
2893.071	60	$z^3G^\circ_5 - e^3H_6$	1	(1.197)	1.17
2889.11	1	$z^1P^\circ_1 - i^1D_2$	2	(0.876)	1.04
2885.141	50	$z^3G^\circ_4 - e^3H_5$	1	(1.049)	1.03
2883.35	1	$z^3P^\circ_2 - g^3F_3$	1	1.465	1.084
2880.644	40	$z^3G^\circ_3 - e^3H_4$	2	(0.757)	0.88
2873.18	2	$z^1D^\circ_2 - g^3D_3$	2	(0.923)	1.205
2862.967	15*hl*	$z^3G^\circ_3 - f^3F_4$	2	0.755	1.129
2862.373	6	$y^3F^\circ_2 - f^1F_3$	2	0.756	0.988
2859.757	5	$y^3F^\circ_2 - g^3D_1$	2	(0.754)	0.62
2855.902	50*hl*	$y^1F^\circ_3 - g^1G_4$	2	(1.034)	1.04
2853.72	4*h*	$y^3P^\circ_2 - h^3D_2$	3	1.478	1.230
2848.34	6	$y^3F^\circ_3 - f^3G_4$	1	(1.086)	1.06
2846.69	5	$y^3D^\circ_2 - f^3P_2$	3	1.166	1.416
2843.659	4	$y^3D^\circ_1 - f^3P_1$	3	0.777	1.528
2838.438	5	$y^3F^\circ_4 - f^3G_5$	1	(1.232)	1.21

TABLE III.—*Continued.*

Wave-length	Spk. int.	Combination	Type	g_1	g_2
2832.55	5	$z^3D^\circ_2 - g^3F_2$	3	1.164	0.666
2825.815	1	$y^1F^\circ_3 - h^1D_2$	1	(1.034)	1.04
2825.51	5	$z^3D^\circ_3 - g^3F_3$	3	1.289	1.089
2821.043	5	$y^1D^\circ_2 - h^1D_2$	3	0.887	1.038
2818.39	3	$z^1D^\circ_2 - e^3S_1$	1	(0.923)	1.446
2815.35	6	$z^3F^\circ_3 - f^3D_2$	1	(1.056)	1.08
2813.72	5	$z^3F^\circ_4 - f^3D_3$	1	(1.247)	1.29
2813.03	3	$z^1G^\circ_4 - f^1F_3$	1	(0.969)	0.94?
2809.34	2	$z^3F^\circ_2 - f^3D_1$	2	(0.664)	0.55
2808.39	150	$b^1D_2 - x^1P^\circ_1$	2	(1.005)	1.00
2807.20	1	$x^3F^\circ_2 - i^1D_2$	3	0.830	1.055
2805.59	5	$z^3G^\circ_3 - f^1G_4$	2	0.763	1.033
2804.53	4	$y^3F^\circ_2 - f^3G_3$	2	(0.754)	0.84
2798.546	40*hl*	$z^3D^\circ_3 - g^3F_4$	1	(1.288)	1.20
2796.366	5	$z^1F^\circ_3 - f^1D_2$	1	(1.017)	1.03
2791.513	25	$z^3D^\circ_2 - g^3F_3$	1	(1.167)	1.08
2780.234	10*h*	$z^3D^\circ_1 - g^3F_2$	2	(0.542)	0.58
2779.778	10	$y^3D^\circ_3 - g^3P_2$	1	(1.308)	1.40
2778.757	10	$z^3G^\circ_5 - g^3F_4$	2?	(1.196)	1.196
2773.86	1	$z^1P^\circ_1 - g^3P_0$	7*a*	0.870	0/0
2761.111	5	$y^3P^\circ_1 - h^3D_1$	3	1.268	0.503
2759.156	3	$z^3H^\circ_4 - e^3H_5$	2	1.178?	1.045?
2758.652	3	$y^1P^\circ_1 - f^1S_0$	7*a*	1.074	0/0
2752.858	10	$y^3D^\circ_2 - g^3P_1$	1	1.156	1.473
2748.317	8	$y^3P^\circ_1 - h^3D_2$	1	(1.267)	1.22
2736.90	2	$z^3H^\circ_5 - e^3H_4$	2	1.03	(0.883)
2736.41	3	$y^3D^\circ_1 - f^3P_2$	2	0.773	1.412
2732.415	10	$z^3G^\circ_4 - g^3F_3$	1	1.06	(1.085)
2727.54	2	$z^3P^\circ_2 - h^1D_2$	3	1.464	1.044
2715.416	10*hl*	$y^3P^\circ_0 - h^3D_1$	7*a*	0/0	0.510
2712.51	1	$z^1P^\circ_1 - g^3P_2$	2	(0.876)	1.41
2709.92	3	$y^3D^\circ_2 - g^3P_2$	3	1.184	1.430
2706.49	2	$z^1P^\circ_1 - h^3D_1$	3	0.878	0.518
2702.159	8	$z^3G^\circ_3 - g^3F_2$	2	(0.757)	0.70
2695.458	35	$z^3H^\circ_6 - e^3H_6$	3	(1.178)	1.14
2694.207	5	$z^1P^\circ_1 - h^3D_2$	2	(0.876)	1.21
2681.501	10	$z^3H^\circ_4 - e^3H_4$	3	0.85	0.88
2675.655	5	$z^3D^\circ_3 - h^1D_2$	2	1.295	1.061
2673.743	3	$z^3P^\circ_1 - f^3P_0$	7*a*	1.443	0/0
2672.906	30	$z^3H^\circ_5 - e^3H_5$	3	1.02	(1.029)
2670.05	2	$x^3F^\circ_3 - g^3P_2$	1	(1.088)	1.399
2666.178	6	$z^3H^\circ_4 - f^3F_4$	3	(0.846)	1.139
2665.679	4	$y^1F^\circ_3 - i^1D_2$	1	(1.034)	1.05
2661.665	3	$z^1F^\circ_3 - f^1G_4$	2	(1.017)	1.04
2661.36	4	$y^1D^\circ_2 - i^1D_2$	3	0.91	1.08
2647.36	4	$z^3F^\circ_3 - f^1F_3$	3	1.03	0.98
2644.70	1	$y^3F^\circ_3 - f^1G_4$	1	(1.086)	1.05
2631.93	8	$y^1F^\circ_3 - f^3P_2$	1	(1.034)	1.421
2631.52	4	$z^3F^\circ_2 - f^1F_3$	2	(0.664)	0.979
2620.03	7	$z^3H^\circ_4 - e^3H_5$	2	(0.846)	1.030
2617.29	1	$z^3G^\circ_4 - g^1G_4$	7*b*	1.05	1.05
2616.314	7*hl*	$z^3H^\circ_4 - f^1G_4$	3	(0.847)	1.02
2613.097	4	$z^3H^\circ_5 - e^3H_6$	2	(1.017)	1.11
2610.335	150	$a^1S_0 - x^1P^\circ_1$	7*a*	0/0	0.990
2601.777	5	$z^3P^\circ_1 - f^3P_1$	3	(1.432)	1.48
2600.869	2	$y^3P^\circ_1 - f^1S_0$	7*a*	1.265	0/0
2596.32	3	$z^1D^\circ_2 - g^3F_2$	3	0.913	0.657
2596.091	20	$z^1G^\circ_4 - e^3H_4$	3	0.98	0.90
2586.37	10	$z^3D^\circ_1 - f^3P_0$	7*a*	0.532	0/0
2582.960	8	$y^3F^\circ_4 - g^3F_3$	2	1.21	1.08
2582.56	6	$z^3F^\circ_2 - f^3G_3$	2	(0.664)	0.83
2580.823	8*hl*	$z^3F^\circ_4 - f^3G_5$	1	(1.247)	1.21
2566.078	10*hl*	$z^3F^\circ_3 - f^3G_4$	1	(1.056)	1.05
2561.848	20	$z^3D^\circ_2 - f^3P_1$	1	1.170	1.515
2560.374	50	$y^3F^\circ_4 - g^3F_4$	3	1.22	1.20
2558.991	3	$z^1F^\circ_3 - f^3F_3$	3	(1.017)	1.12
2552.600	7	$y^3F^\circ_3 - g^3F_2$	2	1.091	0.684
2546.40	20*hl*	$z^3P^\circ_2 - f^3P_2$	3	(1.461)	1.42
2542.40	6	$z^3P^\circ_1 - i^1D_2$	1	1.426	1.052
2541.59	4	$z^1F^\circ_3 - e^3H_4$	1	(1.017)	0.90
2534.98	6	$z^3G^\circ_4 - f^1G_4$	3	0.97	1.01
2533.14	15	$a^3P_2 - x^1P_1$	2	1.487	1.007
2531.60	8	$z^3D^\circ_3 - i^1D_2$	2	(1.288)	1.07
2523.07	5*hl*	$z^3F^\circ_4 - f^3F_4$	3	1.225?	1.125
2519.215	50	$y^3F^\circ_3 - g^3F_3$	7*b*	1.08	1.08
2515.79	4	$z^3F^\circ_2 - f^3F_2$	3	(0.664)	0.74
2501.18	15*h*	$z^3D^\circ_3 - f^3P_2$	1	(1.288)	1.40
2487.588	40	$y^3F^\circ_2 - g^3F_2$	3	0.75	0.68
2479.84	10	$y^3F^\circ_4 - g^1G_4$	3	(1.232)	1.057
2474.51	3	$z^3D^\circ_2 - f^3P_2$	3	(1.167)	1.414
2472.43	10	$z^3H^\circ_4 - g^3F_4$	3	(0.846)	1.208
2471.900	20	$a^3P_0 - x^1P^\circ_1$	7*a*	0/0	1.000
2471.06	5	$z^3P^\circ_2 - g^3P_1$	1	(1.460)	1.49
2455.88	10	$y^3F^\circ_2 - g^3F_3$	2	0.755	1.083
2452.74	8	$z^3P^\circ_1 - g^3P_0$	7*a*	1.450	0/0
2436.42	15*W*	$z^3P^\circ_2 - g^3P_2$	3	(1.460)	1.44
2404.643	6	$z^3P^\circ_1 - g^3P_2$	1	(1.432)	1.42
2403.28	7	$z^3D^\circ_2 - g^3P_1$	1	(1.167)	1.468
2399.66	20*hl*	$z^1G^\circ_4 - g^3F_4$	3	0.963	1.179
2397.237	7*hl*	$z^3H^\circ_4 - g^1G_4$	3	(0.846)	1.039
2319.441	20	$a^3D_2 - x^1P_1$	2	(1.133)	1.02
2256.76	30	$a^1D_2 - x^1P^\circ_1$	1	(0.977)	0.96

field of 81,230 oersteds, while Z 101 was taken at 86,570 oersteds for the perpendicularly-polarized component and 83,770 oersteds for the parallel-polarized component. The spectrum from 2200A to 8000A was covered at dispersions ranging from 0.4 to 1.6A/mm, with three gratings used in the manner previously described.[6] Electrodes for the horizontal arc were made by compressing one part of lanthanum chloride in four parts of silver powder to form 1 inch electrodes of $\frac{1}{8}$ inch diameter.

Russell and Meggers state that the probable error corresponding to unit weight in one of their g values is ± 0.020. The corresponding error for our results is believed to be ± 0.004, this improvement resulting principally from the availability of stronger fields.

Table I contains a list of the Zeeman patterns of La I which we have analyzed. The columns, in order, give: the wave-length in angstroms of the line as taken from the Massachusetts Institute of Technology card catalog; the arc intensity of the line; the term combination which is responsible for the line as assigned by Russell and Meggers (except in a few cases where typographical errors have been corrected); the type of the observed pattern in accordance with the shorthand notation explained below; and the

TABLE IV. g values of terms in La II.

Level	Wave number	g_{LS}	g_{RM}	g Meas.	Number resolved patterns
a^3F_2	0.00	.667	.730	.721	20
a^3F_3	1,016.10	1.083	1.092	1.083	11
a^3F_4	1,970.70	1.250	1.258	1.248	6
a^1D_2	1,394.46	1.000	.987	.977	18
a^3D_1	1,895.15	.500	.520	.498	15
a^3D_2	2,591.60	1.167	1.140	1.133	12
a^3D_3	3,250.35	1.333	1.337	1.334	11
a^3P_0	5,249.70	0/0	0/0	0/0	6
a^3P_1	5,718.12	1.500	1.506	1.497	8
a^3P_2	6,227.42	1.500	1.488	1.481	9
a^1S_0	7,394.57	0/0	0/0	0/0	6
a^1G_4	7,473.32	1.000	1.003	1.000	1
b^1D_2	10,094.86	1.000	1.015	1.005	7
$z^3F^\circ_2$	14,147.98	.667	.676	.664	9
$z^3F^\circ_3$	14,375.17	1.083	1.087	1.056	5
$z^3F^\circ_4$	15,698.74	1.250	1.258	1.247	7
$z^1F^\circ_3$	15,773.77	1.000	1.047	1.017	5
$z^1G^\circ_4$	16,599.17	1.000	.996	.969	4
$y^3F^\circ_2$	17,211.93	.667	.757	.754	9
$y^3F^\circ_3$	18,235.56	1.083	1.090	1.086	5
$y^3F^\circ_4$	19,214.54	1.250	1.243	1.232	7
$z^3H^\circ_4$	17,825.62	.800	.865	.846	8
$z^3H^\circ_5$	18,580.41	1.033	1.082	1.017	1
$z^3H^\circ_6$	19,749.62	1.167	1.17	1.178?	1
$z^1D^\circ_2$	18,895.41	1.000	.931	.923	12
$z^3G^\circ_3$	20,402.82	.750	.775	.757	7
$z^3G^\circ_4$	21,331.60	1.050	1.060	1.049	3
$z^3G^\circ_5$	22,282.90	1.200	1.203	1.197	5
$z^3D^\circ_1$	21,441.73	.500	.547	.542	13
$z^3D^\circ_2$	22,106.02	1.167	1.186	1.167	14
$z^3D^\circ_3$	22,537.30	1.333	1.317	1.288	12
$z^3P^\circ_0$	22,683.70	0/0	0/0	0/0	3
$z^3P^\circ_1$	22,705.15	1.500	1.458	1.431	6
$z^3P^\circ_2$	23,246.93	1.500	1.462	1.459	7
$y^1D^\circ_2$	24,462.66	1.000	.897	.887	14
$y^1F^\circ_3$	24,522.70	1.000	1.032	1.034	8
$y^3D^\circ_1$	25,973.37	.500	.799	.782	12
$y^3D^\circ_2$	27,388.11	1.167	1.191	1.168	14
$y^3D^\circ_3$	28,315.25	1.333	1.312	1.308	12
$x^3F^\circ_2$	26,414.01	.667	.836	.825	15
$x^3F^\circ_3$	26,837.66	1.083	1.081	1.088	7
$x^3F^\circ_4$	28,565.40	1.250	1.246	1.245	3
$z^1P^\circ_1$	27,423.91	1.000	.882	.876	13
$z^1H^\circ_5$	28,525.71	1.000	1.00	1.004	0
$y^3P^\circ_0$	27,545.85	0/0	0/0	0/0	4
$y^3P^\circ_1$	28,154.55	1.500	1.262	1.267	12
$y^3P^\circ_2$	29,498.05	1.500	1.495	1.471	10
$y^1P^\circ_1$	30,353.33	1.000	1.066	1.074	6
$x^3P^\circ_0$	31,785.82	0/0	0/0	0/0	6
$x^3P^\circ_1$	32,160.99	1.500	1.515	1.492	8
$x^3P^\circ_2$	33,204.41	1.500	1.478	1.494	7
$x^1F^\circ_3$	32,201.05	1.000	1.006	1.005	6
e^3G_3	35,452.66	.750	.873	.876	5
e^3G_4	37,172.79	1.050	1.146	1.127	5
e^3G_5	39,018.74	1.200	1.203	1.21	0
e^3F_2	35,787.53	.667	.732	.719	4
e^3F_3	36,954.65	1.083	1.061	1.061	4
e^3F_4	37,790.57	1.250	1.141	1.113	6
e^1F_3	37,209.71	1.000	.953	.944	6
e^1G_4	39,221.65	1.000	1.060	1.059	4
e^3D_1	38,534.11	.500	.495	.497	7
e^3D_2	38,221.49	1.167	1.100	1.071	7
e^3D_3	39,402.55	1.333	1.306	1.274	6
e^1D_2	40,457.71	1.000	1.046	1.036	3
$x^1P^\circ_1$	45,692.17	1.000	.97	.999	3
f^3D_1	49,733.13	.500	.520	.500	5
f^3D_2	49,884.35	1.167	1.141	1.117	4
f^3D_3	51,228.57	1.333	1.331	1.315	1
f^1D_2	51,523.86	1.000	1.02	1.036	3
f^1F_3	52,137.67	1.000	1.00	.987	4
f^3G_3	52,857.88	.750	.89	.861	1
f^3G_4	53,333.37	1.050	1.05	1.036	1
f^3G_5	54,434.65	1.200	1.20	1.21	0
f^3F_2	53,885.24	.667	.77	.751	2
f^3F_3	54,840.04	1.083	1.14	1.088	1
f^3F_4	55,321.35	1.250	1.16	1.136	5
g^3D_1	52,169.66	.500	.67	.621	6
g^3D_2	52,734.81	1.167	1.17	1.154	2
g^3D_3	53,689.56	1.333	1.21	1.218	7
e^3S_1	54,365.80	2.000	1.42	1.455	4
e^1P_1	53,302.56	1.000	—	1.335	2
e^3P_1	55,230.33	1.500	1.57	1.552	2
e^3P_2	56,036.60	1.500	1.22	1.203	1
f^1G_4	56,035.70	1.000	1.03	1.027	4
g^1D_2	55,184.05	1.000	1.08	1.183	3
e^3H_4	55,107.25	.800	.94	.883	7
e^3H_5	55,982.09	1.033	1.04	1.033	3
e^3H_6	56,837.94	1.167	1.18	1.14	0
g^3F_2	57,399.58	.667	—	.675	4
g^3F_3	57,918.50	1.083	1.11	1.085	4
g^3F_4	58,259.41	1.250	1.22	1.196	3
g^1G_4	59,527.60	1.000	1.07	1.046	2
h^1D_2	59,900.08	1.000	1.00	1.035	5
f^3P_0	60,094.84	0/0	0/0	0/0	5
f^3P_1	61,128.83	1.500	1.47	1.528	6
f^3P_2	62,506.36	1.500	1.45	1.416	4
i^1D_2	62,026.27	1.000	—	1.054	4
e^1I_6	62,408.40	1.000	1.01	1.003	0
g^3P_0	63,463.95	0/0	—	0/0	2
g^3P_1	63,703.18	1.500	—	1.471	2
g^3P_2	64,278.92	1.500	—	1.414	3
h^3D_1	64,361.28	.500	—	.506	5
h^3D_2	64,529.90	1.167	—	1.217	4
f^3S_1	60,660.18	2.000	—	1.955	1
1°_3	57,364.12	—	—	1.07	0
4°_4	60,744.17	—	—	1.25	1
$6^\circ_{4,3}$	61,514.46	—	—	.97?	0
7°_4	63,598.87	—	—	1.205	1
8°_3	64,411.17	—	—	.97	0
f^1S_0	66,591.91	0/0	—	0/0	2

observed g values calculated from these data for the lower and upper terms respectively. Values in parenthesis were determined from other patterns and were used in calculating the g value given for the associated level. Details of the patterns observed have been omitted from the final draft to save space, but will be forwarded in typewritten form to anyone concerned.

The notation in Column 4 of Table I indicates patterns observed as follows:

Type 1: Odd multiplicity, $J_1>J_2$, $g_1<g_2$, shade out.
Type 2: Odd multiplicity, $J_1>J_2$, $g_1>g_2$, shade in.
Type 3: Odd multiplicity, $J_1=J_2$, $g_1\neq g_2$, symmetrical.
Type 4: Even multiplicity, $J_1>J_2$, $g_1<g_2$, shade out.
Type 5: Even multiplicity, $J_1>J_2$, $g_1>g_2$, shade in.
Type 6: Even multiplicity, $J_1=J_2$, $g_1\neq g_2$, symmetrical.

TABLE V. Tests of g-sum rule in La I.

	σ	g_{LS}	d_{RM}	d_{HRM}
		Low even terms		
$J=\frac{1}{2}$				
a^4P	7231	2.667	+.039	−.019
a^2P	9044	.667	+.00	+.023
	Sum	3.334	+.04	+.004
$J=1\frac{1}{2}$				
a^2D	0	.800	−.010	−.002
a^4F	2668	.400	+.011	+.005
a^4P	7490	1.733	−.04	−.029
b^2D	8446	.800	+.09	+.142
a^2P	9719	1.333	−.01	−.10
	Sum	5.066	+.04	+.02
$J=2\frac{1}{2}$				
a^2D	1053	1.200	+.003	−.002
a^4F	3010	1.029	+.003	+.001
a^2F	7011	.857	+.04	+.036
a^4P	7679	1.600	−.06	−.102
b^2D	9183	1.200	+.09	+.050
	Sum	5.886	+.08	−.017
$J=3\frac{1}{2}$				
a^4F	3494	1.238	−.016	+.001
a^2F	8052	1.143	−.01	−.006
a^2G	9960	.889	+.021	+.02
	Sum	3.270	−.01	+.02
$J=4\frac{1}{2}$				
a^4F	4121	1.333	−.006	+.005
a^2G	9919	1.111	+.01	+.01
	Sum	2.444	+.00	+.02

Type 7*a*: Limiting cases of types 1 and 2, $J_1>J_2=0$, $g_1\gtrless g_2$, triplet.

Type 7*b*: Limiting cases of types 1, 2, 3, 4, 5, 6, $g_1=g_2$ triplet. Any multiplicity and all singlet combinations.

Table II contains the *g* values of 101 levels in La I as assembled from the data of Table I and other sources. The columns give in order the term designation, the term value, the *g* value of a level of this designation calculated for *LS* coupling from the Landé formula, the *g* value as given by Russell and Meggers, the *g* value as determined in the present work, and the number of well-resolved patterns measured by us from which data were obtained for the level given.

Table III contains data on 507 analyzed Zeeman patterns of La II, the columns corresponding to those of Table I.

Table IV contains the *g* values of 110 levels of La II, including values calculated for *LS* coupling, observed values of Russell and Meggers, and our observed values as averaged from data in Table III. The availability of these two completely independent sets of Zeeman-effect data should make it possible to evaluate very closely the degree of perturbation in La I and II terms.

Comparisons are given in Tables V and VI which show the validity of the Pauli *g*-sum rule and at the same time furnish an indication of the internal consistency of our data and of those of Russell and Meggers. Terms have been segregated in accordance with their inner quantum numbers, the *g* values of all neighboring terms of a given *J*-value and parity being expected to add up to the same *g* sum as though no perturbation were present. The first column in Table V gives the term designation, the second the approximate wave number of the term in cm^{-1}, the third column the *g* value calculated for *LS* coupling, the fourth column the excess or deficiency d_{RM} (+ or −) of the *g* determination by Russell and Meggers over that of pure *LS* coupling, and the last column this same difference (d_{HRM}) from our measurements. The closeness of the sums of these differences to zero is excellent. On the average the Russell and Meggers values appear to be about 1.17 percent too high, in agreement with their expectation that Meggers' fields might have been measured low. On the average our measured departures from the expected *g* sums are less than 0.3 percent, and any consistent departure which might be attributable to an error in field determination is much less than this.

The given values for $J=3\frac{1}{2}$ and $J=4\frac{1}{2}$ in Table V are probably incomplete, since there are doubtless other terms close enough to 10,000 cm^{-1} to produce perturbations, and the ^2G terms in each of these cases are not determined with sufficient accuracy to permit three-figure comparison.

It is of interest to compare the relative sensitivity of detection of perturbations between terms by means of term shifts, *g* values in multiplets and departures from the intensity formulas. The last is the most difficult criterion to apply because intensity anomalies may be due to anomalies in the lower or in the upper term, or in both. Anomalies in *g* values can be readily assigned to the proper term, and appear as an actual loss or gain in the *g* value of this term regardless of any weighting factor. On the other

TABLE VI. Tests of g-sum rule in La II.

Term	Level	g_{LS}	d_{RM}	d_{HRM}
		Low even terms		
$J=1$				
a^3D	1895	.500	+.020	−.002
a^3P	5718	1.500	+.006	−.003
	Sum	2.000	+.026	−.005
$J=2$				
a^3F	0	.667	+.063	+.054
a^1D	1394	1.000	−.013	−.023
a^3D	2591	1.167	−.027	−.034
a^3P	6227	1.500	−.012	−.019
b^1D	10,094	1.000	+.015	+.005
	Sum	5.334	+.026	−.017
$J=3$				
a^3F	1016	1.083	+.009	.000
a^3D	3250	1.333	+.004	+.001
	Sum	2.416	+.013	+.001
$J=4$				
a^3F	1970	1.250	+.008	−.002
a^1G	7473	1.000	+.003	.000
	Sum	2.250	+.011	−.002
		Middle odd terms		
$J=1$				
z^3D°	21441	.500	+.047	+.042
z^3P°	22705	1.500	−.042	−.069
y^3D°	25973	.500	+.299	+.282
z^1P°	27423	1.000	−.118	−.124
y^3P°	28154	1.500	−.238	−.233
y^1P°	30353	1.000	+.066	+.074
x^3P°	32160	1.500	+.015	−.008
x^1P°	45692	1.000	−.03	−.001
	Sum	8.500	.00	−.037
$J=2$				
z^3F°	14147	.667	+.009	−.003
y^3F°	17211	.667	+.090	+.087
z^1D°	18895	1.000	−.069	−.077
z^3D°	22106	1.167	+.019	.000
z^3P°	23246	1.500	−.038	−.041
y^1D°	24462	1.000	−.103	−.113
x^3F°	26414	.667	+.169	+.158
y^3D°	27388	1.167	+.024	+.001
y^3P°	29498	1.500	−.005	−.029
x^3P°	33204	1.500	−.022	−.006
	Sum	10.833	+.074	−.023
$J=3$				
z^3F°	14375	1.083	+.004	−.027
z^1F°	15773	1.000	+.047	+.017
y^3F°	18235	1.083	+.007	+.003
z^3G°	20402	.750	+.025	+.007
z^3D°	22537	1.333	−.016	−.045
y^1F°	24522	1.000	+.032	+.034
x^3F°	26837	1.083	−.002	+.005
y^3D°	28315	1.333	−.021	−.025
x^1F°	32201	1.000	+.006	+.005
	Sum	8.667	+.082	−.026
$J=4$				
z^3F°	15698	1.250	+.008	−.003
z^1G°	16599	1.000	−.004	−.031
z^3H°	17825	.800	+.065	+.046
y^3F°	19214	1.250	−.007	−.018
z^3G°	21331	1.050	+.010	−.001
x^3F°	28565	1.250	−.004	−.005
	Sum	6.600	+.068	−.012
$J=5$				
z^3H°	18580	1.033	+.049	−.016
z^3G°	22282	1.200	+.003	−.003
z^1H°	28525	1.000	.00	+.004
	Sum	3.233	+.05	−.015

hand, intervals can be determined so precisely that they remain one of the most sensitive methods of detecting anomalies.

For example, multiple term La I a^4F has intervals of 627, 484, and 341 cm^{-1} which should be in the ratio of 9:7:5 in pure LS coupling, but actually are in the ratio 9:6.94:4.89. Our g values for the four terms lead to results as follows:

Level	g_{LS}	d_{HRM}	s
$a^4F_{4\frac{1}{2}}$	1.333	+.005	±.004
$a^4F_{3\frac{1}{2}}$	1.238	+.001	±.005
$a^4F_{2\frac{1}{2}}$	1.029	+.001	±.005
$a^4F_{1\frac{1}{2}}$	0.400	+.005	±.003

The figure given first is the g value expected for LS coupling. The second figure is the average observed departure from this value in g units, and the third gives the actual spread of the values as observed by us. It is believed that the actual error in the average values is not greater than ±0.003 unit. The $3\frac{1}{2}$ and $2\frac{1}{2}$ terms show least perturbation. In Table V it is obvious that $a^2D_{2\frac{1}{2}}$ is almost entirely unperturbed by $a^4F_{2\frac{1}{2}}$, and no other term having $J=2\frac{1}{2}$ lies close enough to produce any perturbation. Similarly, $a^4F_{3\frac{1}{2}}$ is more than 4500 wave numbers away from the nearest $3\frac{1}{2}$ term which could be expected to perturb it. Therefore, we may assume that the interval $3\frac{1}{2}$ to $2\frac{1}{2}=484.57$ is normal for the multiplet. Using the expected interval ratio 7:5 we calculate the interval between $2\frac{1}{2}$ and $1\frac{1}{2}$ as

TABLE VI.—*Continued.*

Term	Level	g_{LS}	d_{RM}	d_{HRM}
	High even terms			
$J=1$				
e^3D	38534	.500	−.005	−.003
f^3D	49733	.500	+.020	.000
g^3D	52169	.500	+.17	+.121
e^1P	53302	1.000	—	+.335
e^3S	54365	2.000	−.580	−.545
e^3P	55230	1.500	+.070	+.052
f^3S	60660	2.000	—	−.045
f^3P	61128	1.500	−.030	+.028
g^3P	63703	1.500	—	−.029
h^3D	64361	.500	—	+.006
	Sum	11.500	—	−.080
$J=2$				
e^3F	35787	.667	+.065	+.052
e^3D	38221	1.167	−.067	−.096
e^1D	40457	1.000	+.046	+.036
f^3D	49884	1.167	−.026	−.050
f^1D	51523	1.000	+.02	+.036
g^3D	52734	1.167	+.00	−.013
f^3F	53885	.667	+.10	+.084
g^1D	55184	1.000	+.08	+.183
e^3P	56036	1.500	−.28	−.297
g^3F	57399	.667	—	+.008
h^1D	59900	1.000	.00	+.035
i^1D	62026	1.000	—	+.054
f^3P	62506	1.500	−.050	−.084
g^3P	64278	1.500	—	−.086
h^3D	64529	1.167	—	+.050
	Sum	16.169	—	−.088
$J=3$				
e^3G	35452	.750	+.123	+.126
e^3F	36954	1.083	−.022	−.022
e^1F	37209	1.000	−.047	−.056
e^3D	39402	1.333	−.027	−.059
f^3D	51228	1.333	−.002	−.018
f^1F	52137	1.000	.000	−.013
f^3G	52857	.750	+.14	+.111
g^3D	53689	1.333	−.12	−.115
f^3F	54840	1.083	+.06	+.005
g^3F	57918	1.083	+.03	+.002
	Sum	10.748	+.13	−.039
$J=4$				
e^3G	37172	1.050	+.096	+.077
e^3F	37790	1.250	−.109	−.137
e^1G	39221	1.000	+.060	+.059
f^3G	53333	1.050	.00	−.014
e^3H	55107	.800	+.14	+.083
f^3F	55321	1.250	−.09	−.114
f^1G	56035	1.000	+.03	+.027
g^3F	58259	1.250	−.03	−.056
g^1G	59527	1.000	+.07	+.046
	Sum	9.650	+.17	−.029
$J=5$				
e^3G	39018	1.200	+.003	+.01
f^3G	54434	1.200	.00	+.01
e^3H	55982	1.033	+.01	.000
	Sum	3.433	+.01	+.02
$J=6$				
e^3H	56837	1.167	+.01	−.03
e^1I	62408	1.000	+.01	+.003
	Sum	2.167	+.02	−.03

346 cm^{-1}. The observed value of 341 cm^{-1} indicates that the $1\frac{1}{2}$ term has been raised slightly by a perturbing term below it. The only such term observed is $a^2D_{1\frac{1}{2}}$ which shows a loss in g value to a^4F within the experimental error. Similarly, $a^4F_{4\frac{1}{2}}$ would be 622.5 units above $3\frac{1}{2}$ in *LS* coupling, whereas we observe 627, indicating that this term also has been pushed upward. The deviation of g values is not clear-cut in this case since the sums do not add up to zero, indicating the probable presence of other perturbing terms. Obviously interval shifts remain the most clear-cut indication of incipient departure from *LS* coupling.

In contrast to this case of very small perturbation, it is of interest to examine cases in the odd terms of La I where the perturbations are marked, and where it is possible to isolate a group of terms from others of the same inner quantum number which might also affect the perturbations. The following group gives such a case.

$J=1\frac{1}{2}$

Level	cm^{-1}	g_{LS}	d_{HRM}
y^2D^0	18172	0.800	+.002
y^2P^0	20019	1.333	−.313
y^4F^0	20083	0.400	+.331
y^4D^0	22439	1.200	−.008
	Sums	3.733	+.012

Here the presence below and above the two middle terms of terms which show small perturbations may be taken as first-order evidence of small external perturbation of the center terms. However, it is obvious that the y^2P^0 and y^4F^0 terms, which lie only 64 wave numbers apart, have large mutual perturbations which result in the term of lower g value being increased by about one-third g unit, and that of higher g value being similarly decreased. It is of interest

to attempt to evaluate in a qualitative way the perturbation factor in terms of term separation. A useful criterion is obtained by adding the perturbations without regard to sign, dividing by two, and expressing this value as a percentage of half the sum of the g values involved, which in the case just cited is 37 percent perturbation.

A similar partially isolated group is given by the following odd terms for $J=2\frac{1}{2}$, where the terms z^4G^0 and z^4P^0 are 210 wave numbers apart and show a perturbation on the basis given above of about 42 percent.

$J=2\frac{1}{2}$

Term	cm^{-1}	g_{LS}	d_{HRM}
y^2F^0	16856	0.857	−.047
z^4G^0	17947	0.571	+.482
z^4P^0	18157	1.600	−.425
y^2D^0	19379	1.200	−.014
		Sums 4.228	−.004

It is impossible to predict empirically the degree of perturbation from the closeness of perturbing terms in view of the fact that the perturbation parameters vary with quantum number and other factors, and it appears unfruitful to examine very closely into the origins of the various perturbations until fairly complete equations and data are available for the particular cases under consideration.

Table VI gives tests of the Pauli g-sum rule for La II. Here again, the deviations from the Landé g values as determined by Russell and Meggers are given in the next to the last column, and those from the present work in the last column. In the case of the low even terms we find an average agreement with the g sum rule to within 0.2 percent, while Russell and Meggers sums average 0.85 percent high.

The middle odd terms of La II in Table VI show similar agreement with the g-sum rule, with an average deviation of 0.36 percent and a maximum deviation of 0.53 percent. Here our sums are in general consistently a few tenths of one percent low, while those of Russell and Meggers are again high by an average of 0.93 percent. In the high even terms of La II our maximum deviation from the g-sum rule is 0.64 percent in the cases given for $J=1$, 2, and 3, while the average deviation is 0.41 percent. Here our sums are again slightly low, while the RM value, in the one case where a complete sum is available, is high by about 1 percent.

Our field intensities may in general be about 0.3 of 1 percent high. It is to be noted that in La I $a^4P_{\frac{1}{2}}$ and $a^2P_{\frac{1}{2}}$ balance to within 0.004 unit, instead of 0.04, as Russell and Meggers give, although the ^2S term is missing. The latter should be found to have a g value very close to 2.000.

The results presented in this paper are based on measurements made in part by workers on the M.I.T.-W.P.A. Wave-Length Project during 1939 and 1940. We are especially grateful for this help, and desire also to record our indebtedness to the Rumford Fund of the American Academy of Arts and Sciences for grants in aid to the project. We acknowledge also the kindness of Dr. W. F. Meggers in criticizing this paper in manuscript.

JOURNAL OF THE OPTICAL SOCIETY OF AMERICA VOLUME 35, NUMBER 10 OCTOBER, 1945

Colorimetric Specifications of Wratten Light Filters*

DAVID L. MACADAM
Eastman Kodak Company, Rochester, New York

(Received August 17, 1945)

Colorimetric specifications are given for Wratten light filters, including the tristimulus values, trichromatic coordinates, dominant wave-lengths, purity, and luminous transmittance for ICI illuminants *A* and *C* and for an artificial daylight produced by the use of a Wratten filter. These data are based on the spectral transmittance values published in the seventeenth edition (1944) of the booklet entitled "Wratten Light Filters." Wave-lengths for thirty selected ordinates and for supplementary ordinates are given for colorimetric computations involving the artificial daylight source, which consists of a tungsten filament lamp operated at a color temperature of 2360°K, the light from which is passed through a Wratten filter No. 78.

WRATTEN light filters have been used extensively in photography and in other scientific fields since 1907 and are described fully in the booklet, "Wratten Light Filters," published by the Eastman Kodak Company. These filters consist of specially purified (and in some cases specially synthesized) dyes in gelatin films. From the time of their introduction the production of these filters has been accurately controlled by the use of spectrophotometers and the present filters have essentially the same optical properties as their prototypes. When, from time to time, improved dyes are obtained or formulations are developed which improve the permanence and other important characteristics of the filters, slight changes are made in the standards. The effects of these changes on the spectral transmittances are indicated in successive editions of "Wratten Light Filters," which is revised frequently. The results presented in this paper are based exclusively on the spectral transmittance data published in the seventeenth (1944) edition. Further revisions of the booklet may contain some revised transmittance data. Although the data contained in the filter booklet and used for these colorimetric computations represented the standard filters at the date of publication of the seventeenth edition, some of the standards may have been changed since, and some variations from the standards must be expected in production. Consequently, for any particular samples, the colorimetric specifications, like the spectral transmittance data published in the filter booklet, should be regarded as merely representative and not necessarily exact. Such specifications are primarily useful for the selection of filters according to color, and for good but not necessarily exact estimates of the colorimetric performance of Wratten light filters. When exact data are needed for any particular sample, transmittance data should be obtained for that sample by the accurate use of a reliable spectrophotometer. Colorimetric specifications, if needed, should then be computed from those data.

The selected ordinate method of colorimetric specification, described in the report of the Colorimetry Committee of the Optical Society of America,[1] has been employed in obtaining the present data. The spectral transmittance data tabulated on pages 72 to 86 of the seventeenth edition of "Wratten Light Filters" were plotted, smooth curves were drawn through the plotted points, and the ordinates were selected from these curves. Supplementary ordinates were used whenever necessary, so that the tristimulus values in each instance are accurate within two or three units in the last figure tabulated.

The Wratten number of each filter is indicated in the first column of Table I. The tristimulus values are listed in Columns X, Y, and Z, under the description of the appropriate illuminant. Trichromatic coordinates were computed and checked by verification of the relation: $x+y+z=1$. The essential coordinates are listed in Columns x and y.

* Communication No. 1050 from the Kodak Research Laboratories.

[1] "Quantitative Data and Methods for Colorimetry," J. Opt. Soc. Am. **34**, 648–656 (1944).

TABLE I. Colorimetric specifications of Wratten light filters.

	ICI Illuminant *A*							ICI Illuminant *C*							Lamp at 2360°K with Wratten filter No. 78						
No.	*X*	*Y*	*Z*	*x*	*y*	λ mμ	*p* %	*X*	*Y*	*Z*	*x*	*y*	λ mμ	*p* %	*X*	*Y*	*Z*	*x*	*y*	λ mμ	*p* %
1	.9864	.8966	.3119	.4494	.4085	585	2	.8765	.8951	1.0338	.3124	.3191	574	1.3	.8581	.8951	.8041	.3355	.3500	568	0.7
2	.9810	.8930	.2926	.4528	.4122	582.5	7	.8597	.8891	.9549	.3180	.3288	571	5.5	.8472	.8902	.7515	.3404	.3577	573.2	5.4
2A	.9845	.8973	.2953	.4522	.4122	582.0	6	.8617	.8941	.9603	.3173	.3292	569.5	5.3	.8516	.8953	.7603	.3397	.3571	572.8	5.0
3	.9520	.8857	.1442	.4803	.4469	580.1	50	.7460	.8735	.3683	.3753	.4394	569.2	50.5	.7640	.8808	.3243	.3880	.4473	570.3	48.6
3N5	.3111	.2854	.0422	.4871	.4468	581.1	55	.2423	.2784	.1094	.3845	.4418	570.6	53.7	.2477	.2795	.0978	.3963	.4472	571.7	51.0
4	.9192	.8750	.1113	.4824	.4592	579.0	60.5	.7256	.8587	.2671	.3919	.4638	569.9	61.7	.7475	.8632	.2395	.4040	.4665	571.1	59.2
5	.9265	.8451	.0377	.5121	.4671	581.5	86.5	.6941	.8013	.0710	.4431	.5116	572.4	88.1	.7129	.8056	.0645	.4503	.5089	573.2	87.3
5N5	.3084	.2771	.0093	.5185	.4659	582.2	90	.2304	.2596	.0161	.4552	.5129	573.4	91.7	.2363	.2616	.0143	.4613	.5107	574.1	91.3
6	.9490	.8808	.1574	.4776	.4432	580.0	45.5	.7593	.8650	.4504	.3660	.4169	569.9	42.0	.7711	.8679	.3749	.3829	.4310	571.0	44.6
7	.9277	.8539	.0823	.4977	.4581	581.0	70	.7074	.8252	.1968	.4090	.4772	571.1	69.6	.7270	.8285	.1723	.4208	.4795	572.2	68.9
8	.9206	.8402	.0484	.5088	.4644	581.5	82	.6909	.7999	.0988	.4346	.5032	572.2	83.6	.7116	.8048	.0890	.4433	.5013	573.1	82.8
9	.9273	.8174	.0279	.5231	.4611	582.9	90	.6932	.7565	.0500	.4622	.5044	574.7	91.1	.7124	.7612	.0451	.4691	.5012	574.6	87.6
11	.2580	.3681	.0515	.3808	.5432	551.3	49.2	.2271	.4097	.1138	.3026	.5458	549.6	60.6	.2334	.4062	.1015	.3149	.5481	550.0	58.2
12	.9231	.7923	.0101	.5350	.4592	583.9	96.5	.6870	.7173	.0128	.4848	.5062	576.4	98.0	.7049	.7232	.0130	.4891	.5019	577.1	97.5
13	.1789	.3014	.0477	.3388	.5708	536.2	44	.1680	.3487	.1079	.2690	.5583	540.8	55.9	.1702	.3444	.0973	.2781	.5629	539.9	52.9
15	.9066	.7447	.0059	.5471	.4494	585.6	98.3	.6715	.6584	.0070	.5023	.4925	578.7	99.0	.6963	.6664	.0068	.5084	.4866	579.7	99.0
16	.8884	.6836	.0030	.5641	.4340	588.3	99.3	.6510	.5831	.0035	.5260	.4712	582.2	99.5	.6750	.5935	.0032	.5308	.4667	582.9	99.5
17	.9519	.8942	.1106	.4865	.4570	579.8	61	.7315	.8799	.2609	.3905	.4702	569.1	63.0	.7543	.8824	.2345	.3950	.4622	570.0	55.4
19	.8673	.6318	.0018	.5779	.4209	590.6	99.6	.6268	.5211	.0020	.5450	.4532	585.2	99.6	.6530	.5350	.0020	.5487	.4496	585.7	99.5
21	.8393	.5692	.0009	.5955	.4039	593.8	100.0	.5969	.4503	.0010	.5694	.4296	589.1	99.8	.6240	.4660	.0009	.5719	.4272	589.4	99.8
22	.7662	.4653	.0006	.6219	.3776	599.0	100.0	.5265	.3441	.0004	.6045	.3950	595.4	99.9	.5520	.3619	.0004	.6037	.3958	595.2	99.9
23	.6232	.3266	.0004	.6559	.3438	607.1	100.0	.4041	.2209	.0003	.6463	.3533	604.6	100.0	.4267	.2379	.0003	.6418	.3578	603.4	100.0
23A	.6942	.3845	.0005	.6433	.3562	603.9	100.0	.4588	.2678	.0004	.6311	.3684	600.8	100.0	.4870	.2871	.0004	.6288	.3707	600.4	100.0
23B	.4822	.2461	.0003	.6619	.3378	608.9	100.0	.3088	.1642	.0001	.6526	.3471	606.2	100.0	.3278	.1774	.0002	.6485	.3511	605.0	100.0
24	.5253	.2513	.0003	.6762	.3235	613.6	100.0	.3206	.1602	.0001	.6666	.3332	610.4	100.0	.3412	.1737	.0002	.6624	.3372	609.0	100.0
24A	.5827	.2902	.0002	.6673	.3325	610.5	100.0	.3698	.1909	.0002	.6593	.3404	608.1	100.0	.3948	.2089	.0002	.6538	.3459	606.5	100.0
25	.4980	.2295	.0002	.6843	.3154	616.8	100.0	.3038	.1425	.0001	.6805	.3193	615.3	100.0	.3205	.1556	.0001	.6730	.3268	612.5	100.0
26	.4313	.1897	.0001	.6944	.3055	621.5	100.0	.2564	.1136	.0000	.6929	.3070	620.1	100.0	.2615	.1195	.0001	.6861	.3137	617.5	100.0
27	.5386	.2602	.0002	.6742	.3256	612.9	100.0	.3337	.1673	.0001	.6659	.3339	610.2	100.0	.3523	.1804	.0001	.6611	.3386	608.6	100.0
27A	.5930	.3024	.0003	.6621	.3376	608.9	100.0	.3789	.2021	.0002	.6519	.3477	605.9	100.0	.3980	.2156	.0002	.6483	.3513	605.0	100.0
28	.5278	.2566	.0002	.6727	.3271	612.4	100.0	.3264	.1655	.0001	.6635	.3363	609.4	100.0	.3465	.1773	.0002	.6613	.3384	608.6	100.0
29	.2664	.1066	.0000	.7141	.2858	635.2	100.0	.1484	.0608	.0000	.7093	.2906	631.0	100.0	.1438	.0589	.0000	.7094	.2906	631.0	100.0
30	.7395	.4123	.0946	.5933	.3308	504.4c	52.0	.5504	.2967	.3646	.4542	.2449	496.9c	55.8	.5620	.3191	.2652	.4902	.2784	498.0c	52.8
30A	.6083	.3181	.0050	.6531	.3415	608.5	96	.3935	.2150	.0205	.6256	.3418	607.0	91.3	.4173	.2319	.0141	.6291	.3496	605.5	93.4
31	.4488	.1899	.0948	.6119	.2589	512 8c	81.5	.3254	.1242	.3545	.4047	.1545	514.7c	88.8	.3082	.1249	.2697	.4385	.1777	515.7c	81.5
32	.4274	.1819	.1833	.5392	.2295	549.8c	80.0	.3525	.1355	.6593	.3072	.1181	552.0c	79.3	.3221	.1299	.5064	.3361	.1355	554.0c	79.4
32A	.5396	.2810	.2547	.5018	.2613	558.3c	62.1	.4563	.2457	.8759	.2892	.1557	557.2c	61.4	.4325	.2473	.6800	.3181	.1818	558.1c	59.1
33	.2543	.1007	.0213	.6758	.2676	506.2c	89.2	.1542	.0582	.0794	.5284	.1994	497.5c	88.8	.1438	.0559	.0613	.5509	.2142	500.4c	87.1
34	.0430	.0109	.1058	.2693	.0683	577.7c	93.3	.0923	.0122	.4229	.1750	.0232	432	95.0	.0711	.0118	.2990	.1862	.0309	380	92.4
34A	.1249	.0435	.1187	.4350	.1515	571.5c	90.8	.1421	.0267	.4671	.2235	.0420	563.7c	94.3	.1180	.0290	.3393	.2427	.0596	565.0c	91.5
35	.0340	.0101	.0420	.3949	.1173	573.7c	96.3	.0476	.0067	.1790	.2040	.0287	565.2c	96.0	.0384	.0073	.1187	.2336	.0444	565.4c	95.5
36	.0090	.0026	.0128	.3690	.1066	574.8c	96.2	.0141	.0014	.0566	.1956	.0194	565.7c	98.2	.0122	.0023	.0358	.2426	.0457	564.5c	97.1
38	.2663	.3549	.2607	.3020	.4024	494.1	34.7	.3469	.4223	.8782	.2106	.2563	483.2	41.5	.3173	.4160	.6802	.2245	.2943	485.9	40.4
38A	.0652	.1142	.1914	.1758	.3080	488.4	68.9	.1516	.1630	.6583	.1558	.1675	478.1	72.9	.1252	.1574	.5079	.1584	.1991	480.5	71.7
39	.0220	.0041	.1087	.1631	.0304	452.0	97.0	.0835	.0106	.4316	.1588	.0202	450	99	.0580	.0090	.3065	.1553	.0241	453.5	99
40	.1086	.2860	.0799	.2289	.6027	512.5	51.6	.1272	.3626	.1860	.1882	.5366	514.7	44.6	.1220	.3522	.1681	.1899	.5484	512.3	46.1
40A	.1349	.2858	.0383	.2939	.6227	531.9	55.0	.1390	.3409	.0795	.2486	.6094	538.1	65.4	.1386	.3340	.0708	.2551	.6146	537.3	63.4
43	.0706	.1327	.2236	.1654	.3108	488.8	71.0	.1700	.1907	.7740	.1498	.1681	478.7	75.2	.1378	.1837	.5908	.1510	.2014	481.3	73.7
44	.0327	.1041	.1287	.1232	.3921	494.0	77.2	.0744	.1588	.3841	.1205	.2572	487.2	75.6	.0644	.1543	.3200	.1196	.2864	488.6	76.0
44A	.0330	.0863	.1389	.1278	.3342	490.9	78.6	.0812	.1352	.4309	.1254	.2089	483.7	78.8	.0691	.1296	.3535	.1251	.2347	485.2	78.5
45	.0133	.0289	.0882	.1020	.2216	485.2	91.1	.0406	.0559	.2663	.1119	.1541	480.3	90.0	.0344	.0517	.2240	.1109	.1667	481.2	90.0
45A	.00846	.01373	.05084	.1158	.1880	482.5	90.3	.0248	.0262	.1576	.1189	.1255	477.6	91.3	.0209	.0249	.1314	.1179	.1405	478.8	90.8
46	.0115	.0101	.0748	.1193	.1048	475.9	96.2	.0400	.0231	.2443	.1302	.0751	471.1	95.2	.0325	.0212	.1998	.1282	.0836	472.3	94.9
47	.0222	.0102	.1303	.1364	.0627	468.9	97.0	.0862	.0240	.4730	.1477	.0412	461.3	96.8	.0645	.0216	.3595	.1447	.0485	464.0	96.4
47A	.0152	.0046	.0863	.1433	.0434	463.8	98.2	.0590	.0126	.3199	.1507	.0322	457.8	97.8	.0442	.0101	.2414	.1495	.0342	459.0	98.1

TABLE I.—*Continued.*

No.	ICI Illuminant *A*							ICI Illuminant *C*							Lamp at 2360°K with Wratten filter No. 78						
	X	*Y*	*Z*	*x*	*y*	λ mμ	ρ %	*X*	*Y*	*Z*	*x*	*y*	λ mμ	ρ %	*X*	*Y*	*Z*	*x*	*y*	λ mμ	ρ %
48	.0133	.0082	.0835	.1267	.0781	472.4	97.3	.0472	.0203	.2788	.1363	.0586	467.8	96.3	.0386	.0190	.2263	.1360	.0669	470.3	97.3
48A	.0115	.0036	.0668	.1404	.0440	464.9	98.4	.0449	.0097	.2425	.1510	.0326	457.8	97.7	.0334	.0088	.1860	.1464	.0385	461.0	97.8
49	.0096	.0025	.0558	.1414	.0368	462.9	99.3	.0374	.0071	.2027	.1513	.0287	456.4	98.5	.0286	.0064	.1568	.1491	.0334	458.7	98.2
49A	.0173	.0068	.1023	.1369	.0538	467.4	98.0	.0661	.0178	.3648	.1470	.0396	461.1	97.1	.0504	.0162	.2841	.1437	.0462	463.8	97.0
49B	.00574	.00137	.03331	.1420	.0339	461.8	99.7	.0224	.0041	.1217	.1511	.0277	456.2	98.8	.01732	.00356	.09432	.1503	.0309	457.8	98.6
49C	.00286	.00066	.01658	.1423	.0328	461.3	99.8	.0110	.0020	.0601	.1504	.0274	456.5	99.0	.00861	.00176	.04686	.1504	.0308	457.7	98.6
50	.00475	.00091	.02687	.1460	.0280	458.8	99.9	.01663	.00276	.09110	.1506	.0250	455.9	99.7	.01296	.00249	.07165	.1488	.0286	457.8	99.3
51	.6718	.6868	.1784	.4371	.4468	563.1	20.0	.5958	.7036	.5596	.3205	.3785	558.4	20.8	.5927	.7028	.4444	.3407	.4039	559.5	20.0
52	.1009	.1782	.0132	.3452	.6096	550.4	71.3	.1058	.1967	.0286	.3195	.5941	552.9	77.8	.1077	.1934	.0248	.3305	.5934	553.9	77.1
53	.0401	.0811	.0044	.3193	.6457	548.0	79.5	.0416	.0933	.0076	.2920	.6546	548.3	87.3	.0410	.0909	.0070	.2952	.6544	548.3	86.3
54	.00113	.00287	.00008	.2770	.7034	544.7	93.0	.00128	.00333	.00011	.2712	.7065	545.6	96.4	.00127	.00326	.00010	.2743	.7041	545.7	95.7
55	.0990	.2569	.0340	.2539	.6589	527.0	61.0	.1017	.3188	.0651	.2092	.6568	531.6	70.5	.1039	.3144	.0586	.2179	.6592	531.4	69.0
56	.2964	.4708	.0422	.3662	.5817	553.2	65.9	.2683	.5242	.0822	.3070	.5990	550.6	76.0	.2777	.5212	.0745	.3180	.5967	551.5	73.1
57	.1358	.2868	.0378	.2950	.6229	532.3	55.6	.1340	.3413	.0770	.2428	.6179	537.1	66.3	.1383	.3355	.0686	.2550	.6185	537.5	64.4
57A	.1521	.3197	.0474	.2930	.6158	529.2	51.7	.1504	.3841	.1010	.2367	.6044	534.8	61.6	.1542	.3786	.0902	.2475	.6077	534.4	59.7
58	.0875	.2090	.0137	.2821	.6738	542.7	83.4	.0891	.2451	.0219	.2500	.6885	541.5	86.8	.0903	.2416	.0196	.2569	.6873	542.0	86.0
58A	.0409	.1266	.0115	.2285	.7073	530.3	75.5	.0459	.1569	.0188	.2070	.7082	534.2	83.5	.0441	.1541	.0174	.2045	.7148	532.8	82.5
59	.1449	.3002	.0510	.2921	.6051	525.7	47.3	.1474	.3609	.1102	.2384	.5834	533.8	56.7	.1468	.3570	.0973	.2442	.5939	532.1	54.9
59A	.2512	.4060	.0613	.3496	.5651	540.6	46.0	.2327	.4607	.1413	.2790	.5517	543.4	56.3	.2403	.4565	.1233	.2930	.5567	544.1	54.7
60	.0709	.2087	.0401	.2218	.6528	518.0	58.0	.0785	.2653	.0853	.1828	.6184	522.3	58.5	.0797	.2601	.0768	.1913	.6244	521.1	57.0
61	.0480	.1445	.0112	.2356	.7094	533.0	78.8	.0543	.1764	.0174	.2179	.7119	536.4	86.3	.0513	.1742	.0161	.2123	.7211	534.9	86.0
62	.00724	.02726	.00119	.2029	.7638	534.4	94.4	.0088	.0340	.0016	.1980	.7660	535.2	96.9	.00880	.03312	.00188	.2009	.7562	534.9	94.0
63	.00627	.03555	.01140	.1178	.6680	510.0	76.0	.0086	.0498	.0237	.1047	.6067	509.3	68.8	.00810	.04958	.02177	.1020	.6240	509.0	71.6
64	.0723	.1962	.1122	.1899	.5154	502.3	58.2	.1114	.2643	.3255	.1589	.3772	495.8	52.2	.0986	.2570	.2690	.1578	.4115	497.0	55.4
65	.0163	.0660	.0456	.1274	.5160	500.8	72.6	.0284	.0956	.1217	.1157	.3890	495.5	67.5	.0255	.0931	.1042	.1144	.4179	496.4	69.6
65A	.0142	.0625	.0716	.0958	.4214	495.5	82.6	.0323	.0994	.1956	.0986	.3038	490.2	79.6	.0285	.0969	.1680	.0971	.3303	491.4	80.3
66	.3715	.5307	1508	.3528	.5040	515.8	23.4	.3725	.6005	.4311	.2652	.4273	523.6	21.5	.3665	.5982	.3665	.2753	.4494	518.0	21.1
67	.0421	.1464	.0854	.1537	.5345	502.5	66.3	.0684	.2044	.2371	.1341	.4010	496.8	60.0	.0621	.1989	.1998	.1348	.4316	497.8	62.2
68	.0216	.0597	.0850	.1315	.3590	492.2	76.7	.0466	.0929	.2555	.1180	.2352	485.7	78.5	.0432	.0907	.2110	.1252	.2630	487.0	76.0
69	.0523	.1825	.1006	.1559	.5441	503.2	65.7	.0868	.2496	.2763	.1417	.4078	497.5	57.0	.0815	.2441	.2350	.1454	.4354	498.4	58.4
70	.01794	.00696	.00000	.7205	.2795	641.7	100.0	.00783	.00293	.00000	.7274	.2725	653.0	100.0	.0114	.0043	.0000	.7261	.2739	650.2	100.0
71A	.03257	.01301	.00001	.7145	.2854	635.6	100.0	.01846	.00774	.00000	.7047	.2952	627.8	100.0	.01803	.00742	.00000	.7085	.2915	630.5	100.0
72	.01821	.00941	.00001	.6596	.3401	608.2	100.0	.01163	.00620	.00001	.6521	.3476	606.1	100.0	.01375	.00736	.00001	.6512	.3485	605.8	100.0
73	.01780	.01806	.00004	.4960	.5030	577.6	100.0	.01536	.01610	.00003	.4875	.5115	576.3	100.0	.01593	.01629	.00003	.4940	.5050	577.2	100.0
74	.00658	.02629	.00124	.1929	.7707	533.0	94.5	.00816	.03322	.00165	.1896	.7721	534.0	96.9	.00806	.03262	.00157	.1908	.7721	534.1	96.8
75	.00187	.00767	.01690	.0707	.2901	489.4	94.2	.0044	.0155	.0424	.0707	.2490	487.4	92.1	.0043	.0147	.0375	.0761	.2602	487.9	92.5
76	.00288	.00038	.01440	.1631	.0215	448	98.5	.01096	.00117	.05663	.1594	.0170	447.8	99.7	.00793	.00101	.04166	.1567	.0200	450.8	99.5
77	.4615	.3267	.0030	.5833	.4129	592.0	97.6	.3094	.2808	.0032	.5214	.4732	581.7	98.9	.3140	.2834	.0032	.5228	.4719	582.0	98.9
77A	.3954	.2729	.0022	.5897	.4070	593.0	98.0	.2607	.2336	.0022	.5251	.4705	582.2	99.0	.2546	.2276	.0023	.5255	.4698	582.4	99.0
78	.0816	.0882	.1225	.2792	.3017	483.2	45.4	.1284	.1079	.4338	.1916	.1610	471.8	62.2	.1111	.1060	.3299	.2031	.1938	474.7	58.8
78AA	.1255	.1346	.1462	.3089	.3313	485.0	36.7	.1735	.1575	.5118	.2059	.1869	473.2	53.4	.1541	.1554	.3900	.2203	.2222	476.1	49.8
78A	.2820	.2860	.1974	.3684	.3737	487.2	20.4	.3146	.3119	.6782	.2411	.2391	475.5	34.3	.2930	.3099	.5213	.2606	.2757	478.1	31.0
78B	.4524	.4406	.2339	.4015	.3910	488.4	11.7	.4559	.4638	.7930	.2662	.2708	477.1	21.2	.4342	.4627	.6122	.2877	.3066	479.9	19.1
78C	.7395	.6922	.2796	.4321	.4045	491.2	3.7	.6851	.7052	.9338	.2948	.3034	479.9	7.0	.6657	.7044	.7247	.3178	.3363	482.5	6.2
79	.0854	.0949	.1004	.3042	.3381	486.2	37.4	.1180	.1115	.3467	.2048	.1935	474.6	52.8	.1054	.1101	.2673	.2183	.2281	477.3	49.7
80	.4943	.5108	.2695	.3878	.4008	492.8	14.4	.5064	.5500	.9024	.2585	.2808	482.2	22.8	.4808	.5489	.7007	.2779	.3172	485.2	20.8
85	.8562	.8774	.1441	.4560	.4673	573.0	47.3	.6765	.6225	.4642	.3837	.3530	587.2	29.7	.6844	.6301	.3670	.4070	.3747	588.5	31.6
85B	.8395	.6395	.0975	.5325	.4056	593.5	57.6	.6360	.5707	.3054	.4206	.3774	585.8	46.0	.6512	.5804	.2430	.4416	.3936	587.0	48.4
86	.8071	.5976	.0547	.5530	.4095	592.4	74.3	.5855	.5168	.1504	.4673	.4126	584.5	68.0	.6060	.5292	.1304	.4789	.4181	585.5	68.0
86A	.8731	.7163	.1298	.5079	.4166	589.6	48	.6910	.6679	.3943	.3941	.3810	581.3	39.8	.6917	.6753	.3238	.4091	.3994	581.5	40.2
86B	.9111	.7797	.1768	.4878	.4175	587.9	35	.7371	.7466	.5523	.3620	.3667	578.0	27.4	.7419	.7507	.4470	.3825	.3870	579.6	28.0
86C	.9478	.8388	.2412	.4674	.4137	587.1	18.2	.8039	.8220	.7796	.3342	.3417	577.0	13.3	.7983	.8246	.6181	.3562	.3680	578.3	13.6
88	.000512	.000185	.000000	.7346	.2654	695	100.0	.000149	.000054	.000000	.7346	.2654	695	100.0	.00074	.00027	.00000	.7346	.2654	695	100.0
89	.01131	.00412	.00000	.7332	.2668	679	100.0	.00480	.00177	.00000	.730	.270	660	100.0	.00765	.00293	.00000	.724	.276	646.5	100.0
89A	.00212	.00077	.00000	.7346	.2654	695	100.0	.00061	.00022	.00000	.7346	.2654	695	100.0	.00268	.00097	.00000	.7346	.2654	695	100.0
90	.1437	.1237	.0002	.5369	.4623	583.8	100.0	.1158	.1050	.0002	.5240	.4751	581.8	100.0	.01237	.01096	.00002	.5298	.4694	582.6	100.0
97	.00122	.00078	.00197	.3073	.1965	578.9c	52.5	.00064	.00041	.00108	.3007	.1923	555.0c	48.0	.00101	.00068	.00097	.3797	.2556	521.7c	34.4
101	.4624	.4759	.0177	.4837	.4978	576.4	88	.3721	.4639	.0343	.4276	.5330	569.5	89.7	.3778	.4664	.0318	.4313	.5324	569.8	88.5
102	.4038	.5021	.0330	.4301	.5348	567.2	76.8	.3686	.5086	.0742	.3874	.5346	564.8	79.3	.3758	.5097	.0660	.3949	.5357	565.4	79.0
105	.4409	.1953	.0006	.6924	.3067	621	99.7	.2614	.1224	.0012	.6789	.3180	615.6	99.2	.2723	.1257	.0011	.6819	.3148	615.7	99.1

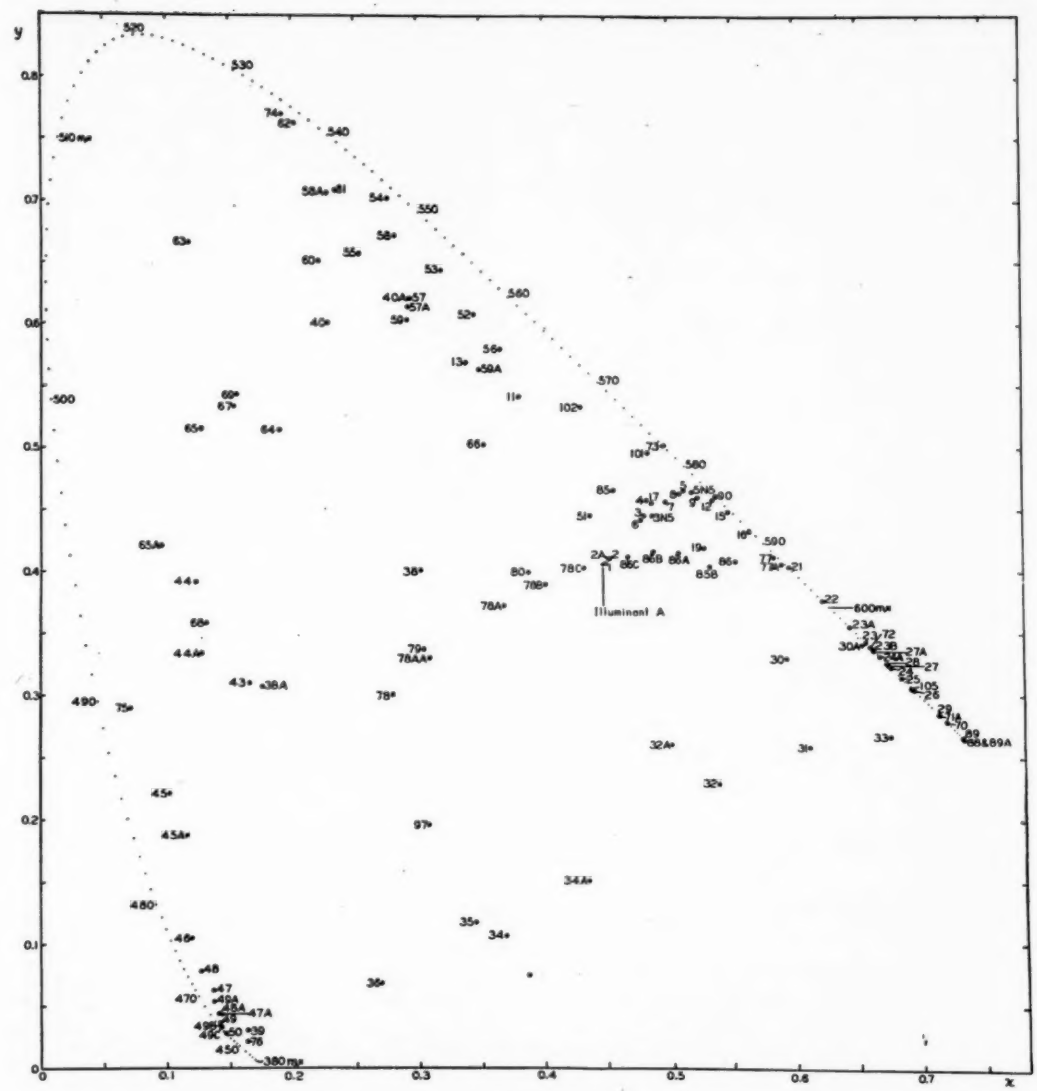

FIG. 1.

Points representing the chromaticities of Wratten light filters, in ICI illuminants *A* and *C*, are indicated in Figs. 1 and 2. Dominant (or complementary) wave-length and purity were determined graphically by using large scale chromaticity diagrams. The dominant wave-lengths are listed in Column λ. Complementary wave-lengths are listed in the same columns, but are followed by the symbol, *c*. Excitation purities are listed in the Columns *p*. The luminous transmittances of the filters, for the several light sources, are indicated by the values of *Y*, since the second distribution function of the ICI system is identical with the standard ICI luminosity function.

When light from an incandescent tungsten-filament lamp operating at a color temperature of 2360°K is transmitted by the standard

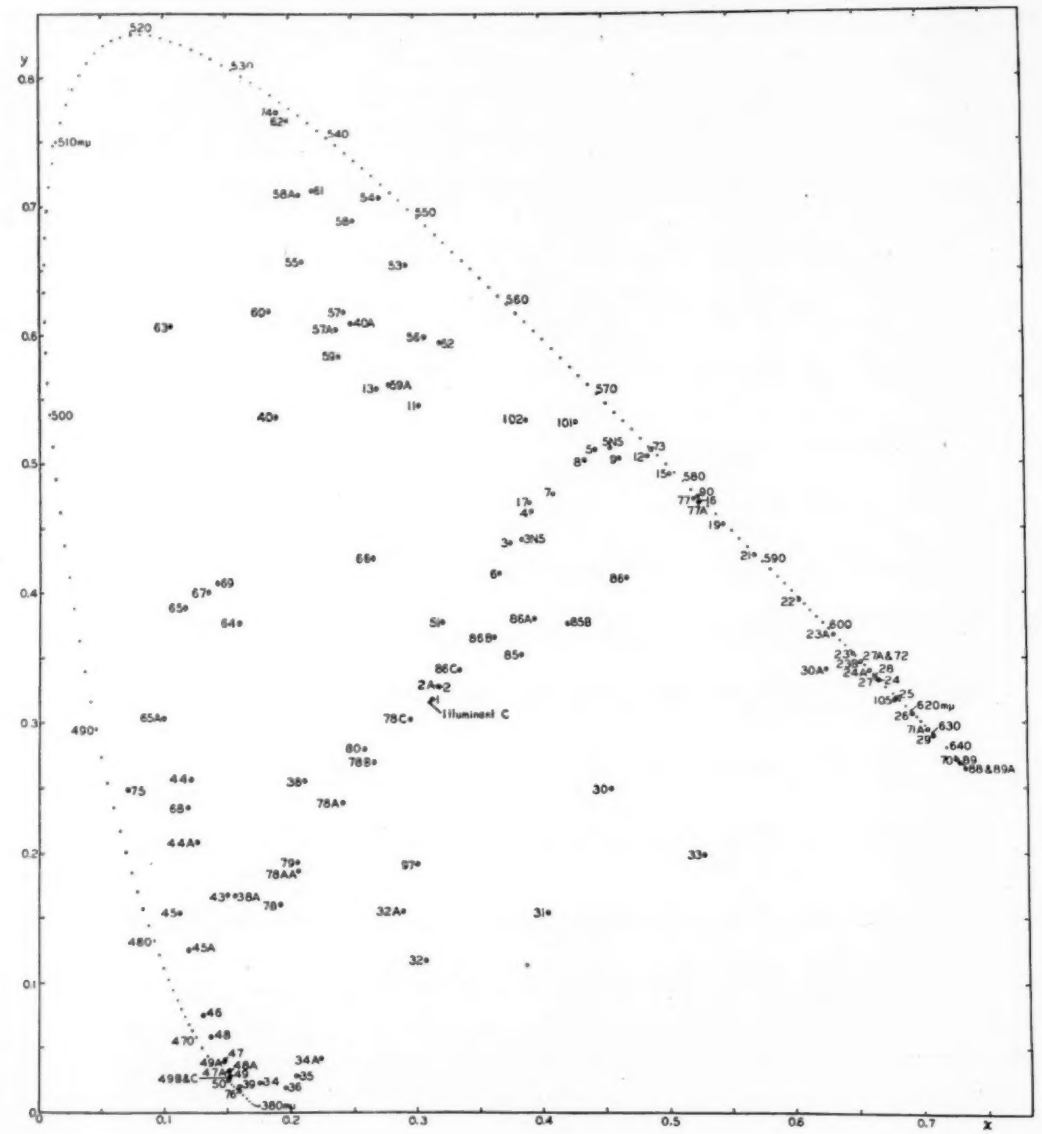

FIG. 2.

Wratten filter No. 78, an artificial daylight quality is produced, which may be specified by the trichromatic coordinates, $x=0.3333$ and $y=0.3476$. These coordinates indicate a light somewhat greener than the most nearly similar Planckian source, which latter has a temperature of about 5500°K. Wave-lengths, for the selection of ordinates from spectrophotometric curves, for colorimetric calculations based on this illuminant are given in Table II.

The first six and the last ordinate of the X set, and the first and the last of the Y and Z sets of ordinates indicated in Table II occasionally require revision, since they are so far from their

TABLE II. Wave-lengths for selected ordinates. Illuminant: 2360°K lamp with Wratten filter No. 78.

Ordinate	X	Y	Z
1	429.0	469.7	416.8
2	442.9	491.4	425.7
3	453.6	503.2	429.8
4	464.6	510.5	433.0
5	485.7	516.7	435.6
6	537.5	522.0	437.9
7	547.8	526.7	440.2
8	555.4	531.0	442.4
9	561.3	535.1	444.6
10	566.6	538.9	446.6
11	571.4	542.6	448.5
12	575.6	546.2	450.4
13	579.4	549.7	452.3
14	583.0	553.2	454.2
15	586.4	556.8	456.1
16	589.6	560.4	457.9
17	592.7	564.1	459.8
18	595.7	567.8	461.6
19	598.6	571.6	463.5
20	601.5	575.5	465.4
21	604.5	579.5	467.6
22	607.7	583.6	469.9
23	611.1	587.8	472.1
24	614.5	592.3	474.4
25	618.5	596.9	477.0
26	623.1	602.0	480.5
27	628.6	608.0	484.9
28	635.9	615.0	490.4
29	646.9	625.7	498.0
30	668.4	648.2	514.4
Factors	0.03196	0.03333	0.03477

TABLE III. Wave-lengths for supplementary ordinates. Illuminant: 2360°K lamp with Wratten filter No. 78.

X	Y	Z
413.5	*441.0*	*403.0*
421.0	453.0	410.0
424.0	*460.5*	*413.5*
429.0	**469.7**	**416.8**
434.8	479.0	421.5
439.0		
442.9		
446.6		
450.1		
453.6		
457.0		
460.6		
464.6		
469.2		
474.8		
485.7		
520.2		
525.4		
528.5		
532.5		
537.5		
541.5		
658.5	638.0	507.5
668.4	**648.2**	**514.4**
679.0	*660.0*	*523.0*
689.5	669.5	531.0
716.0	*695.0*	*547.0*

nearest neighbors and represent integrals extending over wide wave-length ranges. These revisions may be accomplished conveniently by use of the supplementary ordinate method, which is explained with an example in the report of the Colorimetry Committee.[1] The wave-lengths for supplementary ordinates to accompany Table II are given in Table III. Each of the ordinates indicated by a wave-length given in Table II may be replaced, for greater accuracy, with the average of three ordinates whose wave-lengths are indicated in Table III. The original ordinate is one of these three, and its wave-length is indicated in boldface roman type in Table III. The other two ordinates to be averaged with the original have wave-lengths indicated by ordinary roman type preceding and following the boldface numeral. Some of the ordinates at wave-lengths printed in roman type need to be revised occasionally before they are included in the average. The wave-lengths of those most frequently in need of correction are preceded and followed by italicized wave-lengths. The ordinates at the italicized wave-lengths are averaged with the ordinate which they bracket. This average is used in place of the single ordinate in the final averaging by which a revised value is obtained for the ordinate at a wave-length printed in boldface. A majority of the values listed in Table I were revised in this manner, and a few were further corrected by carrying the supplementary ordinate method one stage farther than that indicated in Table III.

JOURNAL OF THE OPTICAL SOCIETY OF AMERICA VOLUME 35, NUMBER 10 OCTOBER, 1945

Entoptic Mapping of the Purkinje Blue Arcs

R. L. Dolecek and Jules de Launay
Physics Department, Texas Technological College, Lubbock, Texas
(Received July 23, 1945)

INTRODUCTION

THE phenomenon of the Purkinje blue arcs* has elicited the interest of many workers of the past. This interest has probably been caused by the realization that a thorough understanding of this phenomenon might result in a better understanding of nerve action and vision.

Purkinje, in 1825, first discovered the phenomenon of the blue arcs. He attributed it to some normal structure of the eye without specifically identifying that structure. Hans Gertz,[1] Hubbard,[2] Otto Gertz,[3] and Troland[4] attributed the phenomenon to secondary excitation of the retinal elements lying near the course of retinal fibers which originate in the region of primary stimulation. Although no actual plots of arcs have been reported in the literature, it has been generally accepted that the form of the arcs coincides with the pattern of the papillo-macular nerve bundle pathways.

Most authors agree substantially on the following facts concerning the form of the arcs and conditions under which they are produced:

1. Arcs may be obtained by the use of a primary stimulus of any color, but are most easily observed with an orange-red source and a dark background.

2. Though the arcs are visible during all stages of dark adaptation, the optimum condition for viewing the arcs seems to be two minutes of dark adaptation after exposure to general room illumination.

3. The stimulus must occur in the general region of the macula.

4. Double and single arcs occur when the stimulus lies on the nasal side of the projected field (temporal side of the fovea on the retina).

5. So called "spikes" occur when the stimulus lies on the temporal side of the projected field.

6. The arcs converge toward the blind spot; their axis of symmetry and the axis of the blue spike coincide with the papillo-foveal line.

7. The form of the arcs coincides closely with the pattern of the papillo-macular nerve bundle pathways.

8. The blue arc phenomenon is transitory in nature, the duration of the arcs being approximately one second after application of primary stimulus to any particular location on the retina.

These facts should be supplemented by several statements (of controversial nature) concerning the form and theory of the Purkinje phenomenon:

9. The oval space enclosed by the blue arcs may be wholly or partially filled with a bluish haze called by Ellis[5] "the blue oval." Ellis[5] states that "the oval may exist alone, when the primary stimulus is feeble, or when the exciting image is nearly a point, or is a narrow line of light."

10. Amberson[6] and Snell[7] postulate, from their observations, the existence of a "central area of blindness for the secondary phenonenon" corresponding closely to the rod-free area. A primary stimulus falling within this area will not evoke blue arcs. Further, Amberson[6] states that in the general macular region, the area in which the primary stimulus must fall to evoke the blue arc phenomenon consists of two oval regions lying on either side of the rod-free area. Ellis[5] disagrees with this postulate, stating that the blue arcs are best defined and most intense when the stimulating image falls within the fovea.

11. Because of variations in experimental technique, the question of color and intensity of the arcs as a function of primary stimulus remains unsettled. This applies also to the occurrence of after images.

12. The general theory of the mechanisms involved in the production of the Purkinje blue arcs is still in a formative stage.

It is the purpose of this study, first: to present a map of the papillo-macular nerve bundle pathways, on the hypothesis that they are represented by the Purkinje blue arcs; second: to show that this map is complete enough to serve as the basis for a critical study of the observations of previous writers and is consistent with histological findings.

EXPERIMENTAL TECHNIQUE

In the design of the experiment, the factors essential for optimum viewing conditions were

* An excellent survey and discussion of the Purkinje blue arc phenomenon is given by B. Friedmann, Arch. Ophthalm. **6**, 663 (1931).

[1] H. Gertz, Zentralbl. f. Physiol. **19**, 229 (1905); Skand. Arch. f. Physiol. **19**, 381 (1907); **21**, 315 (1909).

[2] J. C. Hubbard, Psych. Bull. **7**, 196 (1910).

[3] Otto Gertz, Hosp.-Tid., Københ. (R) **5**, 7, 1197 (1914).

[4] L. T. Troland, J. Opt. Soc. Am. **4**, 160 (1920).

[5] F. W. Ellis, Am. J. Physiol. **82**, 290 (1927).

[6] W. R. Amberson, Am. J. Physiol. **69**, 354 (1924).

[7] P. A. Snell, Arch. Ophth. **1**, 475 (1929).

taken into account. A red primary stimulus viewed on a dark background and small red fixation points of near threshold intensity were used. After suitable dark adaptation, the primary stimulus was applied and a point was marked in the body of the arc during the time interval it appeared projected on the background. This procedure was repeated until the complete arc was plotted.

A variable intensity concentrated tungsten filament type projector was used as the illuminating light source for the primary stimulus. The light from this source, after passing through a No. 242 Corning red filter, was focused on the back of a flat screen (tangent screen) placed at right angles to the line of vision. An interrupting shutter, operated by a magnetic relay under the control of the observer, was placed in the path of the light beam between the source and the tangent screen. The fixation points in the tangent screen were illuminated by a separate uninterrupted variable intensity red source. The interrupting shutter and uninterrupted fixation points were utilized to permit the observer to maintain rigid fixation before, during, and after the application of the primary stimulus. Rigid fixation is one of the essential factors in obtaining consistent data.

The tangent screen, located 35 cm from the eye of the observer, was fitted in a window separating two rooms. One room contained the light sources, filters, and shutter. The other room contained the head rest and recording apparatus. In the order from source to observer, the tangent screen was composed of the following three layers: an opal glass plate, a sheet of opaque paper, and a sheet of graph paper. The opaque paper was ruled with horizontal and vertical lines spaced at centimeter intervals. Needle holes, to serve as fixation points, were made at the intersections of these lines. At the central intersection, a circular aperture subtending 15 minutes of arc at the eye was made. The light from the primary red source was focused on this central aperture. Thus, when the shutter was opened, the aperture served as the primary stimulus for the Purkinje blue arcs. The millimeter graph paper, mounted against the opaque paper, contained two holes, one to expose the primary stimulus, the other to select the desired point of fixation.

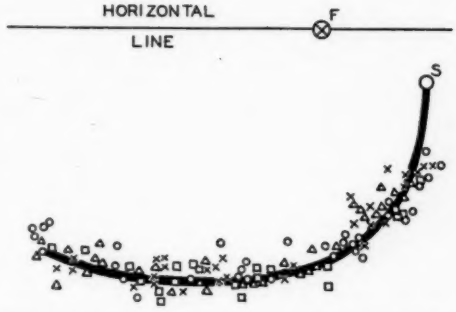

FIG. 1. A composite plot of data obtained on a single arc. The location of the primary stimulus is labelled *S* and of the point of fixation, *F*. The curve is drawn in the center of the distribution. Plot includes data taken at four different sittings.

To facilitate plotting in the dark, a special pencil was constructed. The barrel of this pencil was made of lucite rod. A small lamp was fitted at the "eraser end." The surface of the entire pencil was painted with an opaque material, light being permitted to escape only in a very narrow beam immediately surrounding the pencil lead.

An examination of the data obtained on the same arc, but at different sittings, indicated appreciable error in the repositioning of the eye. This difficulty was overcome by making two improvements in the head rest. Chin rests were molded to fit the contours of the jaw of the individual observer and the forehead rest was fitted with a small round prominence to press against a specific point on the observer's forehead.

EXPERIMENTAL RESULTS

Arcs were plotted for some thirty locations of the primary stimulus. These locations were regularly distributed throughout the region within which a primary stimulus would evoke Purkinje blue arcs. A single arc was plotted throughout its entire length at each sitting, each arc being plotted on a separate sheet of graph paper. To diminish the importance of memory as a factor in plotting, a complete set of graphs of the arcs for the thirty locations of the primary stimulus was made before repeating any of the observations. In all, four sets of observations were made independently by each observer.

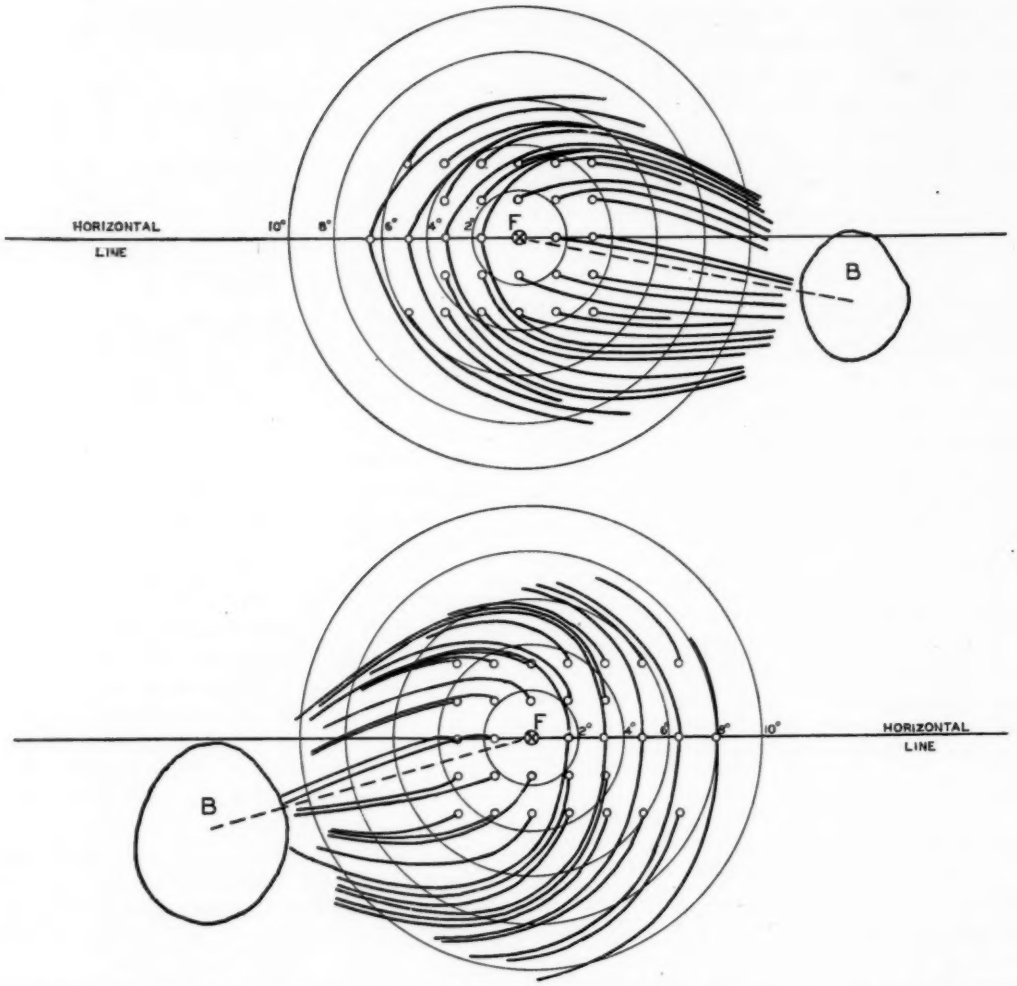

FIG. 2. The projected field plot of the arcs assembled from the data of which Fig. 1 is an example. The blind spot is labelled *B*, the fovea, *F*. The circle at the head of an arc represents the location of the stimulus producing that arc. To serve as a reference scale, concentric circles have been drawn with the fovea as center. The increment in radii corresponds to 2 degrees of visual angle. Above, right eye, R.L.D.; below, left eye, J. de L.

For the purpose of assembling the arcs into a single projected field plot, the data from the four separate graphs of a given arc were plotted on a new sheet, thus forming a composite graph. An example of this composite graph is given in Fig. 1. It is to be noticed (Fig. 1) that the distribution of the points within the body of the arc is uniform although about six months' time lapsed between the first and last trials. As the arcs possess considerable width, as shown in Fig. 1, a curve was drawn through the center of the distribution. The curves produced in this manner for each arc were then assembled into a projected field plot, shown in Fig. 2.

The course of the papillo-macular nerve bundles shown in the histological drawings, as illustrated in the treatises of Atkinson,[8] Polyak,[9]

[8] D. T. Atkinson, *The Ocular Fundus in Diagnosis and Treatment* (Lea and Febiger, Philadelphia, 1937).

[9] S. L. Polyak, *The Retina* (University of Chicago Press, Chicago, Illinois, 1941).

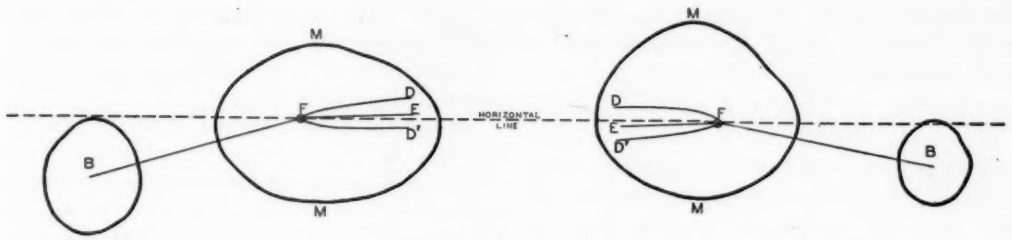

FIG. 3. Summary of data concerning the stimulus field. *M*, boundary of area within which a stimulus will evoke arcs. *DFD'*, boundary of area within which a stimulus will evoke double arcs. *EF*, the locus of points on which a stimulus will produce double arcs of equal intensity. The papillo-foveal line is the line from *F* to the center of the optic disk *B*. The length *BF* of the papillo-foveal line may be used as a standard scale for comparing figures 2 and 3. Left diagram, left eye, J. de L.; right diagram, right eye, R.L.D.

and Wolff,[10] agrees in general with the pathways of the arcs of Fig. 2. However, the drawings do not contain sufficient detail to confirm certain features suggested by the pattern of the arcs in Fig. 2. The pattern shows no actual crossing of pathways though some merging of neighboring arcs occurs near their extremities as they converge to the optic disk. The upper arcs of the projected field are more closely packed than the lower arcs.

Though not shown in Fig. 2, a primary stimulus falling in the fovea or its immediate vicinity evoked the Purkinje phenomenon. Stimulation of the fovea had the peculiar result of evoking a brush-like haze filling the region approximately enclosed by the arcs arising from the points of stimulus shown in Fig. 2 directly above and below the fovea.

In view of the fact that the utmost precaution was exercised to assure complete independence between the two observers in their observation and plotting, a comparison of the two plots shows that on essential features they are in remarkable agreement. One typical difference that may be observed is that the arc leading upward from the second stimulus point to the right of the fovea in the plot of the field for the eye of J. de Launay does not have quite the same pathway among the other arcs as the corresponding pathway in the plot for the eye of R. L. Dolecek.

The axis of symmetry on the temporal side of the projected field coincides with the papillo-foveal line for both observers within a fraction of a degree. However, an axis of symmetry on the nasal side of the projected field, defined as the locus of points along which a stimulus will evoke a pair of arcs of equal intensities, is not coincident with the extended papillo-foveal line, but is approximately a horizontal line. These two axes and the area within which a primary stimulus will evoke the Purkinje phenomenon are shown in Fig. 3. The region enclosed by the lines *D* and *D'* (Fig. 3) is the area within which the stimulus (15 minutes in diameter) is found to evoke double arcs. The axis of symmetry *EF* along which the double arcs are of equal intensity might reasonably correspond to the line of cleavage between the papillo-macular nerve bundles and therefore represent the raphé. The histological drawings, previously mentioned, suggest that the raphé is an extension of the papillo-foveal line. Polyak[9] states, however, that the raphé "is identical with the horizontal meridian connecting the central fovea with the opposite point at the anterior temporal margin of the retina."

In connection with the two line segments (*BF* and *FE*, Fig. 3) forming the axis of symmetry, it might be mentioned that the division of the field into an upper section enclosed in an angle greater than 180° and a lower section enclosed in an angle less than 180° would imply, from purely geometrical considerations, a tendency to a closer packing of the arcs in the upper region.

The entire retina was explored to determine the region or regions within which the application of the primary stimulus (15 minutes in diameter) would evoke the Purkinje phenomenon. The results of the exploration are given in Fig. 3. The

[10] E. Wolff, *The Anatomy of the Eye and Orbit* (The Blakiston Company, Philadelphia, Pennsylvania, 1940).

angular dimensions and location of the oval shaped region (*M*, Fig. 3) correspond to those of the macula as described by Polyak.[9]

DISCUSSION

During the early part of the experiment, it was suspected that a psychological phenomenon, other than the tendency of the eye to move toward the suddenly applied stimulus or the arcs, was affecting the reliability of the data. The tendency of the eye to move was overcome. This was done partly by the use of a stationary uninterrupted point of fixation and partly by subsequent training. The phenonenon affecting the experiment was found to be a distortion of the perceptual geometry of space in darkness as compared to the perceptual geometry of space when viewed in the lighted room. For example, certain arcs, perceived as straight when viewed in the dark, persistently resulted in plots possessing appreciable curvature when viewed in the lighted room. The distortion of the geometry of perceptual space is discussed by Helmholtz.[11] Unless the observer is aware of the nature of this phenomenon, he will experience considerable inconsistency in his data.

Regarding the existence of "blind areas" in the fovea and the regions of the macula extending above and below the fovea, the experimental results of this study substantiate the findings of Ellis[5] and do not agree with the statements of Amberson[6] and Snell.[7] (See item 10 of the Introduction to this paper.)

The results concerning the shape of the Purkinje phenomenon ("blue spikes," "blue ovals," "double arcs") obtained by authors using horizontal or vertical slits as their primary stimulus can be predicted by the use of Fig. 2. One has but to place on Fig. 2 a slit corresponding to the primary stimulus used and the resulting mass of arcs originating within the slit represents their results.

[11] *Helmholtz's Physiological Optics*, translated by J. P. C. Southall, published by the Optical Society of America, §28 (1925).